universität wien

DISSERTATION

Titel der Dissertation

Identification and characterization of potential tumor suppressor genes for ovarian cancer on chromosome 8p22

angestrebter akademischer Grad

Doktor/in der Naturwissenschaften (Dr. rer.nat.)

Verfasserin / Verfasser:	Michael Wittinger
Matrikel-Nummer:	9807194
Dissertationsgebiet (lt. Studienblatt):	Mikrobiologie/Genetik
Betreuerin / Betreuer:	Univ.-Prof. Dr. Pavel Kovarik

Wien, am

Table of Contents

Acknowledgements:

First of all, I would like to express my gratitude to Prof. Dr. Michael Krainer for providing me with the possibility to work in high-quality scientific projects and access to state-of-the-art technology. I also would like to thank cordially Prof. Dr. Pavel Kovarik for taking over the supervision of my thesis.

I would like to thank my collaborators, notably Prof. Dr. Thomas Grunt, Prof. Dr. Maria Sibilia, Prof. Dr. Christian Schöfer, Prof. Dr. Reinhard Horvat, whose expertise, support and motivation was essential for my work.

In addition I want to merit Thomas Pangerl, who painstakingly managed our laboratory, supported me with experiments and always cared that everything in the lab was going on fluently. Special thanks to Dr. Dietmar Pils for providing me his profound basic and technical knownledge and for training me at the beginning of this project. A cheers goes to my other group members, collegues and friends at the Medical University, especially Mag. Mariam Anees, Dr. Peter Horak, Mag. Ahmed El-Gazzar and Dr. Eva-Maria Fuchs.

I am very grateful for my family and friends, they always supported me with spirit and the right perspective towards life. Showing me the real values often made science easier to bear. Especially my sister Dani who accompanied me throughout my lifetime as very best friend and emotional first aid kit. This work would not have been proceeded this way without my girl-friend Cony, who always supported me with unconditional love, alternative perspectives and patience, also in times when professional life was running tumultuously.

1 Summary

Frequent Loss of Heterozygocity (LOH) in specific chromosomal regions of tumors indicates the residence of at least one tumor suppressor gene (TSG) in the corresponding chromosomal region. Chromosome 8p22 is described as LOH hotspot in several epithelial tumors. However, the related genes of this chromosomal band are still very poorly described. The aim of this study was the identification and characterization of potential tumor suppressor genes on chromosome 8p22 in ovarian cancer.

Two out of 22 genes of 8p22 – *hVps37A* and *TUSC3* – turned out to be promising tumor suppressor candidates and were characterized in more detail. It could be shown that hVps37 expression is significantly reduced in primary ovarian tumors relative to normal ovarian epithelias. Furthermore, survival rates of the patients were directly correlated with the hVps37A expression of the corresponding tumors. In-vitro characterization of hVps37A in two ovarian cancer cell lines resulted in an explanatory model of the clinical observations. As part of the ESCRT-I complex hVps37A is involved in the degradation process of activated receptor tyrosine kinases (RTKs) including the well described oncogenes EGFR and HER2. Consequently, hVps37A knockdown led to a hyperactivation of the MAPK (Mitogen Activated Protein Kinase) pathway secondary to accumulating amounts of the activated EGFR (pEGFR) in the cytoplasm. Furthermore, the hVps37-silenced cell lines developed a resistance against the growth inhibitory effect of Cetuximab.

In contrast to *hVps37A*, 29.7% of the tumors analyzed were methylated at the *TUSC3* promoter, acompanied with reduced mRNA expression and unfavourable survival rate of the patients. Therefore, promoter methylation turned out to be an independent prognostic factor for ovarian cancer. *In-vitro*, it could be shown that TUSCS3 resides in the endoplasmatic reticulum and is involved in the N-glycosilation

process of integrin-ß1 and potentially further proteins. Moreover, reconstitution of TUSC3 in ovarian cancer cell lines decreased cellular proliferation.

Overall two promising molecular biomarkers were identified, potentially assisting in the development of more accurate prognostic procedures and therapies for ovarian cancer and beyond.

1.1 Zusammenfassung

Häufiges Auftreten eines Allelverlusts (Loss of Heterozygosity) in einer bestimmten Chromosomenregion bei Tumoren deutet darauf hin, dass in dieser Region mit hoher Wahrscheinlichkeit ein oder mehrere Tumorsuppressorgene (TSG) liegen. Loss of Heterozygosity (LOH) des Chromosoms 8p22 wurde in verschiedenen epithelialen Tumoren bereits häufig beschrieben, jedoch sind die meisten darauf liegenden Gene noch schlecht charakterisiert. Ziel dieser Arbeit war die Identifizierung und Charakterisierung potentieller TSG Kandidaten in dieser Region am Modellsystem des Ovarialkarzinoms.

Aus 22 bekannten Genen dieser Region erschienen zwei Kandidaten – *hVps37A* und *TUSC3* – besonders vielversprechend und wurden genauer charakterisiert. Es konnte gezeigt werden, dass die hVps37A Expression in primären Ovarialtumoren im Vergleich zu gesunden Epithelien des Ovars signifikant erniedrigt ist. Außerdem korreliert die Überlebenswahrscheinlichkeit von Ovarialkarzinom Patientinnen direkt mit der hVps37A mRNA Expression der korrespondierenden Tumore. Eine molekularbiologische Charakterisierung von hVps37A anhand von zwei Ovarialkarzinom Zelllinien lieferte ein Erklärungsmodell für die klinischen Beobachtungen. Als Teil des ESCRT-I Komplexes ist hVps37A am Abbau von Rezeptor Tyrosinkinasen (RTKs) inklusive der Onkogene EGFR und HER2 beteiligt.

Daher führte ein hVps37A Knock-down in unseren Zellmodellen zur Akkumulation des aktivierten EGR (pEGFR) im Cytoplamsa, was wiederum die Hyperaktivierung des MAPK (Mitogen Activated Protein Kinase) Pathways zur Folge hatte. Außerdem erwarben die Zelllinien als Folge des hVps37A Knock-downs eine Resistenz gegenüber der proliferationsinhibierenden Wirkung von Cetuximab.

Im Unterschied zu hVps37A waren 29.7% der untersuchten Tumore am *TUSC3* Promotor methyliert, was mit verringerter mRNA Expression und einer signifikant schlechteren Überlebenswahrscheinlichkeit für die Patientinnen einherging. Somit erwies sich für *TUSC3* die Promotormethylierung als unabhängiger prognostischer Faktor. Rekonstituierung von TUSC3 in Ovarialkarzinomzelllinien führte zu einer verringerten Proliferation. Außerdem konnte gezeigt werden, dass es im endoplasmatischen Retikulum lokalisiert und an der N-Glykosylierung von Integrin-ß1 und potentiell weiteren Proteinen beteiligt ist.

2 Introduction

2.1 Ovarian Cancer

In industrialized countries, ovarian cancer is the leading cause of death from gynaecological malignancies (Jemal et al., 2008). It can be divided into three main groups: Epithelial, stromal and germ cell tumors, whereof epithelial tumors are most common and account for more than 85% of all ovarian cancer cases. Epithelial ovarian tumors may be serous or mucinous and include cystadenocarcinoma, endometrioid carcinoma, clear cell carcinoma, undifferentiated carcinoma, carcinosarcoma and mixed mesodermal tumor. Individual tumors are classified according to the FIGO staging system.

Hereditary causes like mutations of BRCA1, BRCA2, MLH1, MSH2 or GSTM1 are believed to account for 10-15% of ovarian cancer development(Aarnio et al., 1999; Watson et al., 2001). However, the bigger part of ovarian tumors occur spontaneously secondary to somatic mutations of oncogenes and/or tumor suppressor genes, leading to abnormal signalling of specific pathways like the PI3K-AKT, the MAPK or the mismatch-repair (MMR) pathway (Ricciardelli and Oehler, 2009).

2.2 Oncogenes and Tumor Suppressor Genes

Oncogenes and tumor suppressor genes TSGs regulate different cellular mechansims like proliferation, apoptosis or DNA-repair. While oncogenes promote cellular growth, migration, invasion and survival, tumor suppressor genes counterbalance these effects. The rise of malignant tumors including ovarian cancer is a multistep event with subsequent dominant activating mutations of proto-oncogenes or recessive inactivation of TSGs (by mutations, deletions or promoter

methylation), leading to physiological alterations of the cellular phenotype, which is proceeding via a selection process according to the Darwinian evolution.

Tumor suppressor genes are frequently located on LOH (loss of heterozygosity) regions, which are generated by chromosomal loss, somatic recombination or gene conversion (Figure 1). If one allele of a tumor suppressor gene is (e.g. hereditary) inactivated, the remaining wildtype allele can be lost by LOH, leading to transcriptional repression and cancer phenotype. Since repression of TSGs confers an advantage for tumors, a cancer cell-specific selection process accumulates LOH regions bearing at least one tumor supressor genes in cancer. Consequently, LOH regions can be used to indentify novel tumor suppressor genes.

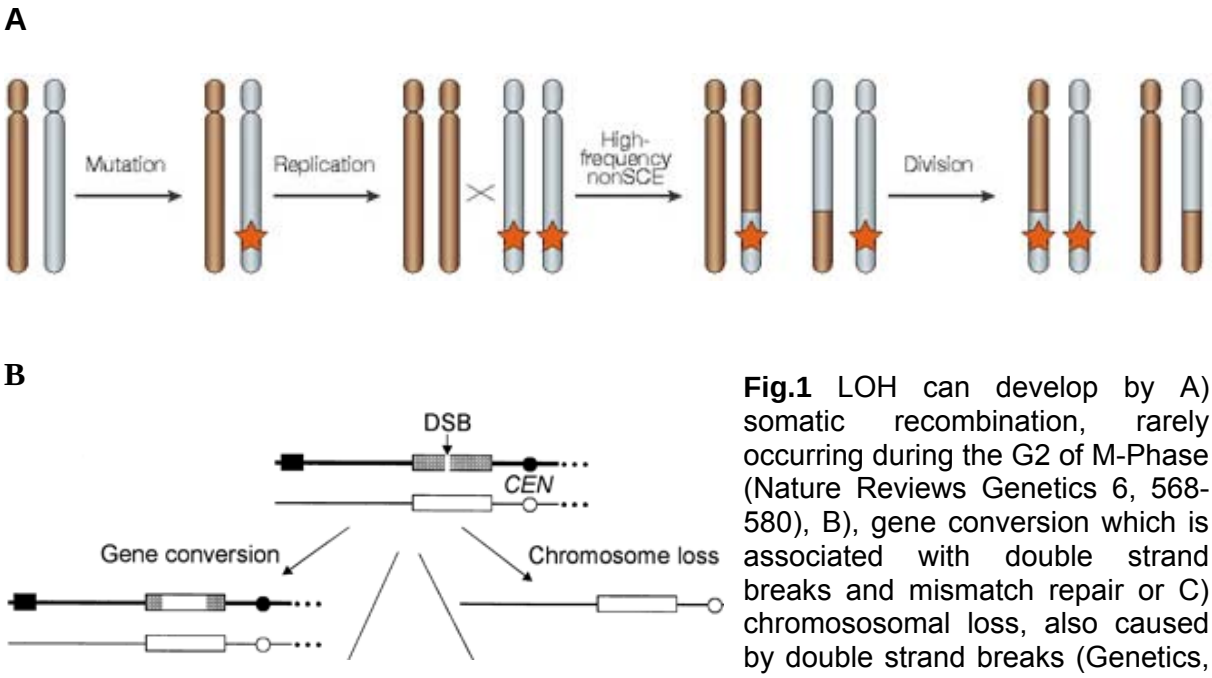

Fig.1 LOH can develop by A) somatic recombination, rarely occurring during the G2 of M-Phase (Nature Reviews Genetics 6, 568-580), B), gene conversion which is associated with double strand breaks and mismatch repair or C) chromososomal loss, also caused by double strand breaks (Genetics, Vol. 153, 665-679, October 1999)

2.3 Anti- Ovarian Cancer Interventions and Tumor Markers

Because of few early stage symptoms and a lack of standard screenings, more than 70% of the ovarian carcinomas have already metastasized beyond the ovary when diagnosed. Consequently, the mortality rate of ovarian cancer patients is relatively high and chemotherapy is mostly needed in addition to debulking surgery.

Due to its high efficiency and low toxicity, the platinum-taxane combined therapy has been established as first-line treatment and also upon tumor recurrence(Sandercock et al., 2002). However, in the course of tumor relapse and subsequent treatments, response rates decrease as a result of gained resistance against first-line therapeutics. Platinum-resistent patients are alternatively treated with agents like gemcitabine, topotecan or etoposide, although there is no standard agreed following-therapy available and response rates are still relatively poor for women who developed resistance against conventional chemotherapy (Agarwal and Kaye, 2003). Currently, a number of promising cytotoxic drugs are under investigation and some of them already proofed to be effective against recurrent ovarian tumors resistant against standard therapies (Krasner et al., 2007). Furthermore, several monoclonal antibodies or small-molecule inhibitors targeting essential components of ovarian cancer-related pathways emerge now as potential future therapeutics (Yap et al., 2009). Angiogenesis inhibitors targeting the VEGFA (vascuolar endothelial growth factor A) (Bevacicumab) or the VEGFR (vascuolar endothelial growth factor receptor) tyrosine kinase domain (pazopanib, sunitinib, sorafenib and cediranib) are currently tested in clinical trials and are giving promising results (Yap et al., 2009). EGFR and HER2 are well described oncogenes of the Erbb-family, frequently overexpressed in ovarian cancer and thus serving as potential targets for anti-tumor interventions. However, single agent administration of anti-EGFR (Cetuximab, Matuzumab, Geftinib, Erlotinib) as well as anti-HER2 (Trastuzumab, Pertuzumab) compounds resulted in modest activity against relapsed cases of ovarian cancer (Yap et al., 2009).

Variations in therapy response are frequently resulting from different genetic profiles and molecular heterogeneity of the tumors. Conventional clinical markers including staging according to FIGO, histotype and grading, response to a first line

chemotherapy and amount of residual tumor after primary debulking surgery are insufficient to account for resistance against ovarian cancer therapies. However, apart from Cancer Antigen 125 (CA-125) (4) there are no specific diagnostic and prognostic molecular markers available in clinical practice (5).

Therefore it is crucial to identify novel prognostic markers facilitating classification of ovarian carcinomas into pathogenetic subtypes and guiding between available therapy options. Aberrations of oncogenes (e.g. EGFR, HER2) or tumor suppressor genes (TSGs) (e.g. p53) of the apoptotic or pro-survival are believed to essentially account for resistance against chemotherapy. In addition to deletions and mutations, TSGs can be downregulated by epigenetic mechanisms like promoter methylation, which holds a particular promise as new molecular marker. They can give insight into the biology of a tumor and in contrast to gene or protein expression analysis, they can be easily detected by PCR-based methods in tumor material as well as in body fluids (6-8).

2.4 Project Aims and Results Summary

In this project, two candidate tumor suppressor genes (hVps37A and TUSC3) which may serve as potential biomoarkers for ovarian cancer, were identified and characterized. They reside on chromosome 8p22, a region of relatively high LOH amounts in epithelial tumors and were selected from 22 known genes on chromosome 8p22, since expression analysis resulted in a significantly reduced expression of hVps37A and TUSC3 in primary ovarian tumors compared to normal epithelial cells. Functional analysis of both candidates yielded promising observations: hVps37A is a member of the ESCRT-I complex, which is crucial for the endosomal sorting process of receptor tyrosine kinases (RTKs) including the oncogenes EGFR and HER2. Knock-down of hVps37A in two ovarian cancer cell

lines was associated with hyperactivation of the MAPK-pathway secondary to the accumulation of activated EGFR (pEGFR) in the cytoplasmic compartment of the cells. Although hVps37A knock-down did not essentially affect cellular proliferation, it reversed the growth-inhibitory effect of the monoclonal EGFR-antagonizing antibody Cetuximab. Furthermore, low hVps37A mRNA expression resulted in unfavourable survival rates of ovarian cancer patients and the prognostic significance of both EGFR and HER2 is strictly dependent on hVps37A protein expression levels.

The *TUSC3* promotor was found to be frequently methylated in primary ovarian tumors, leading to reduced expression levels and having a strong influence on overall as well as progression-free survival, independently of other prognostic factors. *In vitro*, TUSC3 was observed to reside within the endoplasmatic reticulum modifying N-glycosylation patterns of integrin ß1 (and potentially other proteins), resulting in decreased adhesion to collagen I. Moreover, TUSC3 reconstitution in ovarian cancer cell lines was associated with a cell morphology change as well as decreased proliferation and elevated migration.

Overall, hVps37A and TUSC3 bear a high potential as novel tumor suppressor genes in ovarian cancer and hVps37A might be established as first molecular prognostic markers for targeted therapies using monoclonal antibodies against RTKs like the EGFR.

3 Results

3.1 Project 1: The Human Homologue of Vps37A, a Key Component of the ESCRT-mediated Sorting Process in Yeast, is a Potential Biomarker for EGFR-Driven Tumors

Wittinger M[1], El-Gazzar A[1], Pils D[1], Grunt TW[1], Sibilia M[2], Horvat R[3], Schemper M[4], Zeillinger R[5] , Schöfer C[6] and Krainer M[1, *]

[1]Department of Internal Medicine I, Clinical Division of Oncology

[2]Department of Internal Medicine I, Institute for Cancer Research

[3] Clinical Institute of Pathology

[4] Core Unit for Medical Statistics and Informatics

[5] Department of Obstetrics and Gynaecology, Division of Gynaecology

[6] Center for Anatomy and Cell Biology Medical University of Vienna

*Correspondence: Michael Krainer, MD, Department of Internal Medicine I, Medical University of Vienna, Waehringer Guertel 18-20, A-1090 Vienna, Austria, e-mail: michael.krainer@meduniwien.ac.at

Acknowledgements: Bernd Mayer, Peter Horak, Pavel Kovarik for helpful discussions and Thomas Pangerl for technical assistance.

Supported by the Austrian Science Fund (FWF)

Project Number: P17891

3.1.1 Abstract

hVps37A resides on chromosome 8p22, a common LOH region in several cancers. As a potential member of the human ESCRT-I complex, HVPS37A may be crucial for the degradation process of ubiquitinated receptor tyrosine kinases (RTKs). We found HVPS37A expression significantly reduced as well as being the determining influence of the prognostic value of EGFR in ovarian cancer (OC). HVPS37A down-regulation in OC cells led to cytoplasmic pEGFR retention and hyperactivation of the MAPK pathway. Furthermore, based on sustained AKT-pathway activation, HVPS37A-silenced cells became irresponsive towards anti-EGFR antibody inhibition. Overall, we describe a novel prognostic biomarker for OC, clarify its influence on EGFR degradation and, by that, suggest a basis for a further refinement of anti-EGFR intervention in cancer.

3.1.2 Introduction

The ERBB receptor tyrosine kinase (RTK) family comprises four members (ERBB1-4), of which ERBB2 (HER2) and ERBB3 are non-autonomously functional. The epidermal growth factor receptor (EGFR, ERBB1) is a 170 kDa transmembrane RTK that plays an essential role in governing multiple cellular processes, including cell proliferation, survival, and migration (Hynes et al., 2001; Hynes and Lane, 2005). Activation by EGF or EGF-like ligands leads to autophosphorylation of cytoplasmic residues and receptor dimerization (Bogdan and Klambt, 2001). The phospho-tyrosine residue itself serves as a docking platform for several adaptor molecules, triggering the activation of different pathways like the RAS-RAF-MEK-ERK pathway, the PI3K-AKT pathway, and the PLC-gamma-PKC pathway (Scaltriti and Baselga, 2006). Hyperactivation of EGFR-dependent signal transduction often accompanies tumor development, and cancer patients with unbalanced EGFR activity generally present a more aggressive disease leading to unfavorable clinical outcome (Holbro et

al., 2003). It is widely believed that hyperactivation of EGFR-mediated signal transduction can be triggered by the following means: (1) increased ligand expression, (2) elevated EGFR protein expression, (3) specific mutations, rendering EGFR constitutively active, (4) defective down-regulation of EGFR, and (5) cross-talk with heterologous receptor systems (Zandi et al., 2007).

Down-regulation of EGFR and a number of other transmembrane proteins is realized via the endosomal sorting process, which depends on receptor endocytosis as well as subsequent vesicular shuttling towards one of three distinct cytoplasmic compartments (Maxfield and McGraw, 2004) as follows: (I) An internalized receptor can be directed back to the cell surface; (II) receptors enter the trans-Golgi network (TNG), or (III) receptors are transported into the intraluminal vesicles (ILVs) forming multivesicular bodies (MVBs), which are subsequently degraded upon fusion with the lysosome (Katzmann et al., 2002; Raiborg et al., 2003).

MVBs arise upon subsequent binding of four mayor protein complexes (ESCRT-0-III; endosomal complex required for transport) to the limiting membran of sorting endosomes. Protein subunits (termed as vacuolar protein sorting; Vps) of these complexes are well conserved over the eucaryotic kingdom and some of them are described as potential tumor suppressor genes. It is believed that they contribute to cancer prevention by sorting tumor-relevant receptors into the ILVs of MVBs, leading to cessation of the receptor signal (Gruenberg and Stenmark, 2004). This mechanism is reported to regulate cell polarity and proliferation (Giebel and Wodarz, 2006). As an example, mutant vps25 (a member of the ESCRT-II complex) exhibit Notch and Dpp receptor activation, leading to elevated proliferation rates of mutant and adjacent cells, accompanied by loss of epithelial organization (Thompson et al., 2005). Tsg101 (Vps23), the most accuratly described ESCRT-I subunit in mammals,

is suggested to be essential for endosomal trafficking of several activated surface receptors and Tsg101 mutantions may contribute to a tumorgenic phenotype (Babst et al., 2000). Vps37A (vacuolar protein sorting 37 homolog A) was initially described in yeast as further subunit of ESCRT-I (Katzmann et al., 2001). The human homologue of Vps37A (hVps37A), is located on the short arm of chromosome 8 and in this very region, 8p22, high LOH frequencies are described for years in several human cancers including ovarian cancer. Only recently, the tumor suppressor gene DLC1 has been identified on 8p22 by a systematic genomic approach and several further candidates predicted (Pils et al., 2005b; Xue et al., 2008). The expression of hVps37A was found to be reduced or undetectable in hepatocellular carcinoma (HCC) (Xu et al., 2003) by a positional cloning approach as well and independently from its homology to Vps37A and consequently the name HVPS37A (hepatocellular carcinoma related protein) suggested. First functional data showed that overexpression in the HCC cell line SMMC-7721 significantly inhibited cell growth in vitro, whereas siRNA mediated knock-down of HVPS37A in the HCC cell line BEL-7404 resulted in significantly increased cellular proliferation (Xu et al., 2003). In more detailed analysis following the functional studies of Vps37A in yeast it was shown that, via its mod(r) domain hVps37A interacts with Tsg101 and hVps28, as well as with its upstream regulator Hrs (hVps27). In the HeLa cell line, depletion of hVps37A diminishes EGFR degradation (Bache et al., 2004a). With all this information available, hVps37A is still very poorly characterized. Since hVps37A was reported to be involved in the EGFR degradation process and regulating cellular proliferation, we suspected that it might have clinical relevance in OC, which is strongly dependent on EGFR signaling. In fact, low hVps37A expression in primary tumor samples, as well as in recurrent intraperitoneal metastasis, was associated with an unfavorable course of disease for OC patients. Moreover, the well known prognostic influence of EGFR

expression was strictly dependent on the level of hVps37A protein expression. We further aimed to investigate the molecular basis behind this observation in two selected OC cell lines. hVps37A knock-down in OC cells caused accumulation of the activated EGFR (pEGFR) in the cytoplasmic compartment, initiating hyperactivation of the MAPK (mitogen activated protein kinase) pathway. Next we asked, whether hVps37A can interfere with therapeutic interventions targeting the EGFR, and detected that hVps37A-silenced OC cells gain resistance against EGFR inhibition by a monoclonal antibody, but not by small molecules. Taken together, our results identify and characterize a novel prognostic biomarker in OC and, potentially beyond, lead to a more comprehensive understanding of EGFR degradation in general. This also implies there is a chance for a more sophisticated use of targeted therapies in RTK-driven cancer in the future.

3.1.3 Results

3.1.3.1 *hVps37A Expression is Significantly Reduced in Primary Ovarian Tumors and has an Impact on Overall Survival*

hVps37A mRNA expression was quantified in 88 primary ovarian tumors, 38 recurrent intraperitoneal metastases tumors, and 21 normal ovarian tissues (controls). The clinicopathologic characteristics of the patient cohort are outlined in Table 1.

Consistent with our previous results (Pils et al., 2005b), we found that *hVps37A* expression is significantly reduced in primary tumors (p=0.002) compared to the controls. Interestingly, *hVps37A* expression levels in recurrent tumors and normal ovarian tissues were comparable (p=0.397), indicating a selection pressure against *hVps37A* expression, particularly in the early stage carcinogenesis (Figure 2A) Survival curves for *hVps37A* expression dichotomized at the median are visualized as Kaplan-Meier plot (Figure 2B). The influence of *hVps37A* on overall

survival reached statistical significance in a univariate model (p=0.017), as well as in a multivariate model (p=0.027) adjusted for grading, staging and morphologic subtype of the tumors (Table 2).

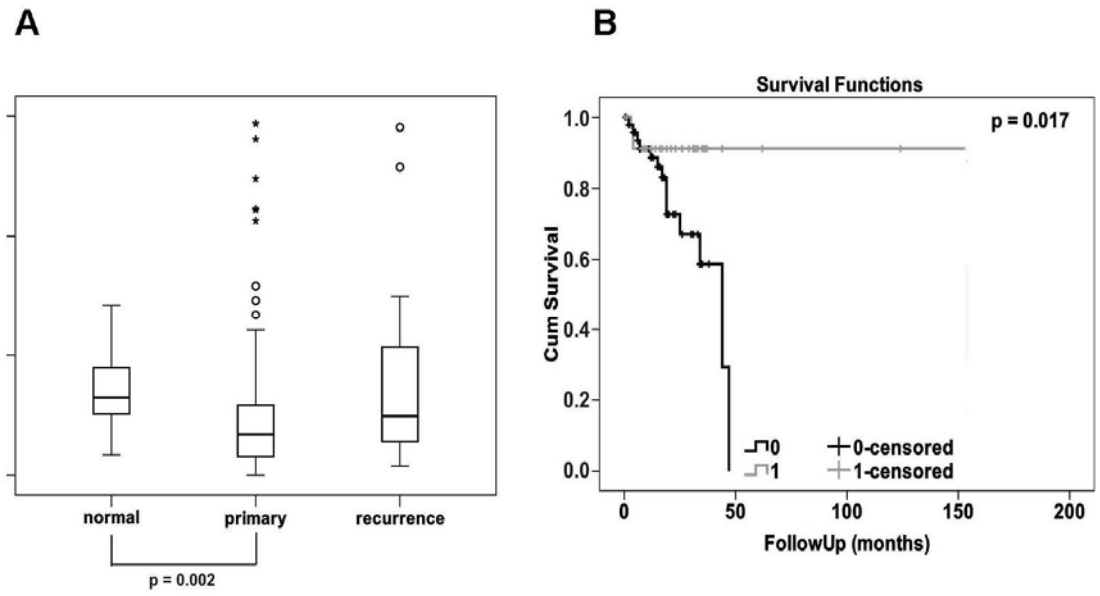

Fig 2. hVps37A Inversely Correlates with Tumor Grade and has an Impact on Survival

(A) hVps37A expression (y-axis) of 88 primary tumors, 38 recurrent tumors, and 21 normal controls was quantified by qRT-PCR and depicted in boxplots. Sample distributions were calculated by the Mann-Whitney *U* test (p-value is indicated). (B) Survival analysis was realized by Cox proportional hazards regression models (Chi-Square=5.185; p=0.023), depicted in plots of the corresponding Kaplan-Meier estimations. Grey/black lines indicate samples high/low hVps37A amounts

Table 1. Characteristics of Patients	cDNA N (percent)	Tissue Microarray: N (percent)
Type		
Normal ovaries	21 (14.3)	
Primary tumors	88 (59.9)	125 (86.8)
Recurrent tumors	38 (25.9)	
Borderline tumors		19 (13.2)
Grade	(1 missing)	(8 missing)
1	2 (1.6)	20 (17.1)
2	50 (40.0)	26 (22.2)
3	73 (58.4)	61 (60.7)
FIGO	(23 missing)	
I	21 (20.4)	31 (24.8)
II	11 (10.7)	14 (11.2)
III	51 (49.5)	72 (57.6)
IV	20 (19.4)	8 (6.4)
Histo	(32 missing)	
Serous	78 (83%)	70 (56)
Non-serous	16 (17%)	55 (44)

Table 2. Univariate and Multiple Cox Proportional Hazards Analysis

	univariate			multivariate		
	Rel. Risk	95% CI	P	Rel. Risk	95% CI	P
hVps37A	4.72	1.33-16.67	0.017*	5.78	1.22-27.80	0.027*
Grade	1.16	0.46-2.91	0.751	2.56	0.76-8.62	0.131
FIGO	9.64	2.93-31.70	<0.001*	16.45	4.11-57.77	<0.001*
Histology	1.29	0.48-3.52	0.614	2.65	0.63-11.24	0.186

CI, confidence interval

3.1.3.2 *hVps37A Expression is Down-Regulated in Human Ovarian Cancer*

Since no commercial hVps37A-specific antibody was available, we raised a polyclonal antibody against a selected peptide of hVps37A in rabbit, followed by affinity purification. First, we stained the MDAH-2774 cell line, in which we knocked

hVps37A down by a shRNA approach. The cells were grown, fixed on chamber slides and stained as described in Experimental Procedures. Upon hVps37A-specific immunocytochemistry (ICC), the control cells exhibited potent hVps37A-specific staining, whereas the hVps37A deficient cell line remained almost negative. These results confirm the hVps37A knock-down in the MDAH-2774 cell line and qualify the antibody for ICC. Further, we immunostained three control ovarian tissues and five ovarian carcinomas with the hVps37A antibody. In accordance with our previous results on mRNA level, we found that the hVps37A protein amount was reduced in ovarian tumors compared to normal epithelia (Figure 3).

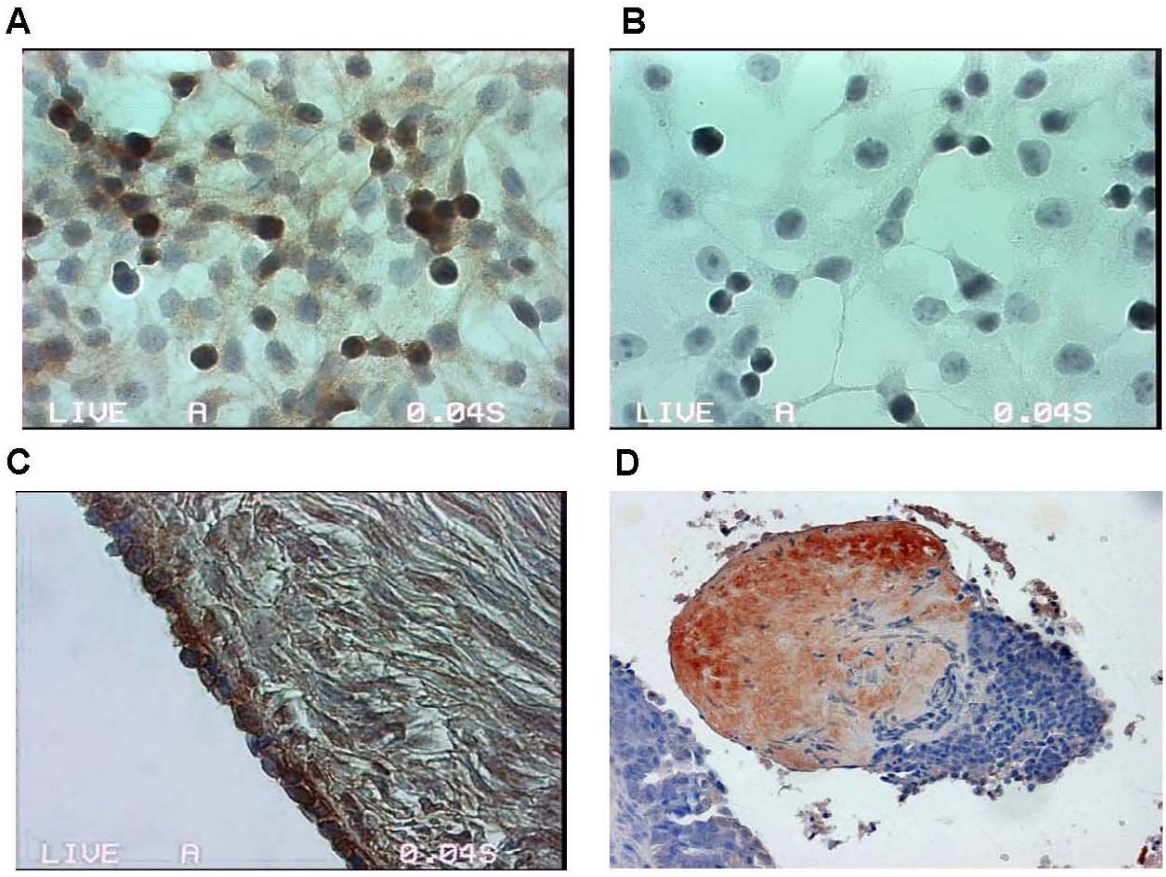

Fig. 3. hVps37A Antibody is Applicable for IHC

MDAH-2274 cells were transfected with (A) a nonsense construct (MDAH Co), or (B) a shRNA sequence directed against hVps37A (MDAH hVps37A-) as negative control. Cells were fixed on chamber slides and stained by our self-established polyclonal antibody specific against hVps37A. Staining specificity of the antibody was further confirmed in normal ovarian epithelial cells (C) and epithelial-derived ovarian tumors (D).

3.1.3.3 *Prognostic Value of EGFR and HER2 is Tightly Related to hVps37A Status*

Since our data of hVps37A suggests a crucial role of hVps37A for endosomal RTK-degradation, it might potentially influence the impact of EGFR/HER2 expression on the survival of OC patients. Thus, we undertook a tissue microarray (TMA) analysis to test this hypothesis. Median follow-up for patients with malignant tumors was 40.0 months (range 0.4–168.7 months), and 38 patients (30.4%) had already died. The TMAs were immunostained for EGFR and HER2 expression, as these receptors represent (1) well-established markers for ovarian carcinogenesis and progression and are (2) subject to hVps37A-dependent receptor degradation. HER2 receptor was stained with the DAKO HercepTest and interpreted following the standard procedures for breast cancer diagnosis. The same interpretation procedure was used for the EGFR. Not unexpectedly, high protein expression of the oncogenes EGFR ($p=0.015$), as well as HER2 ($p=0.003$), was associated with unfavorable overall survival rates, thus confirming our previous results and those of others (Pils et al., 2007a). Further, the TMAs were immunostained with an hVps37A-specific antibody. The tissue staining was graded according to staining intensity and the patient cohort was divided at the median into two subgroups according to hVps37A expression. Interestingly, in the tumors with low hVps37A expression, we observed a strong impact of EGFR ($p=0.008$) as well as HER2 ($p<0.001$) expression levels on overall survival. In case of regular hVps37A expression, the well known prognostic influence of EGFR and HER2 was almost completely lost (Figure 4). This observation suggested a significant influence of the dynamics of receptor decay mechanisms on the clinical relevance of pathologic receptor expression. Thus, EGFR or HER2 overexpression led to more aggressive cancers, almost exclusively under conditions of low hVps37A expression.

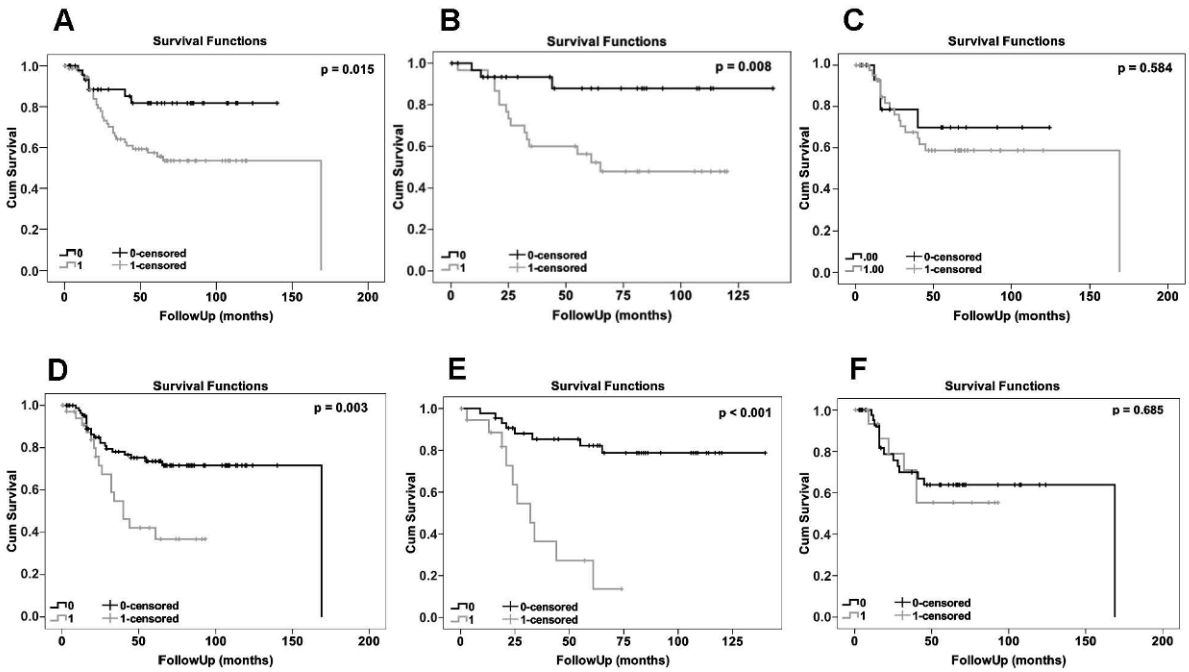

Fig. 4. hVps37A Expression Modulated Prognostic Potential of EGFR and HER2

Tissue microarrays composed of 125 primary ovarian tumor samples and 19 borderline tumors spotted in triplicates and corresponding normal tissue were stained for hVps37A, EGFR (A-C) and HER2 (D-F). (A) A complete set of samples stained against EGFR; (B) hVps37A-low expressing samples stained against EGFR; (C) hVps37A-high expressing samples stained against EGFR; (D) A complete set of samples stained against HER2; (E) hVps37A-low expressing samples stained against HER2; and (F) hVps37A-high expressing samples stained against HER2. Staining intensities were classified as described in Material and Methods. Statistical analysis was realized by Cox proportional hazards regression models for survival analysis, depicted in plots of the corresponding Kaplan-Meier estimations.

3.1.3.4 *Activated EGFR and HER2 Accumulate in hVps37A-Negative Cell Lines*

Since hVps37A was suggested to be involved in the endosomal sorting process of RTKs (Bache et al., 2004a), we supposed that its observed impact on patients' survival may be related to altered receptor levels secondary to hVps37A depletion. EGFR and HER2, two members of the ERBB RTK-family, are established oncogenes crucial for ovarian carcinogenesis. Therefore, we chose them as a cellular model system for further studying the biological processes governed by hVps37A in

ovarian tumors. SK-OV-3 and MDAH-2774 ovarian cancer cell lines bear equal amounts of EGFR while having high (SK-OV-3) or low (MDAH-2774) HER2 expression, respectively (Figurer 5A). Thus, they can be regarded as useful tools to investigate the role of hVps37A in the context of EGFR and HER2 receptor biology. To study the cellular effects of decreased hVps37A expression, hVps37A mRNA was stably knocked down in aforementioned cell lines via a shRNA approach. In order to calculate the silencing efficiencies, hVps37A mRNA and protein levels were determined in each stable clone and quantified relative to the hVps37A expression of the nonsense-controls (Figure 5B-E). For both cell lines, we obtained clones with 60-70% reduction of hVps37A mRNA/protein, leading to elevated levels of activated EGFR. Activated HER2 could only be detected in the SK-OV-3 cell line, where it was found to be increased at similar rates as pEGFR (Figure 5B, D). In contrast, total receptor levels remained unaffected.

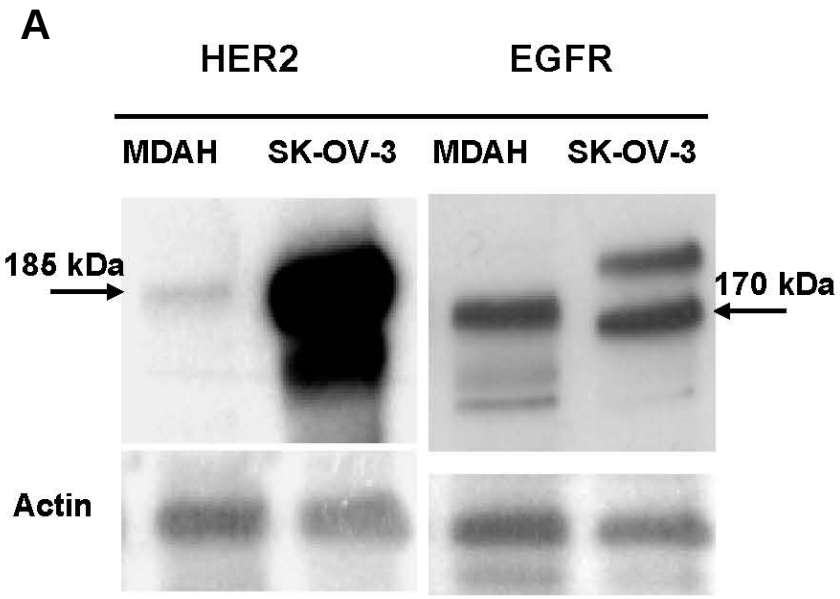

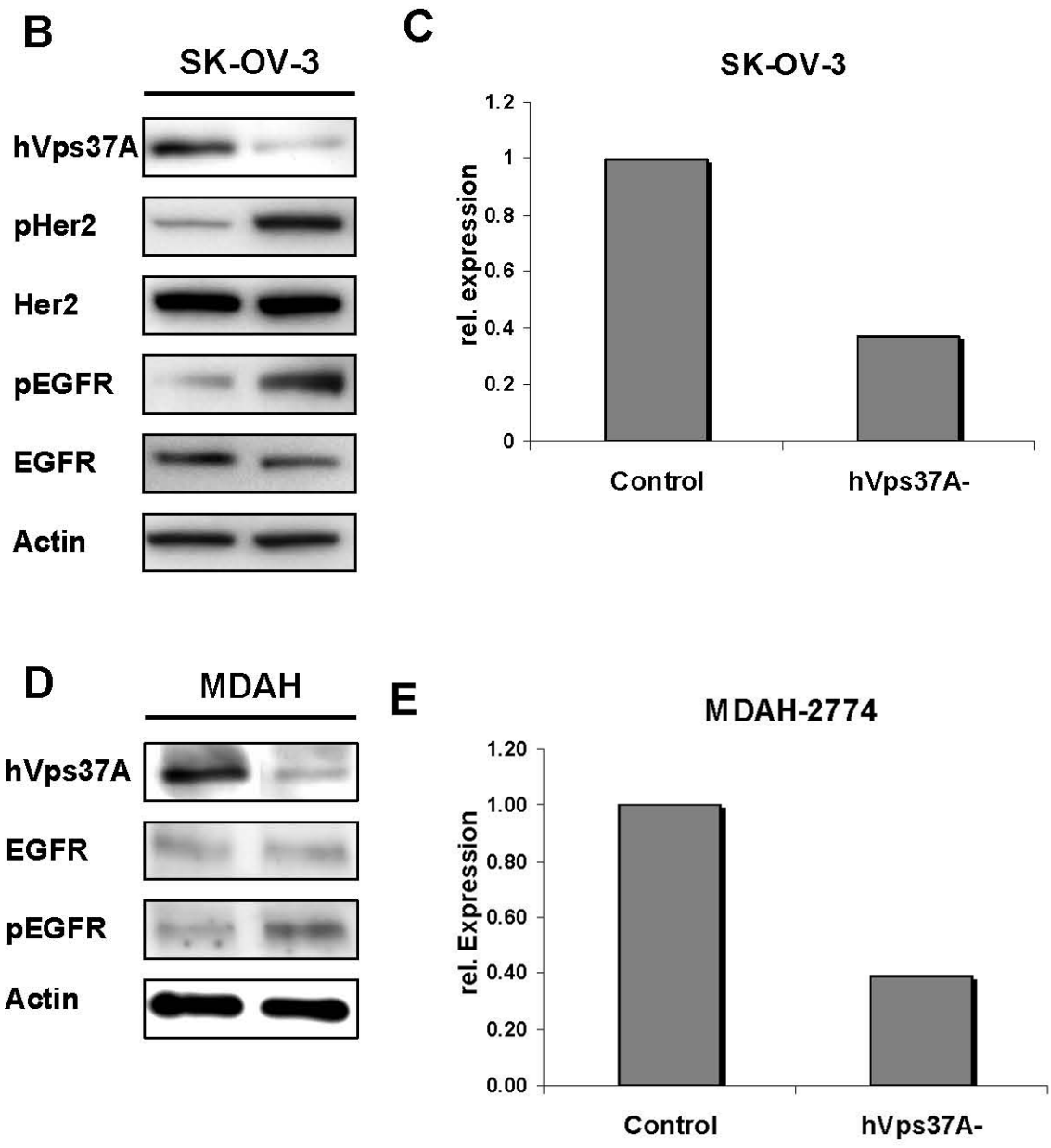

Fig. 5. hVps37A Knock-Down is Associated with pEGF/pHER2 Accumulation

(A) EGFR and HER2 expression was quantified by western blotting in the MDAH-2774 and SK-OV-3 ovarian cancer cell lines.

(B, D) These cell lines were treated with shRNA constructs specific against hVps37A. Knock-down efficiency and receptor levels (EGFR, pEGFR, HER2 and pHER2) were determined by western blotting.

(C, E) Successful knock-down of hVps37A was confirmed on mRNA level by qRT-PCR.

These results were reproduced in five different MDAH clones with reduced hVps37A abundance, as well as in the SK-OV-3 cell line induced or not for silencing of hVps37A. In each stable hVps37A-silenced clone, we observed elevated pEGFR amounts along with constant levels of total EGFR. Thus, the pEGFR/EGFR ratio inversely correlates with hVps37A levels as outlined in Figure 6A. Next, we juxtaposed hVps37A with activated EGFR receptor levels and found elevated pEGFR but constant EGFR levels in all hVps37A-deficient clones analyzed. This resulted in a significant increase of the pEGFR/EGFR ratio (Pearsons C=0.915, $p<0.011$). These observations suggested that activated EGFR accumulated within hVps37A–deficient cells, secondary to defects in cytoplasmic receptor degradation. We further aimed to define the intracellular compartment harboring aberrantly retained pEGFR protein. Therefore, ovary cells were grown on coverslips and probed with an anti-EGFR antibody (Figure 6B). In the control cell lines, the pEGFR was located mainly at the cell membrane (SK-OV-3) or hardly detectable. In contrast, in both hVps37A-deficient cell lines, pEGFR was detected at much higher levels in the cytoplasm (Figure 6B). To verify our observations in a set of standard cell lines (of ovarian and mammary origin), we quantified hVps37A, (p)EGFR and (p)HER2 by immunoblot analysis and plotted the ratios of activated to total receptor versus hVps37A (Figure 6C). No significant association between hVps37A and EGFR ($r = 0.111$; $p=0.695$) was found, yet we observed a significant ($p<0,01$) reciprocal correlation between hVps37A and pEGFR protein expression ($r = -0.683$; $p=0.007$) as well as between hVps37A and pEGF/EGFR protein ratio ($r = -0.707$; $p=0.005$). Moreover, a statistically weak correlation was found between hVps37A and pHER2 protein expression, which did not reach a significance level (data not shown). This may be explained by the fact that many of the cell lines were negative for pHER2 and could, therefore, not be included in the statistical analysis. These observations led to the conclusion that the

observed receptor accumulation was caused by defects in endosomal protein degradation. Therefore, we studied the dynamics of pEGFR degradation in wild-type and hVps37A-deficient MDAH and SK-OV-3 cells. Upon incubation in serum-free media, cells were stimulated with the 100 ng/ml EGF for 15 min to achieve maximal receptor activation, followed by re-incubation in serum-free media. At defined time points, cells were harvested, proteins prepared, and pEGFR expression was determined by Western blotting (Figures 6D, E); pEGFR degradation was significantly impaired in both HCRP-1 deficient cell lines compared with control cells. Interestingly, the EGFR degradation process of the SK-OV-3 cell line was even stronger inhibited compared to the MDAH cell line.

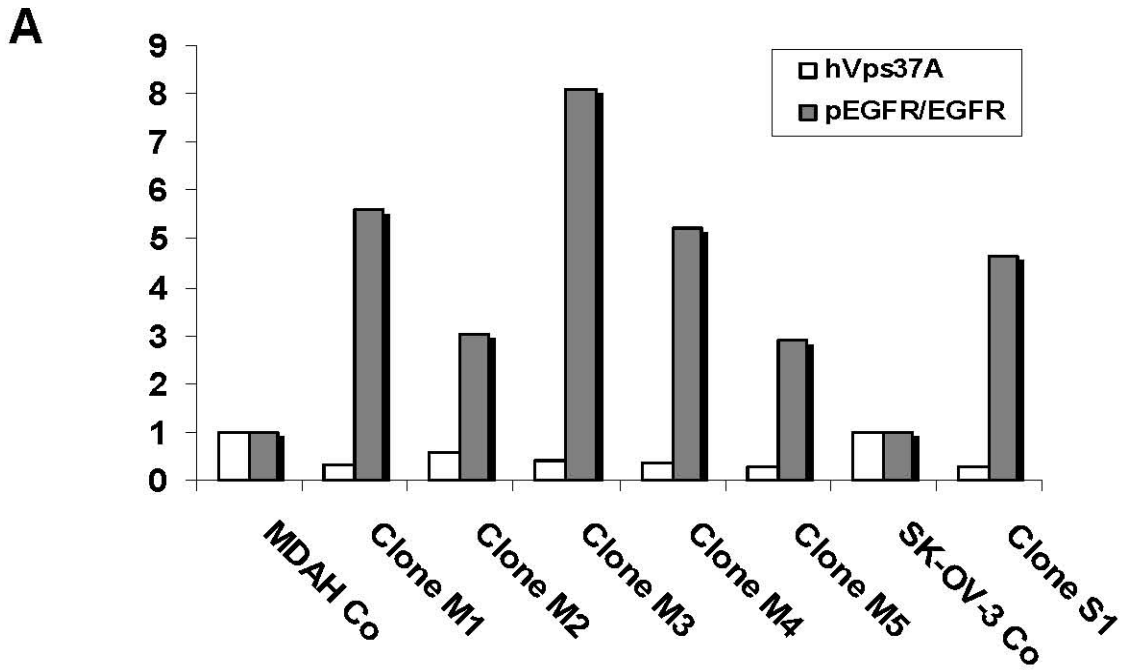

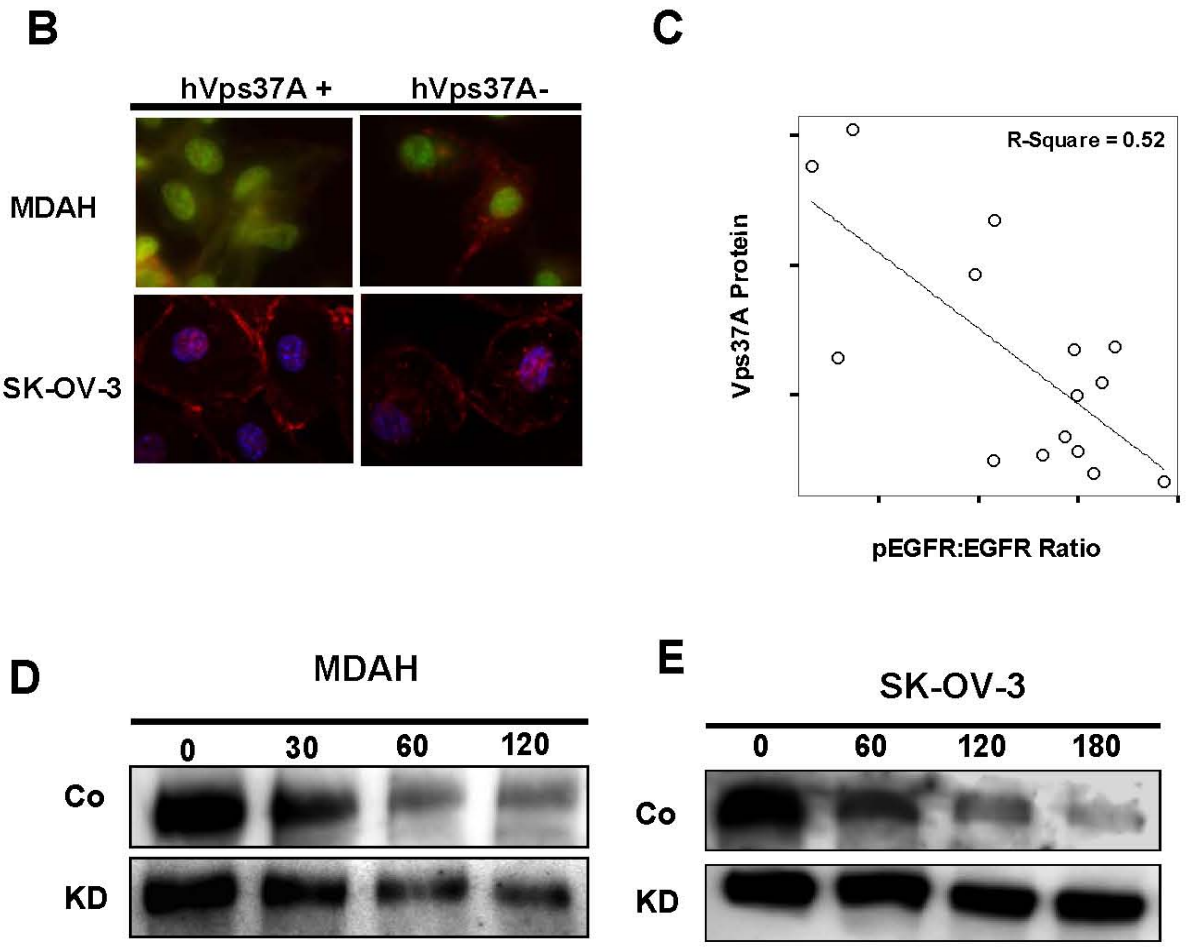

Fig. 6. Receptor Accumulation is Caused by a Defective Degradation Process in Case of Low hVps37A Levels

(A) hVps37A, EGFR and pEGFR amounts were determined in various stable clones in the MDAH and SK-OV-3 cell lines by Western blotting. White columns indicate hVps37A expression; blue columns indicate the ratio of pEGFR to EGFR.

(B) MDAH and SK-OV-3 cells were fixed on chamber slides, incubated with a pEGFR-specific primary antibody and a TRITC-labeled secondary antibody, followed by analysis on a fluorescent microscope.

(C) hVps37A, EGFR and pEGFR amounts were determined in 15 ovarian and breast cancer cell lines by Western blotting. hVps37A expression (y-axis) was plotted versus pEGF/EGFR ratio (x-axis) on a scatterplot and a trendline was calculated (R-Square=0.52). Statistical significance was proved by Pearson Correlation (-0.719) with a p-value of 0.003.

(D, E) MDAH and SK-OV-3 cells were starved in minimal medium for 24 hours, followed by stimulation with 100ng/ml EGF for 15 min and protein harvesting at defined points in time as indicated in minutes. Remaining activated receptor levels (pEGFR) after different time spans were determined by Western blotting, (Co Nonsense Control, KD hVps37A knock-down).

3.1.3.5 *hVps37A Interferes with EGFR Signal Transduction and is Crucial for Anti-EGFR Antibody Treatment*

Characterizing the compensatory changes in EGFR signaling upon hVps37A-knock-down might shed further light on the role of hVps37A in ovarian carcinogenesis. To achieve this, the relative activation of selected ERBB-signalling pathways upon anti EGFR treatment was analyzed in control versus HCRP-1 deficient cells. Not surprisingly, and consistent with our previous findings, hVps37A knock-down was associated with a potent phosphorylation of ERK1/2 (Figures 7A, B). This effect was reversed by treating the cells with an EGFR antibody (Cetuximab) or tyrosine kinas inhibitor (Lapatinib), reducing pERK1/2 to basal levels observed in control cells. Unlike ERK activation, Akt inducibility was not impaired by hVps37A-knock-down. Intriguingly, the inhibitory effect of Cetuximab on AKT-activation was lost upon hVps37A knock-down. This pinpointed towards the fact, that cytoplasmic EGFR degradation is crucial for Cetuximab-dependent inhibition of Akt phosphorylation. In contrast to this, our data suggested that Lapatinib acts independently of hVps37A.

Dysfunctional activation of ERK- and AKT- signal transduction is often reflected by changes in cellular proliferation. Therefore, we determined the proliferation rates of SK-OV-3 and MDAH cell lines (Figures 7C, D). Control cells and induced hVps37A-deficient SK-OV-3 cells exhibited comparable proliferation characteristics (25.5 versus 24.9 hours, respectively). In MDAH cells, the hVps37A knock-down caused a negligible increase in cellular proliferation. Taken together, these results argued for a limited impact of hVps37A onto cellular proliferation under *in vitro* conditions. In contrast, incubation with Cetuximab significantly decreased the proliferation potential of both cell lines, whereas the respective hVps37A-deficient cells remained unaffected. This underscored the notion that the presence of hVps37A is essential for proper degradation of the receptor-antibody complex. In

contrast, EGFR/HER2 inhibition by Lapatinib significantly reduced the proliferation of SK-OV-3 and MDAH cells irrespective of hVps37A expression levels (Figures 7C, D). These results were confirmed by a CellTiter-Blue assay as independent method (data not shown).

Overall, we suggest hVps37A as novel biomarker potentially guiding future therapies in RTK-driven cancers. In order the substantiate our clinical data, we further provided some functional insight into hVps37A dependent receptor decay mechanisms, leading to a better comprehension of the ESCRT mediated degradation process and its implications for tumor biology.

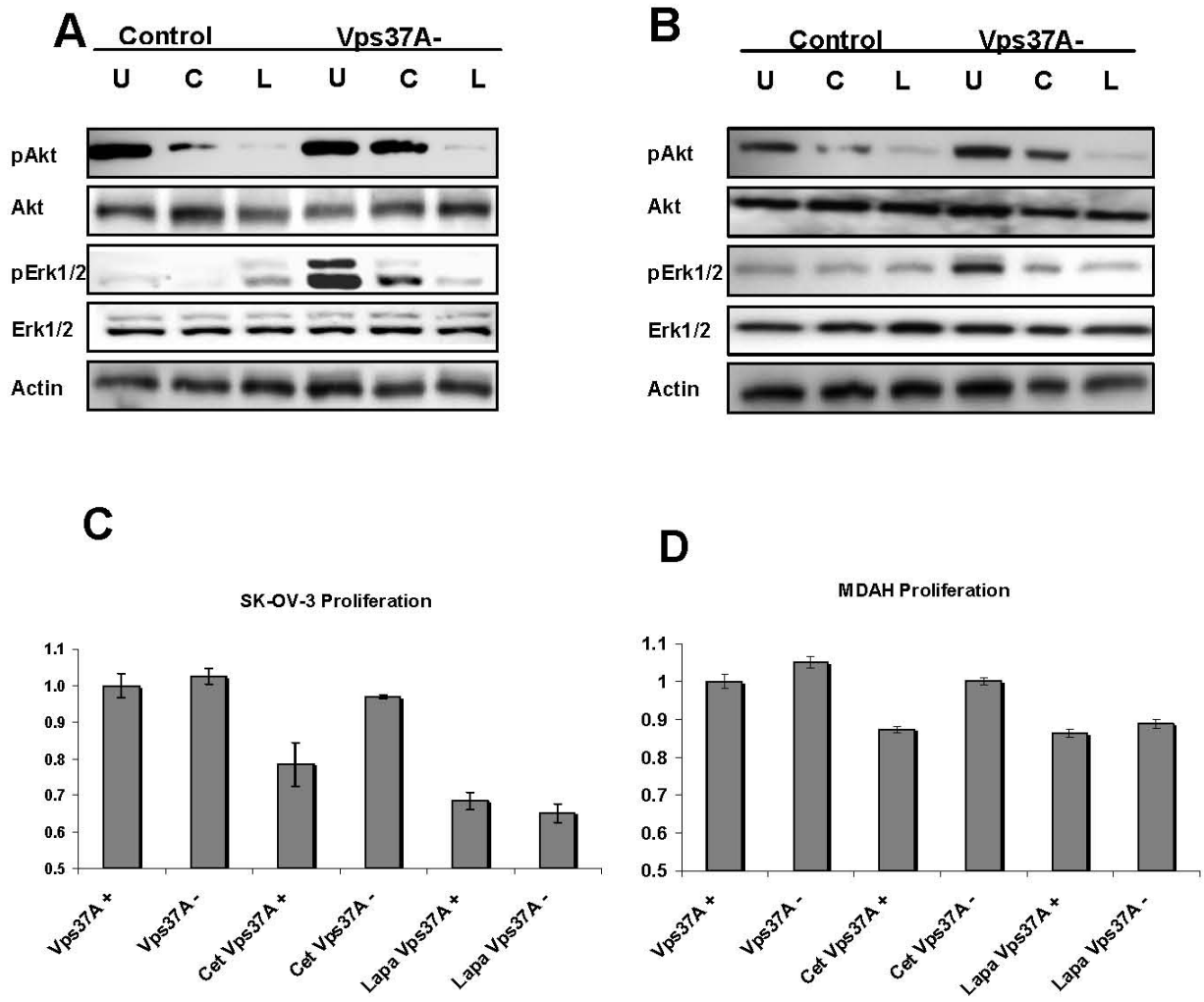

Fig. 7. hVps37A Depletion Confers Cetuximab Resistance Based on Sustained Akt Pathway Activation

hVps37A-silenced and control cell lines (SK-OV-3 (A), MDAH (B)) were incubated with either 20µg/ml Cetuximab (C), or 4µM Lapatinib (L) for 24 hours, or remained untreated (U). Protein levels of important key players of EGFR downstream pathways (pAKT, AKT, pERK1/2, ERK1/2) were determined by Western blotting.

(C, D) Proliferation was estimated by subsequent seeding of 2x105 cells in triplicates into 6 wells. Cell number was determined every 48 hours by a CASY cell counter. This procedure was performed for 8 days overall. Doubling time (dt) was calculated and depicted as 1/dt. The untreated control cell lines were set 1 and served as reference. The columns indicate the mean of three independent experiments; error bars represent +/-SEM.

3.1.4 Discussion

Positive regulation of ERBB RTK family isoforms is often associated with tumor development and progression. One mechanism leading to hyperactivation of ERBB receptors is defective receptor degradation. During this process, activated receptors are translocated to the limiting membrane of sorting endosomes where they are recognized by four major protein sorting complexes (ESCRT 0-III), internalized into endosomes, and degraded upon fusion with the lysosomal compartment(Bache et al., 2004b; Kirisits et al., 2007). In this study, we could demonstrate for the first time that hVps37A, a member of the ESCRT-I complex, is of pivotal importance for ERBB receptor degradation process, has significant impact on the survival of OC patients harboring ERBB overexpressing tumors, and, thus, constitutes a potential novel biomarker with prognostic and potentially therapeutic relevance.

Various tumor-specific genomic aberrations were mapped recently by systemic approaches. The gene of hVps37A is located on the short arm of chromosome 8, one of the most frequently altered regions in human cancer. Within 8p, chromosomal band 22 is a particular deletion hot spot suggesting the residence of potential tumor suppressor genes (TSG) in this area. On 8p22, the most accurately characterized TSG is DLC1, a Rho GTPase-activating protein identified by a deletion

mapping approach and characterized in hepatocellular carcinoma, but most probably playing a role in several cancer types (Durkin et al., 2007; Xue et al., 2008). Further cancer relevant genes are predicted in the area. Being located also in this very genomic region, hVps37A is an intriguing candidate TSG, in particular for cancers which are driven by oncogenic signals mediated by ERBB receptors.

While we could not detect mutations in the coding region of hVps37A (unpublished results), we observed hVps37A expression to be significantly reduced in primary OC, indicative of a negative selection pressure against hVps37A expression. Consistently, depleted hVps37A levels were associated with a more aggressive disease, leading to an unfavorable prognosis for patients with ERBB-overexpressing tumors. For low hVps37A levels, survival analysis revealed an increased probability to die also when corrected for FIGO, grade, and histology of the tumors. To understand this observation on a molecular level, we decided to further elucidate the biological implications of hVps37A expression levels in human OC samples. EGFR is an established driver of ovarian cancer development and a putative target of hVps37A (Bache et al., 2004a; Lafky et al., 2008). Consequently, we quantified activated and total EGFR-, as well as hVps37A protein levels, in 23 ovarian and breast cancer cell lines, and blotted hVps37A expression against the ratio of pEGFR to EGFR, resulting in a significant indirect correlation. Consistent with previous studies (Bache et al., 2004a), these data indicate that hVps37A is involved in protein turnover of EGFR. The same experiment was conducted for HER2, which yielded only borderline statistical significance, most probably due to an insufficient amount of pHER2 positive cases.

In order to further confirm the reciprocal relationship between hVps37A and pEGFR/pHER2 expression, we generated two stable hVps37A-defective ovarian cell line clones (MDAH2774 and SK-OV-3). In each cell line, knock-down of hVps37A

was associated with concomitantly elevated amounts of pEGFR protein expression (and pHER2 for the SK-OV-3 cell line). Via immunofluorescent analysis, we could confirm that aberrantly degraded pEGFR was retained in the cytoplasm under conditions of hVps37A depletion. The kinetics behind this phenomenon was studied by analyzing the influence of hVps37A on the time course of EGFR degradation. Not surprisingly, the degradation process of the activated receptor was strictly dependent on hVps37A expression, as its knock-down resulted in sustained receptor activation upon EGF-stimulation. Interestingly, the degradation inhibitions were found to be potentiated in the SK-OV-3 compared to the MDAH cell line. This observation may be explained by high amounts of HER2 (in SK-OV-3 cells), which is reported to remain more stable at the cell membrane than other receptors of the HER family, and can confer this property to its dimerization partners (Sorkin and Goh, 2008).

Due to the cytosolic orientation of the phosphorylated tail of RTKs, receptors targeted for endosomal degradation are still signaling competently, an effect which may be potentiated by the observed cytoplasmic retention of pEGFR (Pennock and Wang, 2003). In fact, we observed a potent phosphorylation of ERK1/2 upon knock-down of hVps37A. Interestingly, we received no concomitant increase in cellular proliferation. However, there is accumulating evidence that MAPK activation can lead to different responses dependent on the cellular background or intensity and duration of the signal (Lee et al., 2000; Miaczynska et al., 2004; Tang et al., 2002; Zhang and Liu, 2002).

These observations were highly reminiscent of the phenotype of Tsg101, another component of the (ESCRT-I) protein complex. It has been reported that the endosomal degradation of EGFR is impaired in Tsg101-deficient cells (Raiborg et al., 2008). In addition, non-functional Tsg101 causes EGFR accumulation within the cytoplasm (Lu et al., 2003), arguing for non-functional ESCRT-I complexes under

conditions of HCRP-1 knock-down. In line with this, we assume that hVps37A might constitute a novel tumor suppressor in multiple tumor entities, as has been reported for the whole ESCRT-I complex (Tanaka et al., 2008).

Collectively, our data raised the following question: If hVps37A levels significantly regulate the cellular localization of known pro-oncogenes like activated EGFR and HER2, does it possess the potential to modulate their established impact on disease progression? This question was addressed by immunostaining TMAs comprising 125 primary ovarian tumors against hVps37A, EGFR, and HER2. Intriguingly, we found that hVps37A protein levels significantly altered the prognostic impact of EGFR and HER2 expression, which is well described in the literature (Crijns et al., 2006; Pils et al., 2007a). Under conditions of low hVps37A expression, both EGFR and HER2 expression levels highly influenced patients' prognosis, an effect which was completely abrogated under conditions of high hVps37A expression. This observation may be explained by the notion of a disproportionately high number of activated RTK, which are unable to be counterbalanced by reduced hVps37A-mediated degradation.

Although most studies reported EGFR or HER2 overexpression to be associated with an unfavorable prognosis of ovarian cancer patients, the results were often inconsistent (Crijns et al., 2003). Multiple marker testing would thus be beneficial to obtain a more reliable and accurate picture of the tumor. In this work, we established hVps37A as a potential tumor suppressor, significantly modifying the pro-cancerogenic effects of EGFR/HER2 overexpression. If these results can be confirmed in more comprehensive clinical studies, hVps37A-testing should be included – besides EGFR- and HER2 testing – in the characterization of ovarian cancer.

Apparently, individual tumor cells enhance their selective advantage in the course of disease progression via down-regulating hVps37A. This effect would lead to an increase in disease aggressiveness and an unfavorable prognosis. Such tumors should be prone to a disruption of this pathway by a therapy against EGFR, which is a promising molecular target for cancer therapy using monoclonal antibodies or small molecule tyrosine kinase inhibitors (TKIs). In order to assess the influence of hVps37A on those kinds of therapy, SK-OV-3 and MDAH-2774 cell lines were examined for their susceptibility to an EGFR antibody (Cetuximab) and a TKI (Lapatinib), respectively. While there are various mechanisms leading to resistance against anti-EGFR- therapies, including autocrine EGFR activation, mutation of downstream signaling effectors, and cross-activation of alternative RTKs, a recently published study added an additional twist: Cancer cell lines made resistant to Cetuximab by long term exposure developed increased EGFR levels based on defects in receptor degradation (Wheeler et al., 2008). The genetic knock-down of hVps37A and the resulting resistance to Cetuximab in our model confirm and offer a molecular mechanism of this important finding. Cetuximab is a widely used therapeutic antibody directed against EGFR. It down-regulates EGFR signal transduction by various mechanisms, such as competing for extracellular EGFR ligands, forced receptor internalization, and degradation or induction of an immune response to the Fc-region in vivo (Peipp et al., 2008). Further, in addition to the antagonistic effects, Cetuximab also possesses the potential to trigger EGFR activation and dimerization prior to its down-regulation (Mandic et al., 2006; Yoshida et al., 2008). As described above, our results suggest that limited amounts of hVps37A rather inhibit EGFR degradation, leading to cytoplasmic receptor accumulation and hyperactivation of the MAPK pathway. Following incubation with Cetuximab, MAPK pathway activation (ERK1/2) was reduced, yet we observed a

potent compensatory activation of the AKT-pathway in hVps37A-deficient cell lines, arguing for functional signaling capacity of the EGFR-Cetuximab complex within the cytoplasm. The cellular phenotype of this finding is resistance to Cetuximab-related inhibition of proliferation. Our findings are in line with a recent study of Wheeler et al., who generated a Cetuximab-resistant NSCLC cell line. The latter was found to harbor defects in EGFR internalization and degradation, suggesting that these mechanisms are crucial for Cetuximab to be effective (Wheeler et al., 2008). Yet, the notion of constitutive PI3K activation by endosomally located EGFR contradicts a study which reported that PI3K activation is restricted exclusively to the plasma membrane (Haugh and Meyer, 2002).

In contrast to Cetuximab, Lapatinib directly blocks EGFR activation by targeting the ATP-binding domain. This leads to defective EGFR-dependent signal transduction independently of ESCRT mediated receptor down-regulation (Xia et al., 2002). This is in line with our observations, that PI3K/AKT and MAPK pathways, as well as cell proliferation, were inhibited by Lapatinib irrespective of hVps37A expression levels.

Overall, we identified hVps37A as a keyplayer for tumor development being essential for the degradation of RTK oncogenes. We elucidated important aspects of the molecular mechanism and showed the clinical relevance of hVps37A to establish it as a novel TSG and prognostic biomarker in ovarian cancer and beyond.

In order to further examine the clinical significance of our findings, it would be beneficial to assess the impact of hVps37A expression onto the survival of patients sensitive to Cetuximab therapy (or other monoclonal antibodies against EGFR) or not. If an association between hVps37A expression and the efficacy of anti-EGFR therapy would be confirmed in a clinical setting, hVps37A could be considered as a

novel predictive marker to better select patients for the application of monoclonal antibodies in targeted therapies against EGFR- overexpressing tumors.

3.1.5 Material and Methods

3.1.5.1 Patient Material

For mRNA expression analysis, ovarian tumor samples from primary tumors with complete clinical documentation were obtained from patients who underwent optimal debulking surgery at the Charité Hospital in Berlin, Germany (Table 1). Epithelial-enriched normal ovarian and benign cyst samples came from patients diagnosed without malignant disease at the Medical University of Vienna. In total, 21 normal ovarian samples, 88 primary tumors, and 38 recurrent tumors, mostly intraperitoneal metastases after primary surgery followed by platin based chemotherapy, were assessed. Informed consent for the scientific use of biological material was obtained from all patients in accordance with the requirements of the ethics committee of the individual institution.The patient material for the tissue microarray (TMA) is described in detail in Table 1. Microarrays were composed by taking core needle “biopsies” from specific locations in the pre-existing paraffin-embedded tissue blocks and re-embedding them in an array master block, using techniques and an apparatus developed by Beecher Instruments Inc., Micro-Array Technology (Sun Prairie, WI, USA). To achieve good representation of the tumor, three biopsies of tumor material were selected from each patient. None of the patients with borderline tumors died during the follow-up time and were excluded from the survival analysis.

3.1.5.2 *Data Analysis and Statistics*

In order to compare hVps37A expression between primary tumors, recurrent tumors, and normal controls, a Mann-Whitney *U* test was performed. The potential

influence of hVps37A expression on overall survival is presented in plots of the corresponding Kaplan-Meier estimates and quantified using Cox regression, first with a univariate model and then adjusted for grading, staging according to FIGO, and morphologic subtype of the tumor samples. Ninety-five percent confidence intervals were calculated. hVps37A was dichotomized at the median. Histology was dichotomized into serous and nonserous tumors. Tumor stage and grade were used as continuous variables. P-values ≤0.05 were considered to be statistically significant.

In the tissue microarray, staining intensities were analyzed by two independent persons and classified in 0 (missing expression), 1 (low expression), 2 (medium expression), and 3 (high expression). Equal to the mRNA expression analysis experiment, hVps37A was dichotimized into two groups at the median. For EGFR and HER2, results of triplicates and both interpretations were averaged and re-scaled (0-3). HER2, according to standard procedures for breast cancer, was divided into two groups with low (0, 1) or high (2, 3) expression. Since 40% of the tumor samples stained negatively or very weakly positively for EGR, we divided into two groups of positive and negative EGFR expression. Kaplan-Meier plots and survival analysis were calculated as described above. All statistical analyses were performed on SPSS 15 (Chicago, IL, USA).

3.1.5.3 *RNA Isolation, cDNA Synthesis and Quantitative RT-PCR*

Total RNA from cell lines was prepared with the RNeasy Mini Kit (Qiagen, Hilden, Germany) and quality and quantity assessed on RNA Nano Chips (Lab-on-a-Chip, Agilent Technologies, Palo Alto, CA, USA). All steps were accomplished according to the manufacturers' protocols.

cDNA was synthesized from 1µg total RNA using the DuraScript RT-PCR Kit (Sigma-Aldrich, Saint Louis, MO, USA) in a volume of 20µl and subsequently diluted

to a total volume of 100µl. The following Assay-on-Demand™ probes were selected for TaqMan real-time PCR: *FLJ32642*, Hs00329751_m1 and *beta 2-microglobulin (B2M)*, Hs99999907_m1, HPRT1 and GAPDH (Applied Biosystems, Foster City, CA, USA). The real-time PCR reaction mix was composed of 10µl TaqMan® Universal PCR Master Mix (Applied Biosystems) supplemented with 2µl of the obtained cDNA, 1µl of the probe and 8µl of ddH_2O to a total volume of 20µl. The reaction was realized on the 5700 Sequence Detection System (Applied Biosystems, Foster City, CA, USA) with cycle conditions as follows: Initially 50 °C for 2 minutes and 95 °C for 10 minutes, followed by 40 cycles of 95 °C for 15 seconds and 60 °C for 1 minute. Relative expression was calculated from the threshold cycles (Ct) obtained with the GeneAmp 5700 SDS Software v1.3 (Applied Biosystems) as follows: 2^–[(Ct_{gene} mean of duplicated probes – Ct_{gene} mean of duplicated calibrator) – (Ct_{B2M} mean of duplicated probes – Ct_{B2M} mean of duplicated calibrator)].

3.1.5.4 *Silencing of hVps37A in Different Cell Lines*

The SK-OV-3 cell line was cultured equally to the MDAH-2774 cell line except for the use of McCoy´s medium. For applying the Tet-Off inducible system, founder cell lines were generated by transfecting SK-OV-3 cells with the pTet-Off vector (neo^r) encoding a tetracyclin repressible transactivator (tTA). Resistant colonies were selected with 200 µg/ml G418 and characterized by transient transfection with the luciferase reporter plasmid (pTRE-Luc), whose promoter is induced by the transactivator. Luciferase activity in the presence and absence of tetracycline was measured to identify cells with maximal promoter inducibility. Highest induction was 92-fold. These two founder cell lines were used to establish cells inducible for hVps37A-specific shRNA constructs (Open Biosystems; #V2HS_21202, #V2HS_21203), which were cloned into the SIN-TREmiR30-PIG vector (pur^r) downstream of the tetracycline inducible promoter. Thus, presence of tetracycline in

the culture medium would suppress shRNA expression, while its withdrawal would induce the knock-down of hVps37A. Puromycin-resistant colonies were isolated in the presence of tetracycline, and screened for silencing efficiency of hVps37A by qRT-PCR and Western blotting.

The human ovarian carcinoma cell line MDAH-2774 was cultured in RPMI medium with 10% FCS (fetal calf serum), 50 units/ml penicillin G, and 50 µg/ml streptomycin sulfate at 37 °C in a humidified atmosphere of 95% air with 5% CO_2. Three different shRNA constructs complementary exclusively to the *hVps37A* mRNA, in addition to 1 nonsense construct serving as a control, were cloned into the vector pSilencer 4.1-CMV neo. Transfection was performed with Lipofectamine 2000 according to the manufacturers' protocol (Invitrogen, Carlsbad, CA, USA). Stable clones were selected with 700 µg/ml G418, picked, and sub-cultured with 350 µg/ml G418. Silencing efficiency was quantified by qRT-PCR and western blot.

3.1.5.5 *Antibody Production*

Since no commercial hVps37A-specific antibodies were available, we established a polyclonal peptide antibody against hVps37A. The following peptide sequence was selected: MSPYASQGFPFLPPY. Rabbit antiserum raised against this peptide sequence was prepared by Eurogentec (Seraing, Belgium). The serum was affinity purified on beads containing the selected peptide and tested for its applicability in Western blotting and immunohistochemistry.

3.1.5.6 *Protein Preparation and Western Blotting*

The following antibodies were used in the dilution indicated: hVps37A 1:200 (established as described above); primary antibodies (EGFR 1:300, pEGFR 1:100, HER2 1:200, pHER2 1:200, ERK1 1:5000, ERKk2 1:5000 and beta-actin 1:300) and HRP-conjugated secondary antibodies (anti-goat 1:10000 and anti-rabbit 1:10000) were obtained from Santa Cruz Biotechnology, Inc. (Santa Cruz, CA, USA) AKT and

pAKT were purchased from Cell Signaling Technology (Beverly, MA, USA). Upon treatment, cells were lysed and protein was prepared with RIPA+ buffer; protein concentration was determined by a standard Bradford absorbance assay (Sigmal Aldrich, Saint Louis, MO, USA). Equal amounts of proteins (30µg) were separated by SDS-PAGE, blotted on PVDF membranes (GE Healthcare, Buckinghamshire, UK), incubated with the appropriate primary antibody, and visualized via HRP-conjugated secondary antibodies and treatment with the ECL chemiluminescent detection system (GE Healthcare, Buckinghamshire, UK).

3.1.5.7 *Immunohistochemistry*

After deparaffinization and rehydration, the samples were treated with 0.3% H_2O_2/PBS (pH 7.4) for 10 minutes to quench endogenous peroxidase activity and blocked with serum of the secondary antibody diluted 1:50 in PBS. Primary antibodies against EGFR produced in rabbit and hVps37A were diluted 1:100 in serum/PBS and applied on the samples for 1 hour. HER2 was stained using the DAKO HercepTest. The secondary antibody against rabbit was applied for 30 minutes. After visualization with DAB+ (Dako, CA, USA) and counterstaining with hematoxyline/eosin, the slides were mounted in Eukitt (O. Kindler GmbH, Freiburg, Germany) and analyzed on an Olympus BX50 upright light microscope (Olympus Europe, Hamburg, Germany) equipped with the Soft Imaging system CC12.

For the tissue microarray, each sample was treated in an identical manner and the entire cohort was analyzed in one batch on three slides. Reagent conditions, incubation times and temperatures, and antigen retrieval (if necessary) were held identical for each case as previously described.

3.1.5.8 *Fluorescence Microscopy*

Cells were seeded on chamber slides, grown for 48 hours, fixed with 4% paraformaldehyde for 15 minutes, and permeabilized with 0.1% Triton X-100. The

subsequent staining procedure was performed as described for immuno-histochemistry. The cells were incubated with the primary antibody (goat) directed against pEGFR (1:100) for 1 hour. TRITC-conjugated secondary antibody (1:100) was applied on the cells for 45 minutes and counterstain of the nuclei was realized by DAPI (Roche, Manchester, England) or Quinacrine. Afterwards the cells were analyzed on a fluorescence microscope (Nikon Eclipse 800) equipped with a Nikon DS-R1 camera by using the NIS-Elements software.

3.1.5.9 *Proliferation Assays*

2x105 SK-OV-3 (with and without doxycyclin) and MDAH (hVps37A silenced, nonsense control and wildtype) cells were seeded in 6-well plates in media complemented with 10% FCS and treated with 20 µg/ml Cetuximab (Merck, Whitehouse Station, NJ, USA), 4 µM Lapatinib (GlaxoSmithKline plc. London, UK), or were mock-treated. To maintain the logarithmic phase, cells were split at intervals of 48 hours, along with the determination of the cell number by a CASY cell counter (Innovatis AG, Bielefeld, Germany). This procedure was performed in triplicate over a time-span of 6 days and confirmed by a replication of the whole experiment. From the obtained data, doubling times (dt) were calculated and depicted as dt-1.

3.2 Project 2: Methylation of N33 (TUSC3) Independently Predicts Ovarian Cancer Patient Outcomes, Caused by Altered N-Glycosylation Patterns

Dietmar Pils[1], Michaela Petz[1], Angela Alfanz[1], Alfred Gugerell[1], Michael Wittinger[1], Wolfgang Gregor[2], Andreas Gleiss[3], Andreas Kirisits[1], Peter Horak[1], Markus Omann[1], Dan Tong[4], Robert Zeillinger[4], Alexander Mustea[5], Dominique Koensgen[5], and Michael Krainer[1]

From the Department of [1]Internal Medicine I, Division of Oncology, [3]Core Unit for Medical Statistics and Informatics, Section of Clinical Biometrics, [4]Department of Obstetrics and Gynecology, Division of Gynecology, Medical University of Vienna, Austria, [2]Research Group of Molecular Pharmacology and Toxicology, University of Veterinary Medicine Vienna, Austria, and [5]Department of Gynecology and Obstetrics, Charité Campus Virchow-Klinikum, Berlin, Germany.

Supported in part by the Austrian Science Fund (FWF) grant no. P17891 and by the Initiative Krebsforschung.

Address reprint requests to Michael Krainer, MD, Professor of Medicine Department of Internal Medicine I, Medical University of Vienna, Waehringer Guertel 18-20, A- 1090 Vienna, Austria, e-mail: michael.krainer@meduniwien.ac.at

3.2.1 Abstract

BACKGROUND Treatment decisions in ovarian cancer therapy are based on tumor stage, tumor grade, and residual tumor size after debulking surgery, but only few prognostic markers are well established. Here, we present the promoter methylation status of *TUSC3,* a gene on chromosome 8p22, as a new molecular marker and a putative therapeutic target for ovarian cancer.

METHODS *TUSC3* mRNA expression was determined by quantitative RT-PCR in 102 ovarian cancer specimens, followed by promoter-methylation studies via methylation specific PCR. Reconstitution of *TUSC3 in vitro* was used for subcellular localization and functional analysis.

RESULTS *TUSC3* expression was significantly down-regulated by epigenetic regulation in ovarian cancer samples compared to controls (P<0.001). At the time of the initial diagnosis, 29.4% (30/102) of patients had a methylation of the *TUSC3* promoter vs. none of the controls (P=0.003). Methylation of the *TUSC3* promoter had a strong influence on progression-free (HR 2.17, P=0.024) and overall survival (HR 4.11, P=0.008) which was independent from other prognostic factors. *In vitro* reconstitution of *TUSC3* into ovarian cancer cells demonstrated its localization to the endoplasmatic reticulum and triggered cell appearance changes along with decreased proliferation and increased migration. These changes go along with altered N-glycosylation patterns of integrin ß1 in *TUSC3* reconstituted cells, resulting in decreased adhesion to collagen I.

CONCLUSIONS Epigenetic down-regulation of *TUSC3* is a frequent event in ovarian cancer. We show for the first time that TUSC3 is involved in glycosylation of proteins and acts as a tumor suppressor gene with strong and independent impact on ovarian cancer patient prognosis.

3.2.2 Introduction

Epithelial ovarian cancer is the most lethal gynecologic malignancy and with about six percent the fourth most frequent cause of cancer related death in women in industrialized countries. Estimates indicate that one in 70 women will develop ovarian cancer in her lifetime, with a median survival rate of 4.5 years. A recent cancer statistic reported an estimated 22,200 new cases and 16,210 deaths per year in the United States (Jemal et al., 2005).

Early diagnosis represents a major challenge in the treatment of this disease and more than three quarters of cases are diagnosed in late stages (FIGO III and IV). These patients need intensive multimodal therapy consisting of optimal debulking surgery and adjuvant chemotherapy.

Currently used prognostic factors include staging, grading, and the size of residual tumor after initial cytoreductive surgery (Holschneider and Berek, 2000; van der Burg, 2001). Apart from Cancer Antigen 125 (CA-125) (Makar et al., 1992) there are no other specific diagnostic and prognostic molecular markers available in clinical practice. Promoter methylation patterns of tumor suppressor genes (TSGs) hold a particular promise as new molecular markers. They can give insight into the biology of a tumor and in contrast to a gene or protein expression analysis, they can be easily detected by PCR-based methods in tumor material as well as in body fluids (Das and Singal, 2004; Jones and Baylin, 2002; Laird, 2003).

TUSC3 (tumor suppressor candidate 3), originally named *N33*, was identified as a potential TSG in prostate cancer located on chromosome band 8p22 (Bova et al., 1996; MacGrogan et al., 1996). Known homozygous deletions (HDs) of this region in pancreatic (Bashyam et al., 2005; Levy et al., 1999) and prostate cancer cell lines (Arbieva et al., 2000; Bova et al., 1993) contain no other cancer related genes except for *TUSC3*, but mutations of the *TUSC3* coding sequence are rarely

found (Pils et al., unpublished data). Systematicly screening the region on 8p22, we recently showed *TUSC3* to be significantly down-regulated in ovarian cancer tissues and of potential prognostic value (Pils et al., 2005a).

Molecular function of the TUSC3 gene product remains largely unknown. TUSC3 shares a high sequence homology with OST3p, a subunit of the oligosaccharyltransferase complex involved in N-glycosylation of proteins in *Saccharomyces cerevisiae* (Kelleher and Gilmore, 2006; Kelleher et al., 2003a), suggesting TUSC3 might have a similar function in human cells.

Glycosylation is a ubiquitous posttranslational modification of eukaryotic proteins, preferentially of those with contact to the extracellular matrix. In general, it protects proteins from degradation but can also modulate their function (Ohtsubo and Marth, 2006) as well as their immunogenicity (Galonic and Gin, 2007). Changes in glycosylation patterns in tumor cells are well described, but functional knowledge about their origin is limited (Dennis et al., 1999; Kobata and Amano, 2005).

Alterations of relative amounts of sialic acids moieties, which can be generally found at the terminus of oligosaccharide chains on several glycoproteins, were shown to be associated with some cancer cells propreties, such as invasiveness and metastatic potential (Collard et al., 1986; Dennis et al., 1987; Yogeeswaran and Salk, 1981). Increased enzymatic activities of proteins directly involved in sialylation (Kakugawa et al., 2002), or the availability of potential sialylation sites determined by the branching of N-glycans are considered to be crucial for these effects. Well known targets for differential sialylation in tumor cells are, among others, growth factor receptors (Lau et al., 2007) and structural proteins with impact on cell-cell interaction and extra cellular matrix binding, such as integrin ß1 (Seales et al., 2003).

In this report we for the first time identify an epigenetic mechanism inhibiting *TUSC3* expression, which also has a high independent prognostic value in ovarian

cancer. Additionally, we show *in vitro* that decreased *TUSC3* expression alters the N-glycosylation pattern of proteins in ovarian cancer cell lines. Taken together, we present the first evidence that a protein involved in N-glycosylation of proteins acts as a tumor suppressor gene with a major impact on patient survival in ovarian cancer.

3.2.3 Material and Methods

3.2.3.1 *Patient Material and Cancer Cell Lines*

Ovarian tumor samples were obtained from patients who underwent optimal debulking surgery at the Charité Hospital Berlin, Germany. Epithelial-enriched normal ovarian and benign cyst samples came from patients diagnosed without malignant disease at the Medical University of Vienna. In total, 20 benign ovarian samples and 102 primary tumor samples were assessed (Table 3). 84% of patients were treated with a platin-based first line chemotherapy regime. Informed consent for the scientific use of biological material was obtained from all patients in accordance to the requirements of the ethical committee of the individual institutions. The panel of 38 ovarian cancer cell lines was described earlier (Pils et al., 2005a).

Table 3. Clinicopathologic Characteristics of Patients

A) Benign ovarian samples (corresponding mRNA samples)	20 (20)
Age at operation [years]	
Mean ± SD	49.9 ± 11.8
7 Normal ovaries, mean age [yrs]:	51.6
13 Benign cysts, mean age [yrs]:	49.0
B) Tumor samples (corresponding mRNA samples)	102 (99)
Age at diagnosis [years]	
Mean ± SD	58.3 ± 11.0
Histology (1 (1.0%$^{\infty}$) missing)	
Serous	79 (77.4%$^{\infty}$)
Endometrioid	10 (9.8%)
Mucinous	5 (4.9%)
Clear cell	2 (2.0%)
Other	5 (4.9%)
FIGO (2 (2.0%) missing)	
I	17 (16.7%)
II	10 (9.8%)
III	51 (50.0%)
IV	22 (21.6%)
Grading (1 (1.0%) missing)	
1	2 (2.0%)

2	48 (46.1%)
3	51 (50.0%)
Residual disease after initial surgery (3 (2.9%) missing)	
≤ 1cm	86 (84.3%)
> 1cm	13 (12.7%)
First line chemotherapy (3 (2.9%) missing)	
Carboplatin and Taxol	63 (61.8%)
Carboplatin, Taxol and Gemcitabine	17 (16.7%)
Carboplatin or Taxol monotherapy	3 (2.9%)
Carboplatin and other	8 (7.8%)
Other	3 (2.9%)
No	5 (4.9%)
Response to first line chemotherapy (16 (15.7%) missing)	
NED‡	6 (5.9%)
NC†	3 (2.9%)
PD†	12 (11.8%)
PR†	5 (4.9%)
CR‡	43 (42.2%)
Duration of response	
0 – 6 months†,‡	6 (5.9%)
6 – 12 months‡	5 (4.9%)
> 12 months‡	6 (5.9%)
Remissions/progressive disease (3 (2.9%) missing)	
w/o remission	49 (48.0%)
w/ remission	33 (32.4%)
Progressive disease	17 (16.7%)

°Percent based on 102 tumor samples.
†Non-responders to first line chemotherapy.
‡Responders to first line chemotherapy.

3.2.3.2 *DNA and RNA Isolation*

Genomic DNA from about 15 mg of frozen tissue or cell lines was prepared with the DNeasy Tissue Kit (Qiagen, Hilden, Germany) and quantified with the PicoGreen dsDNA Quantitation Kit (Molecular Probes, Inc., Eugene, OR, USA). Total RNA from frozen tissues was extracted with the Agilent Total RNA Isolation Mini Kit (Agilent Technologies, Palo Alto, CA, USA). Total RNA from cancer cell lines was prepared with the RNeasy Mini Kit (Qiagen, Hilden, Germany) and quality/quantity assessed on RNA Nano Chips (Lab-on-a-Chip, Agilent Technologies, Palo Alto, CA, USA).

3.2.3.3 *Methylation-specific PCR (MSP) and DNA-Demethylation*

Bisulfite treatment of 1 µg of genomic DNA was done as described previously (Horak et al., 2005). PCR was performed with 25 ng bisulfite treated DNA, primers published by Xu et al. (Xu et al., 2004) and primers of own design (sequence will be

provided upon request), and AmpliTaq Gold (Applied Biosystems, Foster City, CA, USA). Bisulfite sequencing (primer sequences upon request) was performed directly with the PCR products purified with the QIAquick PCR Purification Kit (Qiagen, Hilden, Germany). DNA demethylation of a cancer cell line was performed by a 72 h treatment with 1 or 2.5 µM 5-aza-2'-deoxycytidine (Sigma-Aldrich, St. Louis, MO, USA) in cell culture medium and relative *TUSC3* expression was evaluated by quantitative real-time RT-PCR.

3.2.3.4 *cDNA Synthesis and Quantitative RT-PCR*

cDNA was synthesized from 1 µg DNase I-digested total RNA using the DuraScript RT-PCR Kit (Sigma-Aldrich, Saint Louis, MO, USA). TaqMan real-time PCR was performed and relative expression was calculated (given as arbitrary 'ratio units (ru)') as described (Pils et al., 2005a) using the following Assay-on-Demand™ probes: *TUSC3*, Hs00185147_m1 and *beta 2-microglobulin*, Hs99999907_m1 (Applied Biosystems, Foster City, CA, USA).

3.2.3.5 *Establishment and Analysis of Two Cell Line Models*

Cells were cultivated in medium (H134: DMEM + 25 mM HEPES (pH 8.0), MIA PaCa-2: α-MEM) with 10% FCS (fetal calf serum), 50 units ml^{-1} penicillin G, and 50 µg ml^{-1} streptomycin sulfate at 37°C in a humidified atmosphere of 95% air with 5% CO_2. For the reconstitution of *TUSC3* expression, the CDS of the IMAGE clone (BC010370 in pDNR-LIB) was cloned into the expression vector pLP-IRESneo. For the TUSC3-FLAG fusion protein the FLAG peptide was cloned in frame behind the C-terminus of *TUSC3*. The empty vector pLP-IRESneo was used as a control (Co). Transfections were performed with lipofectamine 2000 (Invitrogen), stable clones were selected with G418 (H134: 700 µg ml^{-1}, MIA PaCa-2: 800 µg ml^{-1}) and

subcultured with half of these concentrations. The mRNA expression was determined by qRT-PCR as described above. In H134 (an ovarian cancer cell line with methylated *TUSC3*) and MIA PaCa-2 (a pancreas carcinoma cell line with a homozygous deletion of *TUSC3*) *TUSC3* expression was reconstituted with two DNA constructs, one coding for a TUSC3-FLAG fusion protein (TFlag) and one coding for a full length *TUSC3* cDNA (TUSC3).

Proliferation rates were determined with growth curves. Migration and invasion abilities were measured using *in vitro* migration (8.0 µm pore size control chambers) and invasion assays (BD Matrigel invasion chambers). For the collagen I and BSA adhesion assay, cells were incubated on coated 96-well ELISA plates for 30 minutes, washed, and remaining cells were quantified with the Cell Titer-Blue® cell viability assay (Promega, Madison, WI, USA). For colocalization experiments, subcellular fractions (nuclei, mitochondria, lysosomes, microsomes, and cytoplasm) were prepared based on a differential centrifugation protocol (1,000, 9,700, 20,200 and 18,2000 g_{max} for above organelles, respectively (Graham and Rickwood, 1997)) after cell lysis with a Potter pestle. The purity of these fractions was analysed with antibodies against marker proteins (nucleoprin p62, cox 5a, none, ribophorin I, and ß-actin for above fractions, respectively). As primary antibody against FLAG mouse monoclonal anti-FLAG M2 antibody (10 µg ml^{-1}, Sigma Aldrich, Saint Louis, MO, USA) and as secondary antibody a goat anti-mouse HRP-linked antibody (1:10,000, Calbiochem, San Diego, CA, USA) was employed.

3.2.3.6 *Immunoblotting, Immunofluorescence, and Immunocytochemical Staining*

For immunoblotting, 5 µg proteins of the microsomal fraction and, as a control, the same amount of PNGase F digested proteins were separated on a 6% PAA-SDS

gel and blotted on a PVDF membrane. The primary antibody was a polyclonal goat anti-integrin ß1 antibody (1:1,000, R&D, Minniapolis, MN, USA) and the secondary antibody was a donkey anti-goat-HRP-liniked antibody (1:10,000, Santa Cruz Biotechnology, Santa Cruz, CA, USA).

Immunofluorescence staining was performed on formaldehyde-fixed cells with antibodies against FLAG (F2555, Sigma Aldrich) and calnexin (polyclonal rabbit antibody, personal gift of E. Ivessa) and counterstained with phalloidin (F-actin). For a morphological overview, the whole cells were stained with either hematoxylin/eosin or phalloidin (F-actin)/DAPI (nuclei).

For immunocytochemical staining cells on Lab-Tek™ Chamber Slides™ (Nagle Nunc International, Rochester, NY, USA) were formaldehyde-fixed and permeabilized with 0.5% Triton X-100. Endogenous peroxidase activity and slides were blocked with 3% H_2O_2/PBS and 0.2% fish gelatine, respectively. After incubation with polyclonal goat anti-integrin ß1 antibody (1:500, R&D, Minniapolis, MN, USA) and biotinylated rabbit anti-goat antibody (1:200, Vector Laboratories, Burlingame, CA, USA) or with the biotinylated sialic acid-specific lectin SNA (1:200, Vector Laboratories, Burlingame, CA, USA), the streptavidin ABComplex-HRP (ABC-Kit from Dako, Glostrup, Denmark) was employed and subsequently DAB+ (Dako) staining was performed. Finally cells were counterstained with hematoxyline/eosin and mounted in Eukitt (O. Kindler GmbH, Freiburg, Germany) (Pils et al., 2007b). Microscopy was performed on an Olympus BX50 upright light microscope (Olympus Europe, Hamburg, Germany) equipped with the Soft Imaging system CC12.

3.2.3.7 *Statistical Analysis*

Continuous variables are presented as mean and standard deviation, categorical variables as absolute and relative frequencies. In order to compare

frequencies between two or more groups, a Fisher's exact test or a Fisher-Freeman-Halton test, respectively, was performed. Mean values and 95% confidence intervals for *TUSC3* expression were calculated on a logarithmic scale and then transformed back to the original scale. In order to compare *TUSC3* expression between two or more groups a T-test or one-way ANOVA, respectively, was performed using the log-transformed expression as independent variable. Analogously, the potential influence of methylation on *TUSC3* expression was investigated using a T-test at the logarithmic scale. The potential influence of *TUSC3* methylation on progression free and overall survival is presented in plots of the corresponding Kaplan-Meier estimates and quantified using Cox proportional hazards regression models. As time point for progression the date of the documentation of the first relapse or the first documentation of the disease progression starting at the time of the first diagnosis was used. Univariate Cox models were used to demonstrate the influence of known prognostic factors and the potential new prognostic factor. Phenotypical changes and changes in binding to collagen- and BSA-coated surfaces of cell lines TUSC3 and TFlag were compared each with a control using t-tests with subsequent Bonferroni-Holm correction. P-values ≤ 0.05 were considered to be statistically significant. All computations have been performed using SAS software Version 9.1 (SAS Institute Inc., Cary, NC, USA, 2001); graphics were produced using SPSS software Version 13.0 (SPSS Inc. Headquarters, Chicago, Illinois, USA).

3.2.4 Results

3.2.4.1 *TUSC3 mRNA is Down-regulated in Ovarian Cancer*

TUSC3 mRNA expression was significantly decreased in ovarian cancers (n=99, median 0.105 ru) compared to benign ovarian tumors (n=20, median 0.465 ru, $P<0.001$) (Fig. 8A, Table 4). Ovarian cancer cell lines have generally low levels of

TUSC3 mRNA, in keeping with their dedifferentiated and highly proliferative phenotype. We did not detect any significant differences in *TUSC3* expression between different age groups, different FIGO stages, or different grades of ovarian cancer patients. Interestingly, expression of *TUSC3* in the subset of non-serous ovarian tumors, which are known to have worse outcomes than the purely serous tumors, was significantly lower (uncorrected *P*=0.037) (Table 4).

Table 4. Comparison of *TUSC3* Expression by Clinicopathologic Characteristics

Clinicopathologic Characteristics	Expression of *TUSC3* (mean)	Comparison (*P*)
Benign ovarian samples		
Mean	0.465	
CI	0.347-0.623	
Tumor Samples (compared to benign ovarian samples)		<0.001†
Mean	0.105	
CI	0.082-0.135	
Age		
≤ 50	0.085	0.299†
> 50	0.114	
Histology		
Serous	0.121	0.037†
Non-serous	0.064	
FIGO		
I	0.084	0.764‡
II	0.124	
III	0.104	
IV	0.126	
Grading		
1	0.068	0.188‡
2	0.135	
3	0.086	

‡ANOVA (calculated after logarithmic transformation, means and CI are given after back-transformation to the original scale).
†T-Test (calculated as above).

3.2.4.2 *Methylation of the TUSC3 Promoter and Reconstitution of Expression by DNA-Demethylation*

We have previously shown that the mRNA expression of *TUSC3* was undetectable or at the lower limit of detection in eight out of 38 ovarian cancer cell lines (Pils et al., 2005a). *TUSC3* promoter was methylated in seven out of these eight cell lines, as opposed to four out of thirty methylated cell lines with higher *TUSC3* mRNA levels (Fig. 8B and 8C). We observed a significant link between *TUSC3*

mRNA expression and the promotor methylation status of the respective cell line (*P*<0.001) (Fig. 8A and 8C), pointing towards epigenetic transcriptional regulation of *TUSC3* by DNA methylation. In order to further investigate the epigenetic regulatory mechanism, we treated the ovarian cancer cell line MZ6, which shows low *TUSC3* mRNA levels as well as promoter hypermethylation, with increasing concentrations of the demethylating agent 5-aza-2'-deoxycytidine (Aza). Indeed, demethylation of the TUSC3 promoter with Aza led to an induction of *TUSC3* mRNA after 72h (Fig. 8D).

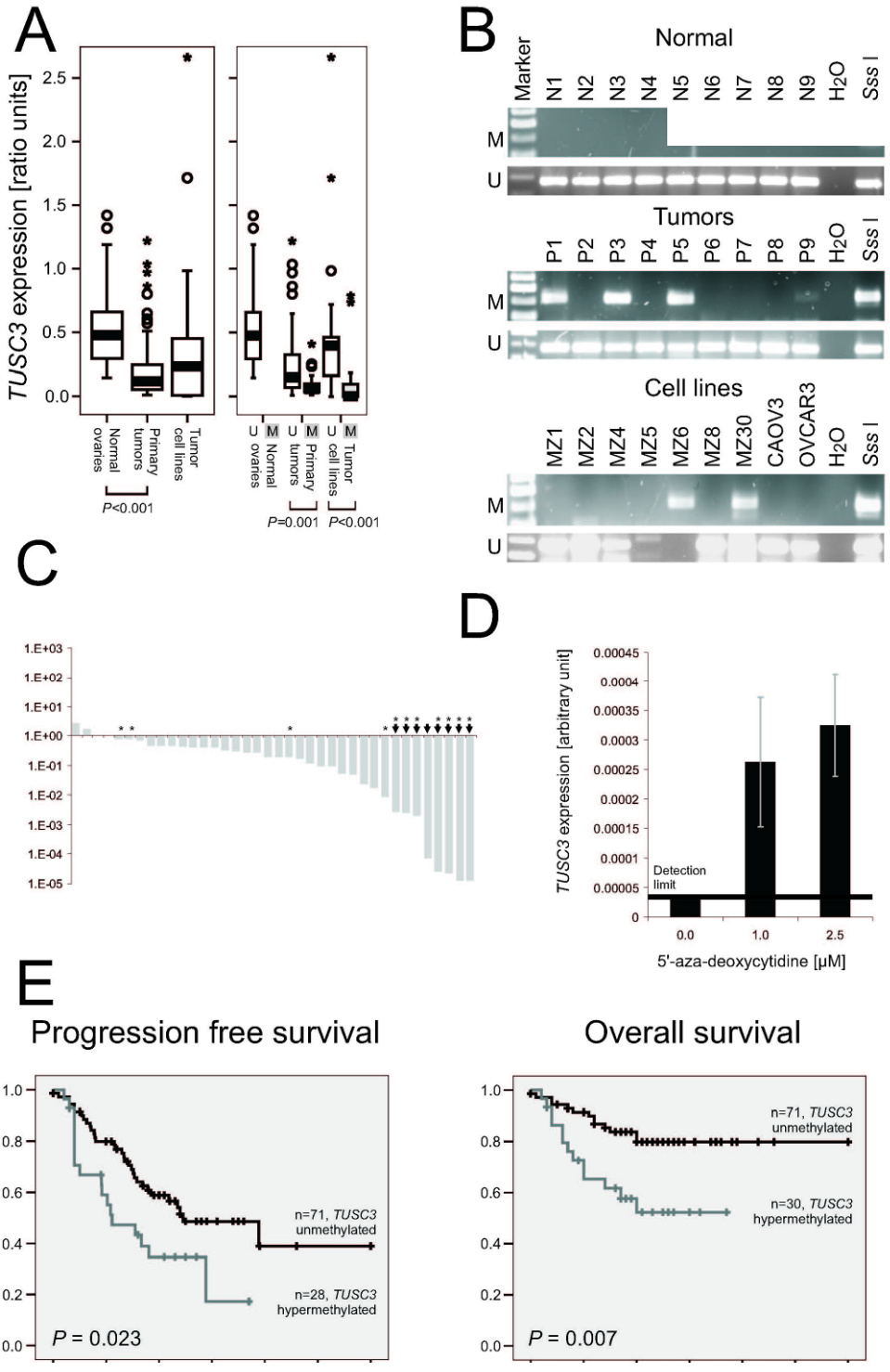

Fig.8. A) Box plots of the expression of TUSC3, given in arbitrary units (ratio units) in benign ovarian tissue samples, ovarian tumor samples, and ovarian cancer cell lines (left) and expression of TUSC3 subdivided in unmethylated (U) and hypermethylated (M) fractions (right). Statistical analysis: T-test on logarithmic scale. B) Representative ethidium bromide agarose-gels showing methylation-specific PCR products of nine benign ovarian tissue samples (top), nine ovarian tumor samples (center), and nine ovarian cancer cell lines (bottom). We used Sss I (CpG methylase) methylated human DNA and H2O for positive and negative controls, respectively. C) Expression of TUSC3 in 38 ovarian cancer cell lines. Cell lines with silenced TUSC3 expression are marked with arrows and cell lines with methylation-specific PCR products are marked with asterisks. D) Reconstitution of TUSC3 expression after 72-hour incubation with 1 or 2.5 μM 5-aza-2'-deoxycytidine in the ovarian cancer cell line MZ6. TUSC3 expression was below the detection limit in the mock-treated samples. Experiments were done in triplicates and mean values of relative TUSC3 expression (based on the expression of β-2-microglobulin) with standard deviations are plotted. E) Plots of Kaplan-Meier estimates for progression free and overall survival of patients with tumor samples with hypermethylated or unmethylated TUSC3. As time point for progression, the date of the documentation of the first relapse or the first documentation of the disease progression, starting at the time of the first diagnosis was used. P-values are from the univariate Cox regression analysis (Table 2).

As a next step, we wanted to gain more insight into the CpG methylation frequency within the *TUSC3* promoter region as well as to validate the results of the methylation specific PCR. We assessed the methylation status of individual CpG-islands localized within the *TUSC3* promoter region by bisulfite sequencing of three hypermethylated cell lines and two controls. The bislufite sequencing analysis revealed that most of the CpGs within the region of interest in the methylated cell lines are indeed methylated at higher frequencies (75%) than in the unmethylated control cell lines (10%) (data not shown).

3.2.4.3 *TUSC3 Methylation in Primary Ovarian Tumor Samples and Correlation with TUSC3 Expression and Clinicopathologic Parameters*

Next, we extended the methylation analysis of the *TUSC3* promoter to a panel of 102 primary ovarian tumor samples and 20 benign ovarian controls. Statistical analysis revealed no significant association of *TUSC3* promoter methylation frequency with any clinicopathological parameters like tumor histology, grading, FIGO staging or age of the patients (Table 5). In this cohort, hypermethylation of the *TUSC3* promoter was observed in 30 out of 102 (29.8%) ovarian cancer tissues but none of the controls (*P*=0.003; Fig. 8B). Consequently, mean *TUSC3* mRNA expression in the methylated group was significantly reduced (0.065 ru) compared to the unmethylated group (0.135 ru, *P*=0.001), hinting towards methylation dependent gene-silencing of *TUSC3* in primary ovarian tumors.

Table 5. Comparision of Clinicopathologic Characteristics with Frequency of Hypermethylation of *TUSC3*

Clinicopathologic Characteristics	Hypermethylation of *TUSC3*	Comparison (*P*) †
Benign ovarian samples	0 / 20 (0%)	
Primary Tumor Samples	30 / 102 (29.4%)	0.003
Age		0.218
≤ 50	5 / 26 (19.2%)	
> 50	25 / 75 (33.3%)	
Histology		0.200
Serous	21 / 79 (26.6%)	
Non-serous	9 / 22 (40.9%)	
FIGO		0.948
I	5 / 17 (29.4%)	
II	2 / 10 (20.0%)	
III	15 / 51 (29.4%)	
IV	7 / 22 (31.8%)	
Grading		0.102
1	2 / 2 (100.0%)	
2	15 / 48 (31.2%)	
3	13 / 51 (25.5%)	

†Fisher's Exact Test and Fisher-Freeman-Halton Test, respectively.

Influence of *TUSC3* methylation status on progression free and overall survival

TUSC3 promoter methylation was associated with higher rates of progressive disease (32.1% vs. 11.3%), prompting us to further investigate its influence on ovarian cancer prognosis. We found that patients with methylated *TUSC3* promoter had significantly shorter progression free (RR 1.97, *P*=0.023) and overall survival rates (RR 2.92, *P*=0.007) as shown by Kaplan Meier estimates (Fig. 8E) with a median progression free survival of 11.1 months in the methylated group vs. 24.6 months in the unmethylated group (Fig.8E). Cox proportional hazards analysis revealed a significant association between *TUSC3* promoter methylation and progression free (RR 2.17, *P*=0.024) as well as overall survival (RR 4.12, *P*=0.008) which was independent from other risk factors, including response to chemotherapy, the strongest predictive factor in our analysis (interaction term not significant; Table 6). The hazard ratio of methylated vs. unmethylated *TUSC3* promoter status for progression free survival was significant (RR 1.97, *P*=0.023) and only slightly inferior to the increase of one FIGO stage (RR 2.82, *P*<0.001) or residual disease after surgery (RR 3.04, *P*=0.001). Similarly, the significant influence of *TUSC3* methylation on overall survival (RR 2.92, *P*=0.007) was comparable to the increase of one FIGO stage (RR 2.52, *P*=0.002), histological subtype (serous vs. non-serous RR 2.37, *P*=0.037) and residual disease after surgery (RR 5.28, *P*<0.001), adding to the few prognostic factors available at the time when individual therapeutic options have to be explored.

Table 6. Univariate and Multiple Cox Proportional Hazards Analysis

	Progression free survival			
	Univariate		Multiple	
	Relative risk (95% CI)‡	*P*	Relative risk (95% CI)‡	*P*
Age at diagnosis	1.02 (0.99-1.05)	0.184		
Histology (non-serous *v* serous)†	1.16 (0.58-2.32)	0.683		
FIGO stage	**2.82** (1.87-4.26)	<0.001	used	
Grading	0.98 (0.58-1.65)	0.933		
Residual disease (>1cm *v* ≤1cm)†	**3.04** (1.53-6.02)	0.001	used	
Therapy response (no *v* yes) †	**4.91** (2.64-9.10)	<0.001	used	
Methylation of *TUSC3* (yes *v* no)†	**1.97** (1.10-3.53)	0.023	**2.17** (1.11-4.24)	0.024
	Overall survival			
	Univariate		Multiple	
	Relative risk (95% CI)‡	*P*	Relative risk (95% CI)‡	*P*
Age at diagnosis	**1.06** (1.02-1.10)	0.003	used	
Histology (non-serous *v* serous)†	**2.37** (1.05-5.32)	0.037	used	
FIGO stage	**2.52** (1.41-4.49)	0.002	used	
Grading	0.76 (0.38-1.53)	0.446		
Residual disease (>1cm *v* ≤1cm)†	**5.28** (2.19-12.70)	<0.001	used	
Therapy response (no *v* yes) †	**9.56** (3.56-25.65)	<0.001	used	
Methylation of *TUSC3* (yes *v* no)†	**2.92** (1.35-6.29)	0.007	**4.12** (1.45-11.65)	0.008

‡CI, confidence interval. †Categorical variable. Bold, statistically significant.

3.2.4.4 *Generation and In-vitro Characterization of TUSC3 Cancer Cell Line Models*

In order to decipher the function of *TUSC3,* we stably reconstituted TUSC3 *in vitro* in two cancer cell lines (H134 and Mia PaCa-2), which have either low or lack *TUSC3* expression. We transfected a full length (TUSC3) or a FLAG tagged (TFlag) *TUSC3* mRNA-construct (Fig. 9A), resulting in a considerably altered phenotype.

First, proliferation of *TUSC3*-reconstituted cells was significantly decreased (by 23%, corr. *P*=0.007 for H134 and 26%, corr. *P*=0.005 for Mia PaCa-2, respectively) compared to vector transfected controls (Fig. 9A).

Second, transwell migration rate of the H134 ovarian cancer cell line was significantly enhanced by 272% (*P*<0.001) in TUSC3 as well as by 253% in TFlag transfected cell lines (*P*<0.001) (Fig. 9A). Interestingly, we observed incongruous results in the MIA PaCa-2 cell line, where migration ability was significantly inhibited upon TUSC3 reconstitution (-62%, *P*=0.001 in the TFlag transfected cell line and -

57%, *P*=0.001 in the TUSC3 transfected cell line, respectively, Fig 9A). Invasiveness, as tested by a matrigel-transwell assay, was not significantly affected (ranging only from 0.1% to 1.0% for all cell lines, data not shown).

Finally, TUSC3 reconstitution induced a change in cellular morphology of ovarian cancer cells, from an epitheloid-like to a rather mesenchymal phenotype. This phenomenon is reminiscent of the epithelial-mesenchymal transition decribed in several tumors and might develop secondary to a disorganized actin stress-fiber network (Fig. 9B).

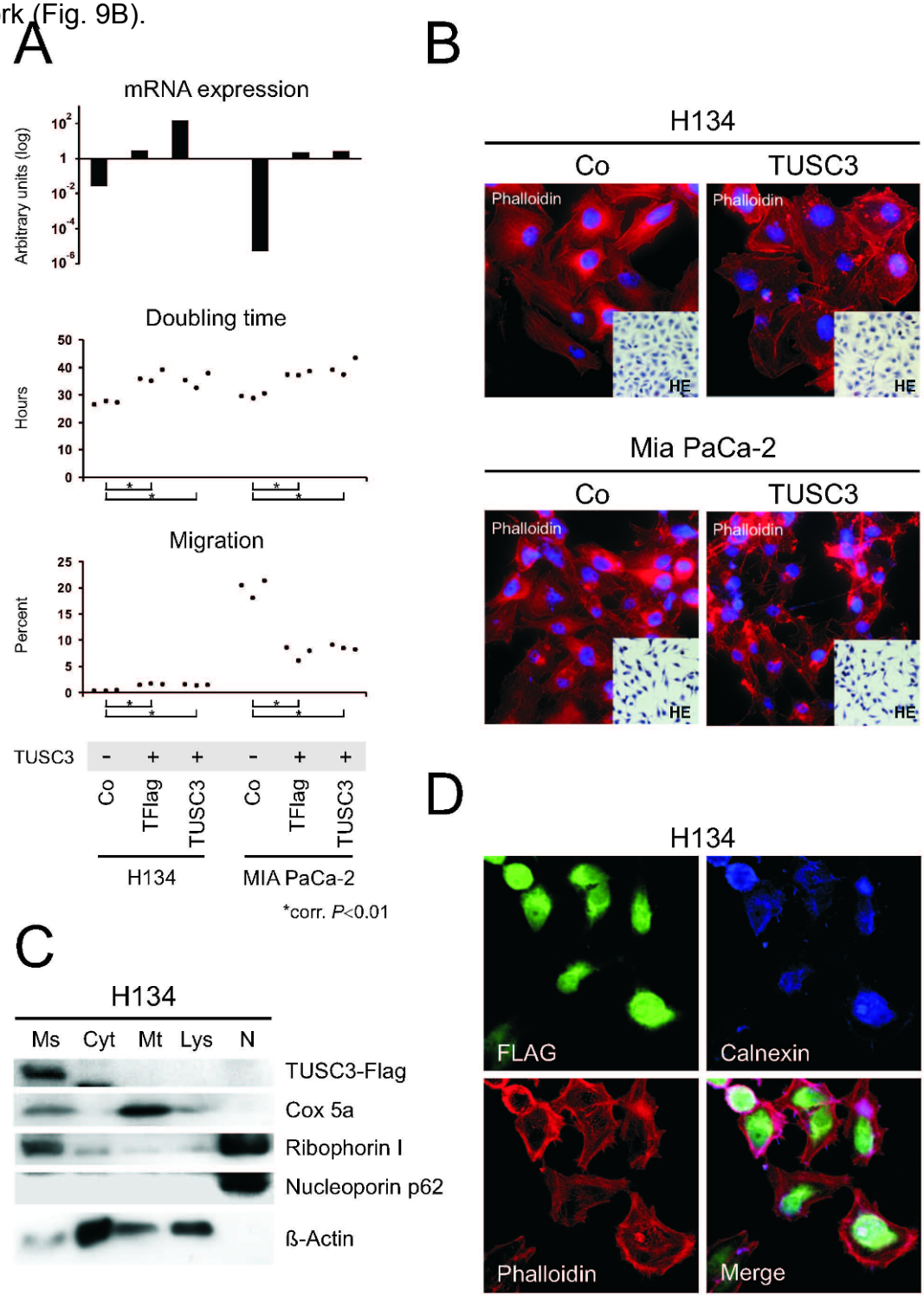

Fig.9. A) In vitro characterization of cell line models with reconstituted TUSC3 expression (H134 and MIA PaCa-2). mRNA expression is shown in arbitrary units, doubling time in hours and migration abilities, determined by transwell assays, in percent of total cell numbers. Experiments were performed in triplicates, the significance was calculated by the T-test and corrected for multiple testing. B) Morphological overview stains with phalloidin (F-actin) and DAPI (nuclei) (large picture) and HE stains (inset) are shown for all cell lines. C) Western blot analysis of subcellular fractions for FLAG-tagged TUSC3 (TUSC3-Flag) in the ovarian cancer cell line H134. Fractions (Ms, microsomes; Cyt, cytoplasm; Mt, mitochondria; Lys, lysosomes; and N, nuclei) were probed with ribophorin I, ß-actin, cox 5a, no marker, and nucleoporin p62, respectively. D) Colocalization experiment of fixed H134 cells stained for the TUSC3-FLAG fusion protein with anti-FLAG, for an integral endoplasmic reticulum protein with anti-calnexin, and with phalloidin as a counterstain.

3.2.4.5 *Subcellular Localization of TUSC3*

To determine the subcellular localization of TUSC3 we applied two independent approaches. First, western blot analysis of the FLAG tagged TUSC3 fusion protein in highly enriched subcellular fractions of H134 cells (microsomes, soluble cytoplasm, mitochondria, lysosomes, and nuclei) showed its localization to the microsomal fraction, comprised of the endoplasmic reticulum (ER) and some minor amounts of cytoplasmic membranes (Fig. 9C). As a second approach, we used an immunofluorescent colocalization experiment, which revealed a perfect overlap of the *TUSC3*-FLAG protein and calnexin, an integral protein of the endoplasmic reticulum (Fig. 9D). These two methods confirm with certainty the expected subcellular localization of TUSC3 in the H134 cell line, namely the endoplasmatic reticulum.

3.2.4.6 *Functional Analysis of TUSC3*

TUSC3 might function as potential subunit of the oligosaccharyltransferase complex in the endoplasmic reticulum. To investigate this putative function of TUSC3 in N-glycosylation, we performed a western blot analysis of a well known glycosylation target, integrin ß1, in the microsomal fractions of H134 and MIA PaCa-2

cells. As a control, a complete removal of N-glycosylated oligosaccharides was achieved by digestion with PNGase F, resulting in bands of equal mobilty at ~80 kDa, consistent with the calculated molecular weight of roughly 85 kDa (Fig. 10A). In both cell lines the ratio between mature, fully glycosylated, and incompletely glycosylated precursor integrin ß1 increased upon *TUSC3* reconstitution (by a factor of 2.0 and 2.6 for H134 and MIA PaCa-2, respectively; Fig. 10A). Additionally, a ~10 kDa shift towards higher mobility of the mature integrin ß1 was observed, suggesting a different N-glycosylation pattern in the reconstituted cells.

Changes of sialylation levels of the mature integrin ß1, which cause a mobility shift have been described previously and might regulate its binding affinity to collagen I (Seales et al., 2003). Accordingly, immunohistochemical staining for sialylated proteins using the sambucus nigra lectin (SNA) revealed a significant increase in sialylation in *TUSC3*-positive cells compared to *TUSC3*-negative cells (Fig. 10B).

To assess the impact of the observed glycosylation modifications of integrin ß1 on collagen I binding in our cell line models, we performed adhesion assays on collagen I-coated surfaces. Adhesion of the *TUSC3* reconstituted cells to a collagen I-coated surface was significantly increased despite their lower levels of mature ß1 integrin, possibly suggesting defective glycosylation or sialylation patterns (Fig. 10C). Hence, loss of *TUSC3* might lead to decreased collagen binding and subsequent migration of cells in ovarian cancer, leading to their increased tumorigenicity.

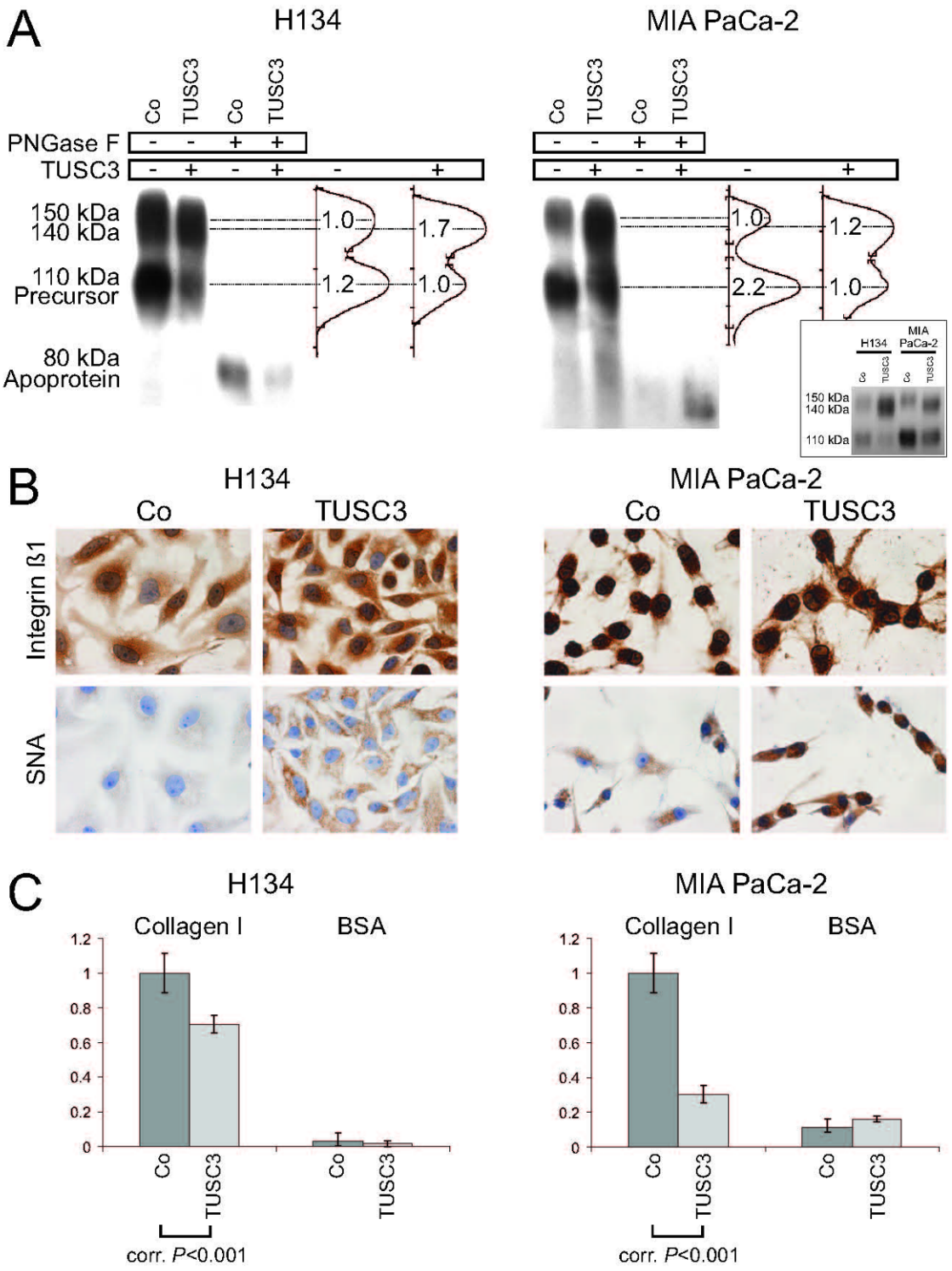

Fig.10. A) Western blot analysis of integrin ß1 in H134 and MIA PaCa-2 cell lines. Integrin ß1 revealed two bands, one at ~110 kDa representing the precursor ß1-pool in the ER, and one at ~140-150 kDa representing the mature ß1 protein. In TUSC3-reconstituted cell lines the band representing mature ß1 showed a ~10 kDa shift towards higher mobility. Treatment of proteins with the deglycosylating enzyme, PNGase F, eliminated the differential mobility and resulted in one band approximately at the position of the calculated apoprotein mass (~80 kDa).

Adjacent to the blots, quantification curves are shown. Bands with the smaller values were set to unity for each cell line model. The molecular weight shift and the change of the mature / precursor ratio was more pronounced after a shorter run (inset). B) Immunocytochemical stains for integrin ß1 and sialylated poteins in general (SNA) are shown for the cell line models H134 and MIA PaCa-2. Cells were counterstained with hematoxylin/eosin. C) Adhesion of cells to 96-well plates coated with collagen I and BSA (as a control) were tested in octuples and the significance calculated by the T-test and corrected for multiple testing. Binding of the control cells to collagen I was arbitrarily set to unity.

3.2.5 Discussion

TUSC3, originally named *N33*, was originally discovered as a candidate TSG in the mid 1990 and is located on chromosome 8p22 within a region of frequent homozygous deletions. Mutational analysis performed in prostate cancer and various other tumor entities failed to reveal a significant rate of protein disruptive mutations and the interest in *TUSC3* consequently vanished.

Using publicly available gene expression profiling data, we have systematically screened the region on 8p22 for differentially regulated genes and identified *TUSC3* as a candidate TSG in ovarian cancer. A quantitative expression analysis confirmed the significant down-regulation of *TUSC3* in ovarian cancer tissues and a consequent explorative analysis yielded significant correlations with some clinical parameters, in particular linking reduced *TUSC3* expression at the time of diagnosis with unfavorable overall survival rates (Pils et al., 2005a). Similar results were recently obtained in head and neck tumors, where loss of *N33* (*TUSC3*) was significantly correlated with poor survival (Guervos et al., 2007). In addition, the frequency of LOH on chromosome band 8p22 in colorectal cancer was shown to be very high (up to 67%) and accompanied by a significantly reduced expression of *TUSC3* in these tumors (Andersen et al., 2007).

In this work we validated our previous observations in a larger, completely independent patient population and showed for the first time and epigenetic

mechanism as the molecular basis of reduced *TUSC3* expression in ovarian cancer tissues. Furthermore, we established the methylation status of the *TUSC3* promoter as a potent independent prognostic marker for progression free and overall survival in ovarian cancer.The frequency of *TUSC3* promoter methylation in ovarian tumor tissues was more than 30% compared to none in tissues derived from regular ovaries and from benign ovarian cysts. Methylation status significantly correlated with expression in tumor samples and cell lines, further establishing the epigenetic regulation as the main cause for low TUSC3 expression in tumors.

Recently, the gene product of *TUSC3* was acknowledged as a human homologue to *S. cerevisiae* Ost3p shown to be associated with the oligosaccharyltransferase complex by copurification experiments (Kelleher et al., 2003a). Oligosaccharyltransferase is an integral membrane protein complex in the ER that catalyzes N-linked glycosylation of secreted as well as membrane bound proteins. Whereas the loss of Ost3p in yeast results in underglycosylation of selected acceptor substrates *in vitro* (Karaoglu et al., 1995) the molecular function of TUSC3 in the human oligosaccharyltransferase protein complex remained unclear (Kelleher et al., 2003a). Aberrant glycosylation of proteins can be found in essentially all *in vitro* cancer models and human cancers, and many glycosylated epitopes constitute tumor-associated antigens (Hakomori, 2002; Kobata and Amano, 2005) causing a long-standing debate whether aberrant glycosylation is a result or a cause of cancer.

Our functional analysis adds some small, but crucial data to the incremental understanding of the causal connexion between *TUSC3*, glycosylation and cancer. We were able to show the subcellular localization of TUSC3 to the ER, as predicted from its homology to OSTP3p, by using FLAG-tagged fusion constructs. In both cell line models high *TUSC3* expression correlated significantly with decreased proliferation. This fact is consistent with the role of TUSC3 as a TSG. Poor prognosis

of patients with TUSC3 negative (promoter methylated) cancers might be partly dependent on the increased proliferation of cancer cells as shown by our *in vitro* data. The inter-cell line phenotypic variability of the migration and invasion properties observed in our experiments, might be explained by the differences in the tissue of origin (ovary vs. pancreas) of the individual cancer cell lines. This observation is not surprising, judged by the highly variable and tissue dependent *TUSC3* expression levels in whole genome expression profiles (data not shown).

The glycosylation pattern of the mature integrin ß1 protein and the ratio of mature to precursor protein changed uniformly upon *TUSC3* reexpression in two carcinoma cell lines of different origins (ovary and pancreas). Furthermore, the amount of sialylated glycoproteins was substantially decreased in both *TUSC3*-negative cell lines. Therefore, we conclude that TUSC3 is involved in the post-translational maturation (i.e. glycosylation) of integrin ß1 and probably other glycoproteins. Integrin ß1 signalling is regulated by extracellular matrix (ECM) binding, affecting multiple cellular functions such as proliferation, changes in cytoskeletal organization and motility, Modifications of integrin ß1 glycosylation are a well confirmed regulatory mechanism for ECM binding and subsequent signalling (Seales et al., 2003). Local tumor dissemination to the peritoneum (transcoelomic metastasis) is the predominant mechanism of tumor progression in ovarian cancer and the main reason for the poor prognosis of this disease. The current hypothesis proposes tumor cell aggregates, so-called spheroids, rather than single cells may be responsible for this dissemination. Collagen I is a major component of the peritoneal mesothelium and promotes integrin ß1-mediated spheroid adhesion and dissemination (Burleson et al., 2006; Burleson et al., 2004a; Burleson et al., 2004b; Lessan et al., 1999). Therefore, the significantly increased affinity of *TUSC3*-negative cells to collagen I, caused by differential integrin ß1 glycosylation, provides an

intriguingly plain explanation for the strong tumor suppressive function of TUSC3, cumulating in a prominent impact on patient outcome (as shown in univariate and multiple cox regression analyses). Furthermore, changes of integrin ß1 glycosylation were shown to affect cell migration by cytoskeletal rearrangements as indicated by a disorganized actin stress-fiber network (Guo et al., 2002), which we also observed in our cell line models.

Regardless of the detailed molecular function of TUSC3, *TUSC3* promoter methylation is a promising new prognostic marker for ovarian cancer, which deserves to be evaluated prospectively. Given the poor prognosis, the availability of DNA demethylating agents and inhibitors histone deacetylases (e.g. decitabine and zebularin) (Momparler, 2005) and the superior response to intraperitoneally administered chemotherapy compared to systemic chemotherapy (Armstrong et al., 2006), patients with hypermethylated *TUSC3* genes may profit from the combination of epigenetic modifiers with conventional chemotherapy. An even more specific approach could be an antagonistic therapy targeting integrin ß1, especially in patients with *TUSC3* promoter methylation. A deeper understanding of the role of *TUSC3* in protein glycosylation may offer additional possibilities for therapeutic interventions in the future.

ACKNOWLEDGMENTS

We thank Cornelia Sax and Dr. Brigitte Wolf for their excellent technical support, Dr. Erwin Ivessa for providing the antibody for calnexin, and Dr. Werner Aufsatz for providing the protocol for bisulfite treatment.

4 Concluding Remarks and Future Directions

The short arm of chromosome 8 is frequently altered in human cancer. 8p22 is a particular deletion hot spot suggesting the presence of tumor suppressor genes (TSG) in this area. The most accurately characterized TSG in this region is DLC1, a Rho GTPase-activating protein, which identified by a deletion mapping approach. Originally, it has been characterized in hepatocellular carcinoma, but most likely plays a role in several cancer types (Durkin et al., 2007; Xue et al., 2008). Using publicly available gene expression profiling data, we have systematically screened the region on 8p22 for differentially regulated genes and identified hVps37A and TUSC3 as candidate TSGs in ovarian cancer. Quantitative expression analysis confirmed the significant down-regulation of hVps37A and TUSC3 in ovarian cancer tissues and a consequent explorative analysis yielded significant correlations with some clinical parameters. In particular, we could link reduced hVps37A and TUSC3 mRNA expression in tumors to unfavorable overall survival rates (Pils et al., 2005b).

In this work our previous results were validated in a larger, completely independent patient population. Subsequently, hVps37A and TUSC3 were characterized in more depth with respect to their molecular function and corresponding clinical implications. hVps37A prooved to be essential for the degradation process of EGFR and HER2 and determined their prognostic significance for overall survival in ovarian cancer. Moreover, low hVps37A expression confered resistance against the EGFR antagonistic antibody Cetuximab *in vitro*.

The promoter region of *TUSC3* was found to be frequently methylated in ovarian tumor samples, associated with reduced mRNA expression and unfavorable survival rates. Furthermore, we identified TUSC3 to localize to the endoplasmatic reticulum and to function in N-glycosylation of integrin-ß1 and potentially several

other proteins. Overall, we describe two molecular markers, which determine patient survival and response to targeted therapies. Since only few molecular markers are available for ovarian cancer, clinical utilization of TUSC3 or hVps37A would potentially lead to advances in ovarian cancer diagnosis and treatment.

In order to reach a final conclusion about their clinical value, more experiments will have to be conducted. As mentioned above, hVps37A knock-down in ovarian cancer cell lines introduced a resistance mechanism against the monoclonal antibody Cetuximab, caused by ineffective EGFR degradation. Ongoing studies of our group aim to determine clinical impact of hVps37A expression on response of Non Small Cell Lung Cancer (NSCLC) patients to Cetuximab therapy. In case a significant correlation can be observed and reproduced in other EGFR overexpressing cancer entities, we will establish hVps37A as molecular marker for Cetuximab based therapy in clinical practice. A patent describing a procedure to predict Cetuximab response rates based on hVps37A expression was recently submitted by our group.

In order to shed more light on hVps37A function, we recently established a mouse xenograft model applying the above described SKOV-3 Tet-Off cell line. Preliminary results indicate, that tumor growth in mice is elevated upon hVps37A knock-down. TUNEL assays as well as Ki-67 assays of the corresponding tumors will show if enhanced tumor growth is a result of elevated proliferation of reduced apoptosis rates. A 3D cell culture experiment showed that hVps37A-silenced cells gained the ability to invatde a collagen matrix more efficiently. In line with current literature (Arora et al., 2008; Yang et al., 2004), this finding may be traced back to dysregulated EGFR-downstream pathways (Figure 7A, B). Overall, we have promising upcoming results which will be validated over the next months.

We will also further investigate cellular function and clinical impact of TUSC3. IHC on tissue microarrays containing primary ovarian tumor samples should confirm

the negative impact of low TUSC3 expression obtained by RNA-expression analysis. The knowledge of TUSC3 cellular localization is a prerequisite for the understanding of its function. According to a recently published study, TUSC3 is weakly associated to the oligosaccharyltransferase complex in the endoplasmatic reticulum (Kelleher et al., 2003b). We plan dual-immunofluorescence staining experiments of fixed cancer cells using several cell-compartment markers in addition to antibodies directed against TUSC3 or a C-terminal TUSC3 tag in order to prove and substantiate our previous findings. Furthermore, in-vivo experiments using mouse xenografts of overexpressing and silenced *TUSC3* cell lines will be performed to evaluate the potential influence of TUSC3 expression on tumor growth. The expected attenuation of tumor formation mediated by TUSC3 will be examined by immunohistochemistry and TUNEL assays on histological sections.

5 References

Aarnio, M., Sankila, R., Pukkala, E., Salovaara, R., Aaltonen, L. A., de la Chapelle, A., Peltomaki, P., Mecklin, J. P., and Jarvinen, H. J. (1999). Cancer risk in mutation carriers of DNA-mismatch-repair genes. International journal of cancer *81*, 214-218.

Agarwal, R., and Kaye, S. B. (2003). Ovarian cancer: strategies for overcoming resistance to chemotherapy. Nature reviews *3*, 502-516.

Andersen, C. L., Wiuf, C., Kruhoffer, M., Korsgaard, M., Laurberg, S., and Orntoft, T. F. (2007). Frequent occurrence of uniparental disomy in colorectal cancer. Carcinogenesis *28*, 38.

Arbieva, Z. H., Banerjee, K., Kim, S. Y., Edassery, S. L., Maniatis, V. S., Horrigan, S. K., and Westbrook, C. A. (2000). High-resolution physical map and transcript identification of a prostate cancer deletion interval on 8p22. Genome Res *10*, 244.

Armstrong, D. K., Bundy, B., Wenzel, L., Huang, H. Q., Baergen, R., Lele, S., Copeland, L. J., Walker, J. L., and Burger, R. A. (2006). Intraperitoneal cisplatin and paclitaxel in ovarian cancer. NEnglJMed *354*, 34.

Arora, P., Cuevas, B. D., Russo, A., Johnson, G. L., and Trejo, J. (2008). Persistent transactivation of EGFR and ErbB2/HER2 by protease-activated receptor-1 promotes breast carcinoma cell invasion. Oncogene *27*, 4434-4445.

Babst, M., Odorizzi, G., Estepa, E. J., and Emr, S. D. (2000). Mammalian tumor susceptibility gene 101 (TSG101) and the yeast homologue, Vps23p, both function in late endosomal trafficking. Traffic (Copenhagen, Denmark) *1*, 248-258.

Bache, K. G., Slagsvold, T., Cabezas, A., Rosendal, K. R., Raiborg, C., and Stenmark, H. (2004a). The growth-regulatory protein HCRP1/hVps37A is a subunit of mammalian ESCRT-I and mediates receptor down-regulation. Mol Biol Cell *15*, 4337-4346.

Bache, K. G., Slagsvold, T., and Stenmark, H. (2004b). Defective downregulation of receptor tyrosine kinases in cancer. The EMBO journal *23*, 2707-2712.

Bashyam, M. D., Bair, R., Kim, Y. H., Wang, P., Hernandez-Boussard, T., Karikari, C. A., Tibshirani, R., Maitra, A., and Pollack, J. R. (2005). Array-based comparative genomic hybridization identifies localized DNA amplifications and homozygous deletions in pancreatic cancer. Neoplasia *7*, 556.

Bogdan, S., and Klambt, C. (2001). Epidermal growth factor receptor signaling. Curr Biol *11*, R292-295.

Bova, G. S., Carter, B. S., Bussemakers, M. J., Emi, M., Fujiwara, Y., Kyprianou, N., Jacobs, S. C., Robinson, J. C., Epstein, J. I., and Walsh, P. C. (1993). Homozygous deletion and frequent allelic loss of chromosome 8p22 loci in human prostate cancer. Cancer Research *53*, 3869.

Bova, G. S., MacGrogan, D., Levy, A., Pin, S. S., Bookstein, R., and Isaacs, W. B. (1996). Physical mapping of chromosome 8p22 markers and their homozygous deletion in a metastatic prostate cancer. Genomics *35*, 46.

Burleson, K. M., Boente, M. P., Pambuccian, S. E., and Skubitz, A. P. (2006). Disaggregation and invasion of ovarian carcinoma ascites spheroids. JTranslMed *4*, 6.

Burleson, K. M., Casey, R. C., Skubitz, K. M., Pambuccian, S. E., Oegema, T. R., Jr., and Skubitz, A. P. (2004a). Ovarian carcinoma ascites spheroids adhere to extracellular matrix components and mesothelial cell monolayers. GynecolOncol *93*, 170.

Burleson, K. M., Hansen, L. K., and Skubitz, A. P. (2004b). Ovarian carcinoma spheroids disaggregate on type I collagen and invade live human mesothelial cell monolayers. Clin ExpMetastasis *21*, 685.

Collard, J. G., Schijven, J. F., Bikker, A., La, R. G., Bolscher, J. G., and Roos, E. (1986). Cell surface sialic acid and the invasive and metastatic potential of T-cell hybridomas. Cancer Research *46*, 3521.

Crijns, A. P., Boezen, H. M., and Schouten, J. P. (2003). Prognostic factors in ovarian cancer: current evidence and future prospects. Eur J Cancer S *99*, 127-145.

Crijns, A. P., Duiker, E. W., de Jong, S., Willemse, P. H., van der Zee, A. G., and de Vries, E. G. (2006). Molecular prognostic markers in ovarian cancer: toward patient-tailored therapy. Int J Gynecol Cancer *16 Suppl 1*, 152-165.

Das, P. M., and Singal, R. (2004). DNA methylation and cancer. JClinOncol *22*, 4632.

Dennis, J. W., Granovsky, M., and Warren, C. E. (1999). Glycoprotein glycosylation and cancer progression. BiochimBiophysActa *1473*, 21.

Dennis, J. W., Laferte, S., Waghorne, C., Breitman, M. L., and Kerbel, R. S. (1987). Beta 1-6 branching of Asn-linked oligosaccharides is directly associated with metastasis. Science *236*, 582.

Durkin, M. E., Yuan, B. Z., Zhou, X., Zimonjic, D. B., Lowy, D. R., Thorgeirsson, S. S., and Popescu, N. C. (2007). DLC-1:a Rho GTPase-activating protein and tumour suppressor. J Cell Mol Med *11*, 1185-1207.

Galonic, D. P., and Gin, D. Y. (2007). Chemical glycosylation in the synthesis of glycoconjugate antitumour vaccines. Nature *446*, 1000.

Giebel, B., and Wodarz, A. (2006). Tumor suppressors: control of signaling by endocytosis. Curr Biol *16*, R91-92.

Graham, J. M., and Rickwood, D. (1997). Subcellular fractionation, a practical approach, (New York: Oxford University Press).

Gruenberg, J., and Stenmark, H. (2004). The biogenesis of multivesicular endosomes. Nat Rev Mol Cell Biol *5*, 317-323.

Guervos, M. A., Marcos, C. A., Hermsen, M., Nuno, A. S., Suarez, C., and Llorente, J. L. (2007). Deletions of N33, STK11 and TP53 are involved in the development of lymph node metastasis in larynx and pharynx carcinomas. Cell Oncol *29*, 327.

Guo, H. B., Lee, I., Kamar, M., Akiyama, S. K., and Pierce, M. (2002). Aberrant N-glycosylation of beta1 integrin causes reduced alpha5beta1 integrin clustering and stimulates cell migration. Cancer Research *62*, 6837.

Hakomori, S. (2002). Glycosylation defining cancer malignancy: new wine in an old bottle. ProcNatlAcadSciUSA *99*, 10231.

Haugh, J. M., and Meyer, T. (2002). Active EGF receptors have limited access to PtdIns(4,5)P(2) in endosomes: implications for phospholipase C and PI 3-kinase signaling. J Cell Sci *115*, 303-310.

Holbro, T., Civenni, G., and Hynes, N. E. (2003). The ErbB receptors and their role in cancer progression. Exp Cell Res *284*, 99-110.

Holschneider, C. H., and Berek, J. S. (2000). Ovarian cancer: Epidemiology, biology, and prognostic factors. Seminars in Surgical Oncology *19*, 3.

Horak, P., Pils, D., Haller, G., Pribill, I., Roessler, M., Tomek, S., Horvat, R., Zeillinger, R., Zielinski, C., and Krainer, M. (2005). Contribution of epigenetic silencing of tumor necrosis factor-related apoptosis inducing ligand receptor 1 (DR4) to TRAIL resistance and ovarian cancer. MolCancer Res *3*, 335.

Hynes, N. E., Horsch, K., Olayioye, M. A., and Badache, A. (2001). The ErbB receptor tyrosine family as signal integrators. Endocr Relat Cancer *8*, 151-159.

Hynes, N. E., and Lane, H. A. (2005). ERBB receptors and cancer: the complexity of targeted inhibitors. Nat Rev Cancer *5*, 341-354.

Jemal, A., Murray, T., Ward, E., and Samuels, A. (2005). Cancer statistics, 2005. Ca-A Cancer Journal for Clinicians *55*, 259.

Jemal, A., Siegel, R., Ward, E., Hao, Y., Xu, J., Murray, T., and Thun, M. J. (2008). Cancer statistics, 2008. CA: a cancer journal for clinicians *58*, 71-96.

Jones, P. A., and Baylin, S. B. (2002). The fundamental role of epigenetic events in cancer. NatRevGenet *3*, 415.

Kakugawa, Y., Wada, T., Yamaguchi, K., Yamanami, H., Ouchi, K., Sato, I., and Miyagi, T. (2002). Up-regulation of plasma membrane-associated ganglioside sialidase (Neu3) in human colon cancer and its involvement in apoptosis suppression. ProcNatlAcadSciUSA *99*, 10718.

Karaoglu, D., Kelleher, D. J., and Gilmore, R. (1995). Functional characterization of Ost3p. Loss of the 34-kD subunit of the Saccharomyces cerevisiae oligosaccharyltransferase results in biased underglycosylation of acceptor substrates. JCell Biol *130*, 567.

Katzmann, D. J., Babst, M., and Emr, S. D. (2001). Ubiquitin-dependent sorting into the multivesicular body pathway requires the function of a conserved endosomal protein sorting complex, ESCRT-I. Cell *106*, 145-155.

Katzmann, D. J., Odorizzi, G., and Emr, S. D. (2002). Receptor downregulation and multivesicular-body sorting. Nat Rev Mol Cell Biol *3*, 893-905.

Kelleher, D. J., and Gilmore, R. (2006). An evolving view of the eukaryotic oligosaccharyltransferase. Glycobiology *16*, 47R.

Kelleher, D. J., Karaoglu, D., Mandon, E. C., and Gilmore, R. (2003a). Oligosaccharyltransferase isoforms that contain different catalytic STT3 subunits have distinct enzymatic properties. MolCell *12*, 101.

Kelleher, D. J., Karaoglu, D., Mandon, E. C., and Gilmore, R. (2003b). Oligosaccharyltransferase isoforms that contain different catalytic STT3 subunits have distinct enzymatic properties. Molecular cell *12*, 101-111.

Kirisits, A., Pils, D., and Krainer, M. (2007). Epidermal growth factor receptor degradation: an alternative view of oncogenic pathways. The international journal of biochemistry & cell biology *39*, 2173-2182.

Kobata, A., and Amano, J. (2005). Altered glycosylation of proteins produced by malignant cells, and application for the diagnosis and immunotherapy of tumours. ImmunolCell Biol *83*, 429.

Krasner, C. N., McMeekin, D. S., Chan, S., Braly, P. S., Renshaw, F. G., Kaye, S., Provencher, D. M., Campos, S., and Gore, M. E. (2007). A Phase II study of trabectedin single agent in patients with recurrent ovarian cancer previously treated with platinum-based regimens. British journal of cancer *97*, 1618-1624.

Lafky, J. M., Wilken, J. A., Baron, A. T., and Maihle, N. J. (2008). Clinical implications of the ErbB/epidermal growth factor (EGF) receptor family and its ligands in ovarian cancer. Biochimica et biophysica acta *1785*, 232-265.

Laird, P. W. (2003). The power and the promise of DNA methylation markers. NatRevCancer *3*, 253.

Lau, K. S., Partridge, E. A., Grigorian, A., Silvescu, C. I., Reinhold, V. N., Demetriou, M., and Dennis, J. W. (2007). Complex N-glycan number and degree of branching cooperate to regulate cell proliferation and differentiation. Cell *129*, 123.

Lee, S. W., Fang, L., Igarashi, M., Ouchi, T., Lu, K. P., and Aaronson, S. A. (2000). Sustained activation of Ras/Raf/mitogen-activated protein kinase cascade by the tumor suppressor p53. Proc Natl Acad Sci U S A *97*, 8302-8305.

Lessan, K., Aguiar, D. J., Oegema, T., Siebenson, L., and Skubitz, A. P. (1999). CD44 and beta1 integrin mediate ovarian carcinoma cell adhesion to peritoneal mesothelial cells. AmJPathol *154*, 1525.

Levy, A., Dang, U. C., and Bookstein, R. (1999). High-density screen of human tumor cell lines for homozygous deletions of loci on chromosome arm 8p. Genes ChromosomesCancer *24*, 42.

Lu, Q., Hope, L. W., Brasch, M., Reinhard, C., and Cohen, S. N. (2003). TSG101 interaction with HRS mediates endosomal trafficking and receptor down-regulation. Proceedings of the National Academy of Sciences of the United States of America *100*, 7626-7631.

MacGrogan, D., Levy, A., Bova, G. S., Isaacs, W. B., and Bookstein, R. (1996). Structure and methylation-associated silencing of a gene within a homozygously deleted region of human chromosome band 8p22. Genomics *35*, 55.

Makar, A. P., Kristensen, G. B., Kaern, J., Bormer, O. P., Abeler, V. M., and Trope, C. G. (1992). Prognostic value of pre- and postoperative serum CA 125 levels in ovarian cancer: new aspects and multivariate analysis. ObstetGynecol *79*, 1002.

Mandic, R., Rodgarkia-Dara, C. J., Zhu, L., Folz, B. J., Bette, M., Weihe, E., Neubauer, A., and Werner, J. A. (2006). Treatment of HNSCC cell lines with the EGFR-specific inhibitor cetuximab (Erbitux) results in paradox phosphorylation of tyrosine 1173 in the receptor. FEBS Lett *580*, 4793-4800.

Maxfield, F. R., and McGraw, T. E. (2004). Endocytic recycling. Nat Rev Mol Cell Biol *5*, 121-132.

Miaczynska, M., Pelkmans, L., and Zerial, M. (2004). Not just a sink: endosomes in control of signal transduction. Curr Opin Cell Biol *16*, 400-406.

Momparler, R. L. (2005). Epigenetic therapy of cancer with 5-aza-2'-deoxycytidine (decitabine). SeminOncol *32*, 443.

Ohtsubo, K., and Marth, J. D. (2006). Glycosylation in cellular mechanisms of health and disease. Cell *126*, 855.

Peipp, M., Dechant, M., and Valerius, T. (2008). Effector mechanisms of therapeutic antibodies against ErbB receptors. Curr Opin Immunol *20*, 436-443.

Pennock, S., and Wang, Z. (2003). Stimulation of cell proliferation by endosomal epidermal growth factor receptor as revealed through two distinct phases of signaling. Mol Cell Biol *23*, 5803-5815.

Pils, D., Horak, P., Gleiss, A., Sax, C., Fabjani, G., Moebus, V. J., Zielinski, C., Reinthaller, A., Zeillinger, R., and Krainer, M. (2005a). Five genes from chromosomal band 8p22 are significantly down-regulated in ovarian carcinoma. Cancer *104*, 2417.

Pils, D., Horak, P., Gleiss, A., Sax, C., Fabjani, G., Moebus, V. J., Zielinski, C., Reinthaller, A., Zeillinger, R., and Krainer, M. (2005b). Five genes from chromosomal band 8p22 are significantly down-regulated in ovarian carcinoma: N33 and EFA6R have a potential impact on overall survival. Cancer *104*, 2417-2429.

Pils, D., Pinter, A., Reibenwein, J., Alfanz, A., Horak, P., Schmid, B. C., Hefler, L., Horvat, R., Reinthaller, A., Zeillinger, R., and Krainer, M. (2007a). In ovarian cancer the prognostic influence of HER2/neu is not dependent on the CXCR4/SDF-1 signalling pathway. Br J Cancer *96*, 485-491.

Pils, D., Pinter, A., Reibenwein, J., Alfanz, A., Horak, P., Schmid, B. C., Hefler, L., Horvat, R., Reinthaller, A., Zeillinger, R., and Krainer, M. (2007b). In ovarian cancer the prognostic influence of HER2/neu is not dependent on the CXCR4/SDF-1 signalling pathway. BrJCancer *96*, 485.

Raiborg, C., Malerod, L., Pedersen, N. M., and Stenmark, H. (2008). Differential functions of Hrs and ESCRT proteins in endocytic membrane trafficking. Exp Cell Res *314*, 801-813.

Raiborg, C., Rusten, T. E., and Stenmark, H. (2003). Protein sorting into multivesicular endosomes. Curr Opin Cell Biol *15*, 446-455.

Ricciardelli, C., and Oehler, M. K. (2009). Diverse molecular pathways in ovarian cancer and their clinical significance. Maturitas.

Sandercock, J., Parmar, M. K., Torri, V., and Qian, W. (2002). First-line treatment for advanced ovarian cancer: paclitaxel, platinum and the evidence. British journal of cancer *87*, 815-824.

Scaltriti, M., and Baselga, J. (2006). The epidermal growth factor receptor pathway: a model for targeted therapy. Clin Cancer Res *12*, 5268-5272.

Seales, E. C., Jurado, G. A., Singhal, A., and Bellis, S. L. (2003). Ras oncogene directs expression of a differentially sialylated, functionally altered beta1 integrin. Oncogene *22*, 7137.

Sorkin, A., and Goh, L. K. (2008). Endocytosis and intracellular trafficking of ErbBs. Exp Cell Res *314*, 3093-3106.

Tanaka, N., Kyuuma, M., and Sugamura, K. (2008). Endosomal sorting complex required for transport proteins in cancer pathogenesis, vesicular transport, and non-endosomal functions. Cancer science *99*, 1293-1303.

Tang, D., Wu, D., Hirao, A., Lahti, J. M., Liu, L., Mazza, B., Kidd, V. J., Mak, T. W., and Ingram, A. J. (2002). ERK activation mediates cell cycle arrest and apoptosis after DNA damage independently of p53. J Biol Chem *277*, 12710-12717.

Thompson, B. J., Mathieu, J., Sung, H. H., Loeser, E., Rorth, P., and Cohen, S. M. (2005). Tumor suppressor properties of the ESCRT-II complex component Vps25 in Drosophila. Developmental cell *9*, 711-720.

van der Burg, M. E. (2001). Advanced ovarian cancer. CurrTreatOptionsOncol *2*, 109.

Watson, P., Butzow, R., Lynch, H. T., Mecklin, J. P., Jarvinen, H. J., Vasen, H. F., Madlensky, L., Fidalgo, P., and Bernstein, I. (2001). The clinical features of ovarian cancer in hereditary nonpolyposis colorectal cancer. Gynecologic oncology *82*, 223-228.

Wheeler, D. L., Huang, S., Kruser, T. J., Nechrebecki, M. M., Armstrong, E. A., Benavente, S., Gondi, V., Hsu, K. T., and Harari, P. M. (2008). Mechanisms of acquired resistance to cetuximab: role of HER (ErbB) family members. Oncogene *27*, 3944-3956.

Xia, W., Mullin, R. J., Keith, B. R., Liu, L. H., Ma, H., Rusnak, D. W., Owens, G., Alligood, K. J., and Spector, N. L. (2002). Anti-tumor activity of GW572016: a dual tyrosine kinase inhibitor blocks EGF activation of EGFR/erbB2 and downstream Erk1/2 and AKT pathways. Oncogene *21*, 6255-6263.

Xu, X. L., Yu, J., Zhang, H. Y., Sun, M. H., Gu, J., Du, X., Shi, D. R., Wang, P., Yang, Z. H., and Zhu, J. D. (2004). Methylation profile of the promoter CpG islands of 31 genes that may contribute to colorectal carcinogenesis. World JGastroenterol *10*, 3441.

Xu, Z., Liang, L., Wang, H., Li, T., and Zhao, M. (2003). HCRP1, a novel gene that is downregulated in hepatocellular carcinoma, encodes a growth-inhibitory protein. Biochem Biophys Res Commun *311*, 1057-1066.

Xue, W., Krasnitz, A., Lucito, R., Sordella, R., Vanaelst, L., Cordon-Cardo, C., Singer, S., Kuehnel, F., Wigler, M., Powers, S.*, et al.* (2008). DLC1 is a chromosome 8p tumor suppressor whose loss promotes hepatocellular carcinoma. Genes Dev *22*, 1439-1444.

Yang, Z., Bagheri-Yarmand, R., Wang, R. A., Adam, L., Papadimitrakopoulou, V. V., Clayman, G. L., El-Naggar, A., Lotan, R., Barnes, C. J., Hong, W. K., and Kumar, R. (2004). The epidermal growth factor receptor tyrosine kinase inhibitor ZD1839 (Iressa) suppresses c-Src and Pak1 pathways and invasiveness of human cancer cells. Clin Cancer Res *10*, 658-667.

Yap, T. A., Carden, C. P., and Kaye, S. B. (2009). Beyond chemotherapy: targeted therapies in ovarian cancer. Nature reviews *9*, 167-181.

Yogeeswaran, G., and Salk, P. L. (1981). Metastatic potential is positively correlated with cell surface sialylation of cultured murine tumor cell lines. Science *212*, 1514.

Yoshida, T., Okamoto, I., Okabe, T., Iwasa, T., Satoh, T., Nishio, K., Fukuoka, M., and Nakagawa, K. (2008). Matuzumab and cetuximab activate the epidermal growth factor receptor but fail to trigger downstream signaling by Akt or Erk. Int J Cancer *122*, 1530-1538.

Zandi, R., Larsen, A. B., Andersen, P., Stockhausen, M. T., and Poulsen, H. S. (2007). Mechanisms for oncogenic activation of the epidermal growth factor receptor. Cell Signal *19*, 2013-2023.

Zhang, W., and Liu, H. T. (2002). MAPK signal pathways in the regulation of cell proliferation in mammalian cells. Cell Res *12*, 9-18.

6 Side Project:

BAMBI Translocates into the Nucleus after TGF-ß Treatment, Promotes Oncogenic characteristics *In-vitro* but without Negative Impact on Patient Outcome in Ovarian Cancer

Dietmar Pils[1], Michael Wittinger[1], Michaela Petz[1], Alfred Gugerell[1], Wolfgang Gregor[2], Angela Alfanz[1], Thomas Pangerl[1], Peter Horak[1], Reinhard Horvat[3], Robert Zeillinger[4], Wolfgang Mikulits[5], Michael Krainer[1]

[1]Department of Internal Medicine I, Division of Oncology, Medical University of Vienna, Austria,
[2]Research Group of Molecular Pharmacology and Toxicology, University of Veterinary Medicine Vienna, Austria,
[3]Clinical Pathology, Medical University of Vienna, Austria,
[4]Department of Obstetrics and Gynecology, Division of Gynecology, Medical University of Vienna, Austria.
[5]Department of Internal Medicine I, Division: Inst. of Cancer Research, Medical University of Vienna, Austria.

Correspondence: Professor M. Krainer and Dr D. Pils, Department of Internal Medicine I, Division of Oncology, Medical University of Vienna, A-1090 Vienna, Austria.

E-mails: michael.krainer@meduniwien.ac.at and dietmar.pils@univie.ac.at

RUNNING TITLE: BAMBI modulates TGF-ß signalling in ovarian cancer

KEYWORDS: TGF-ß signalling; BAMBI; NMA; Ovarian cancer; Co-translocation; Signaltransduction

6.1 Abstract

TGF-ß signalling via Smads plays a central role in carcinogenesis. *BAMBI* was initially described as pseudoreceptor antagonizing TGF-ß receptor activation thus impairing signalling. We demonstrate for the first time a nuclear cotranslocation of BAMBI with Smad2/3 upon TGF-ß treatment employing intracellular localisation experiments.

Overexpression of *BAMBI* led to increased proliferation, migration, and resistance to TGF-ß-mediated apoptosis. Although – *prima facie* – this fits to the thesis of BAMBI as pseudoreceptor, it could also be explained by modulation of TGF-ß signalling in the nucleus, leading to the observed pro-oncogenic properties. The tumor promoting impact of *BAMBI* mRNA expression *in vitro* could not be confirmed in primary tumor samples. Whereas nearly all tumor samples showed up-regulation of BAMBI compared to undetectable BAMBI in healthy ovarian epithelia no impact of BAMBI expression on overall survival could be observed. These findings suggest a more complex view of Smad-mediated transcription regulation, including BAMBI as novel modulator.

6.2 Introduction

Epithelial ovarian cancer is the most lethal gynecologic malignancy and with about six percent the fourth most frequent cause of cancer-related death of women in western countries. Estimates indicate that one of 70 women will develop ovarian cancer in her lifetime with a median survival rate of approximately 4.5 years. Recent cancer statistics estimated 22,430 new cases and 15,280 deaths per year in the United States (Jemal et al. 2007).

Loss of accurate response to growth inhibiting signals, such as transforming growth factor (TGF)-ß occurs frequently during cancerogenesis. TGF-ß affects various cellular processes including regulation of differentiation, migration, apoptosis, and proliferation of epithelial cells (Massague et al. 2000b; Bierie and Moses 2006c). The three TGF-ß isoforms (TGF-ß1, TGF-ß2 and TGF-ß3) recognize type I, II, and III TGF receptors (TGF-ßRI, TGF-ßRII and betaglycan or endoglin, respectively) to initiate signalling via the activation of transcriptional co-regulators named Smads (Bierie and Moses 2006b). In detail, activation of the TGF-ßRI triggers Smad2 and Smad3 phosphorylation which subsequently translocate from the cytoplasm to the nucleus as a complex with Smad4. Interacting with specific DNA binding sites they induce or repress the transcription of corresponding target genes (Miyazono et al. 2000).

The functional TGF-ßRII/TGF-ßRI heteromeric signalling complex is is described as tumor promoter acting via SMAD-dependent but also alternative pathways(Siegel and Massague 2003; Derynck and Zhang 2003; Moustakas and Heldin 2005; Barrios-Rodiles et al. 2005). Smad-independent TGF-regulated networks include signalling mocules like RHOA, cell division cycle 42 (CDC42), RAC1, Ras, phosphatidylinositol 3-kinase (PI3K), protein phosphatase 2A (PP2A), mitogen-activated protein kinase

kinase kinase 1 (MAP3K1, also known as MEKK1), TGF-activated kinase 1 (TAK1) (Bierie and Moses 2006a).

Resistance against antiproliferative effects of TGF-ß signalling contributes to the development of many epithelial cancers (Massague et al. 2000a; Gotzmann et al. 2004), including ovarian cancer (Yamada et al. 1999; Baldwin et al. 2003; Nilsson and Skinner 2002; Rodriguez et al. 2001). Although accumulating knowledge concerning TGF-ß resistance is available, the mechanisms are poorly understood in ovarian cancer. Recently, Sunde et al. found a number of genes involved in TGF-ß signalling which are differentially expressed in ovarian cancer specimens compared to normal ovarian surface epithelium. In particular, genes that inhibit TGF-ß signalling were up-regulated in advanced-stage ovarian cancers while genes that enhance TGF-ß signalling were down-regulated (Sunde et al. 2006).

The pseudoreceptor BAMBI (BMP and activin membrane-bound inhibitor), formerly also called NMA, is known inhibitor of the TGF-ß signalling pathway (Sekiya et al. 2004a; Onichtchouk et al. 1999d; Degen et al. 1996; Sekiya et al. 2004d). BAMBI exhibits structural homology to TGF-ßRI but lacks an intracellular kinase domain (Onichtchouk et al. 1999c).

Expression of *BAMBI* has been shown to be aberrantly elevated in most colorectal and hepatocellular carcinomas, caused by ß-catenin signalling (Sekiya et al. 2004b). In HepG2 hepatoma cells, transcription of *BAMBI* is regulated via a feedback loop which confers binding of Smad3 and Smad4 to the Smad-responsive elements of the *BAMBI* promoter (Sekiya et al. 2004c).

The significance of TGF-ß signalling raised the question of the function of BAMBI in ovarian cancer. Thus, we characterised the role of BAMBI in an ovarian cancer cell line and evaluated the impact of *BAMBI* expression on ovarian cancer patients outcome.

6.3 Results

6.3.1 Generation and Analysis of BAMBI Overexpressing SKOV3 Cells

We employed the ovarian cancer cell line SKOV3 because of its low endogenous *BAMBI* expression. For overexpression of *BAMBI* the full length ORF of *BAMBI* was cloned into the pLP-IRESneo vector. This construct or the empty vector as control were stably transfected into SKOV3 cells and *BAMBI* expression was determined. On the mRNA level the SKOV3 BAMBI clone showed a 35.5-fold overexpression compared to the SKOV3 control cell line (Co) (Fig. 1A) which resulted in a clearly visible BAMBI band on Western blots (Fig. 1B). *BAMBI* overexpression significantly enhanced cellular proliferation (doubling time -37.0%, P=0.010; Fig. 1C) as well as increased migration capability in trans-well migration assays (+581.2%, P=0.004) compared to the control (Fig. 1D). Interestingly, altered migration was not associated with a morphologic phenotype as shown by HE and phalloidin staining for F-actin (Fig. 1G) The relatively low invasiveness of the SKOV3 cell line in matrigel invasion assays was not essentially affected by BAMBI overexpression (Fig. 1E). Supplementation with 2.5 ng ml^{-1} TGF-ß resulted in a 7.6% inhibition of proliferation in the control cells, whereas SKOV3 BAMBI cells were not affected (Fig. 1F). Apoptosis as detected by FACS analysis with Annexin V-FITC decreased from 30% in the SKOV3 Co cells to 7% in the SKOV3 BAMBI cells upon induction by TGF-ß (data not shown). In another cell line with low endogenous BAMBI expression, MDAH 2774, proliferation decreased significantly (26.7%, P=0.005) upon TGF-ß supplementation, consistent with enhanced TGF-ß sensitivity (9.8% and 19.0% apoptosis in the absence and presence of TGF-ß, respectively, corresponding to an increase of +93.9%) (data not shown).

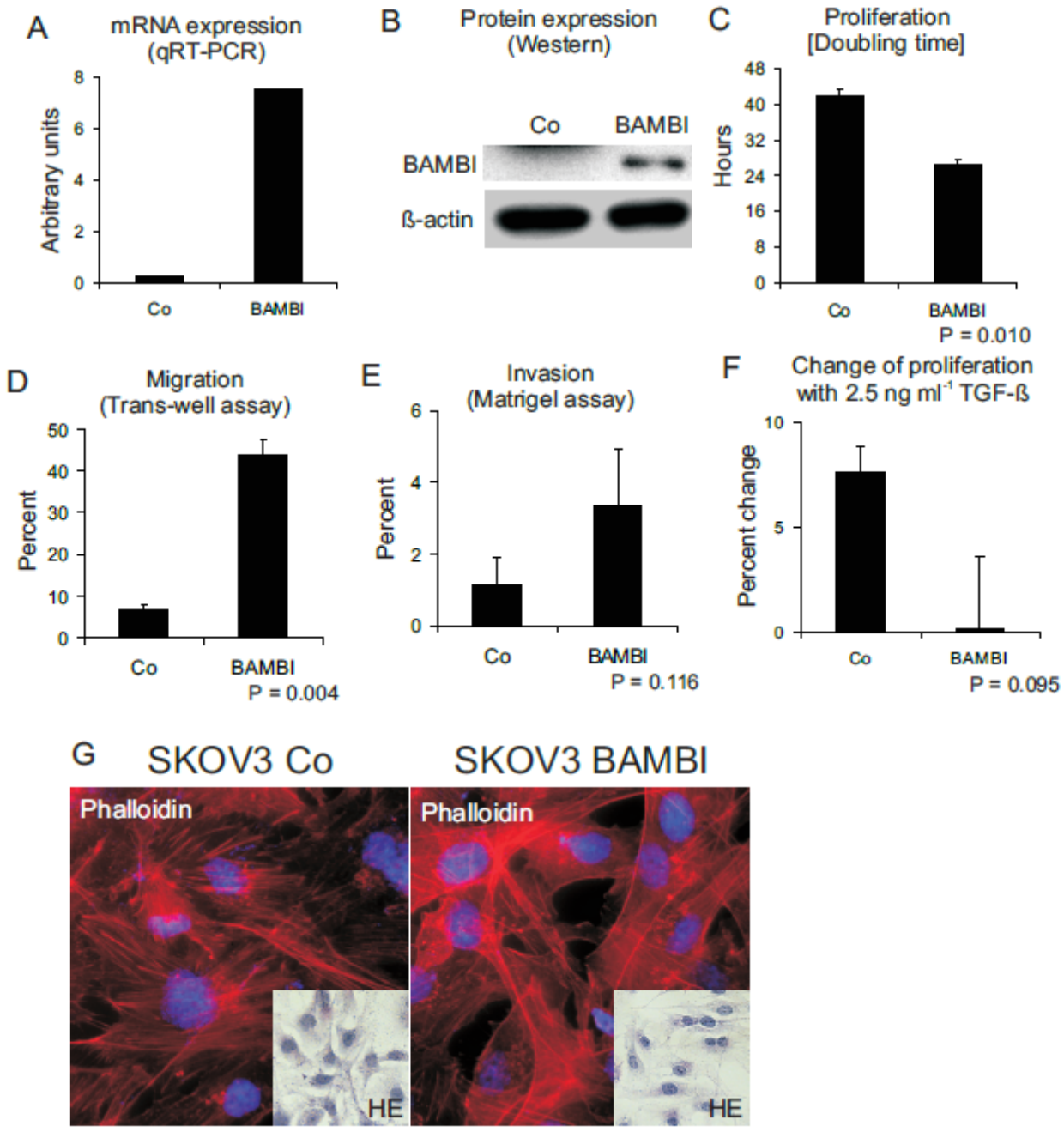

Figure 1 In vitro characterization of the BAMBI-overexpressing SKOV3 cells. Relative BAMBI mRNA (A) and BAMBI protein levels (B) were higher in SKOV3 BAMBI cells as compared to SKOV3 control (Co) cells. Upon BAMBI overexpression proliferation (C) as well as migration rates (D) increased significantly, whereas increase in invasion was not significant (E). Sensitivity to growth inhibition by TGF-ß was reduced in the SKOV3 BAMBI cells compared to SKOV3 Co cells (F). Stain for whole cell morphology (hematoxylin and eosin, HE) and for F-actin (phalloidin with DAPI as counterstain) (G). Data are given in mean and standard deviations of triplicate experiments.

6.3.2 TGF-ß Signalling in Ovarian Cancer Cell Lines and Intracellular Localization of BAMBI

Canonical TGF-ß signalling leads to phosphorylation of Smad2 and Smad3 proteins, which translocate together with Smad4 into the nucleus. The impact of *BAMBI* overexpression on this process was investigated by immunocytochemical staining of BAMBI and Smad2/3 proteins. As expected, Smads translocate into the nucleus upon stimulation of the cells with TGF-ß for 10 minutes, exhibiting decreased cytoplasmic and increased nuclear staining intensities. Interestingly, elevated nuclear staining of BAMBI in TGF-ß-treated cells indicates a cotranslocation with Smads (Fig. 2). Since BAMBI was described as pseudoreceptor with a transmembrane region directly binding to TGF-ß (Onichtchouk et al. 1999b) this result was highly unexpected.

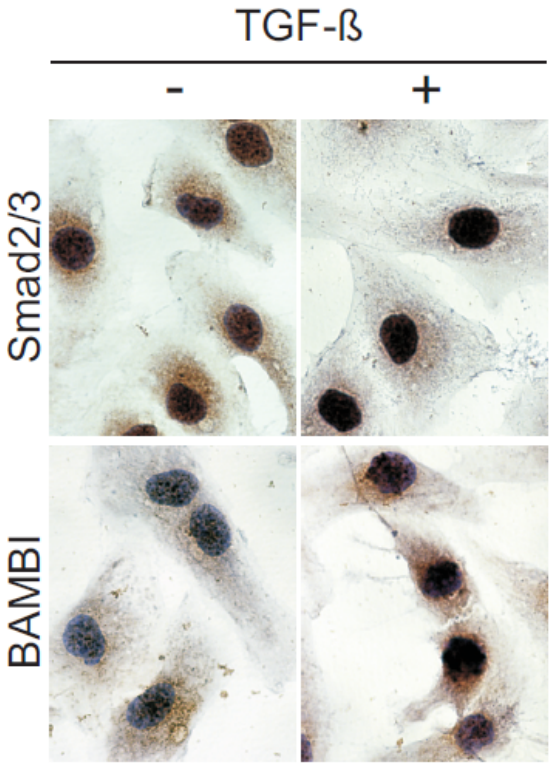

Figure 2 Regulation of *BAMBI* mRNA expression by TGF-ß in MDAH 2774 clones. MDAH clones with initially low (MDAH Co) or high (MDAH BAMBI) *BAMBI* expression levels were grown in triplicates in the presence of different concentrations of TGF-ß, resulting in a concentration-dependent and significant upregulation of *BAMBI* transcripts.

In order to verify this this observation and eleminating localization artefacts from *BAMBI* overexpression in the SKOV3 BAMBI clone, this experiment was confirmed by immunofluorescent colocalization experiments on another ovarian cancer cell line

with substantial endogenous *BAMBI* expression, namely H134. Again, cytoplasmic BAMBI as well as Smad2/3 diminished and accumulated in the nucleus upon TGF-ß treatment (Fig. 3A), corroborating the finding of BAMBI and Smad cotranslocation in the SKOV3 BAMBI cells. Consistent with the translocation of Smads into the nucleus, staining of phosphorylated Smad2 (p-Smad2) exhibited high p-Smad2 levels in the nucleus upon TGF-ß treatment whereas staining was nearly undetectable in untreated cells (Fig. 3A), indicating traditional TGF-ß signalling including phosphorylation of the Smads.

Since unspecific nuclear staining by fluorescent conjugates could provide artefacts, localisation of BAMBI was further analyzed by immunoblotting of subcellular fractions.

Therefore, purified fractions of the nuclei, the microsomes (with a minor contribution of cytoplasmic membranes), and the soluble cytoplasm were prepared from the H134 and MDAH 2774 cell lines (to avoid over-expresion artefacts not from SKVO3 BAMBI). Western blots were probed for nucleoporin p61 as a nuclear marker and ß-actin as a cytoplasmic marker as fraction quality controls.

Upon TGF-ß stimulation, Smad2 and Smad3 translocate to the nucleus together with BAMBI in a nearly stoichiometrical ratio in both cell lines (Fig. 3B), substantiating our immunocytochemical and immunofluorescence staining experiments.

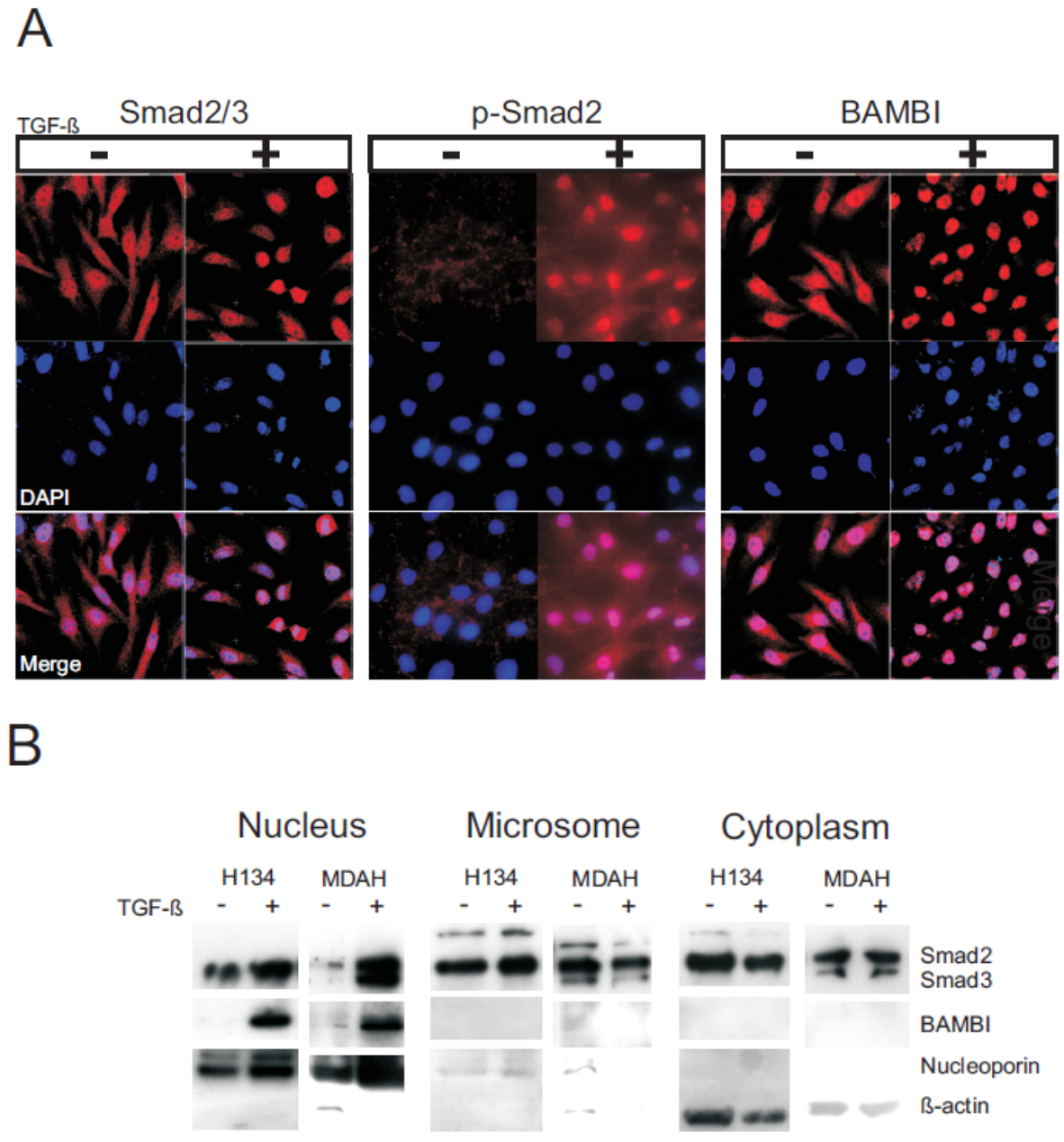

Figure 3 Smad2/3-BAMBI-cotranslocation in H134 and MDAH 2774 clones. Immunofluorescence staining for Smad2/3 and BAMBI in H134 cells revealed a shift of fluorescence from the cytoplasm to the nucleus upon treatment with TGF-ß (counterstained with DAPI) (A). Western blot analysis of subcellular fractions of both MDAH 2774 clones and H134 cells (B). The quantity of subcellular fractions was evaluated by staining with the nuclear and cytoplasmic markers nucleoporin p61 and ß-actin, respectively. Smad2/3 and BAMBI levels in the nuclear fraction increased significantly upon treatment of the cells with TGF-ß, for both MDAH 2774 clones even in a nearly stoichiometric ratio. (Band intensities before TGF-ß treatment were set to unity and the calculation was performed on a longer-exposed film after normalization to the nucleoporin band intensities. In the H134 cells we could not detect BAMBI in the nucleus before incubation with TGF-ß, therefore no calculation was possible).

6.3.3 BAMBI mRNA Expression in 69 Ovarian Cancer Samples and Correlation with Clinicopathologic Parameters

Next we addressed the question if BAMBI expression has the potential to influence survival rates of ovarian cancer patients. Therefore we quantified the BAMBI mRNA of 69 ovarian cancer patients relative to ß-2-microglobulin by RT-qPCR. Clinicopathologic characteristics of the patients are shown in Table 2. The tumor samples represent a typical distribution of ovarian cancer patients frequenting a university hospital. In particular, 74% of tumors were of serous type and 68% of patients displayed an advanced stage of tumor progression (FIGO III and IV). The mean follow up time was 20.6 months with 25% of cases of death. We observed no significant *BAMBI* mRNA expression variations between any groups of histological type, FIGO stage, Grade, or in patients without recurrences compared to patients with recurrences or progressive disease (Table 2). Kaplan-Meier estimation showed no difference in overall survival if samples were divided into three groups at the 33.3 and 66.6 percentile (Fig. 5), nor after dichotomisation at the. median, 25% or 75% percentiles, respectively. On the other hand, the FIGO stage – one of the strongest predictive clinical parameters – showed a clear significant impact on overall survival according to Kaplan-Meier estimates (Fig. 5). Multivariate analysis using different or all of the clinicopathologic parameters as given in Table 2 together with *BAMBI* expression never revealed a significant impact of *BAMBI* expression on overall survival (data not shown).

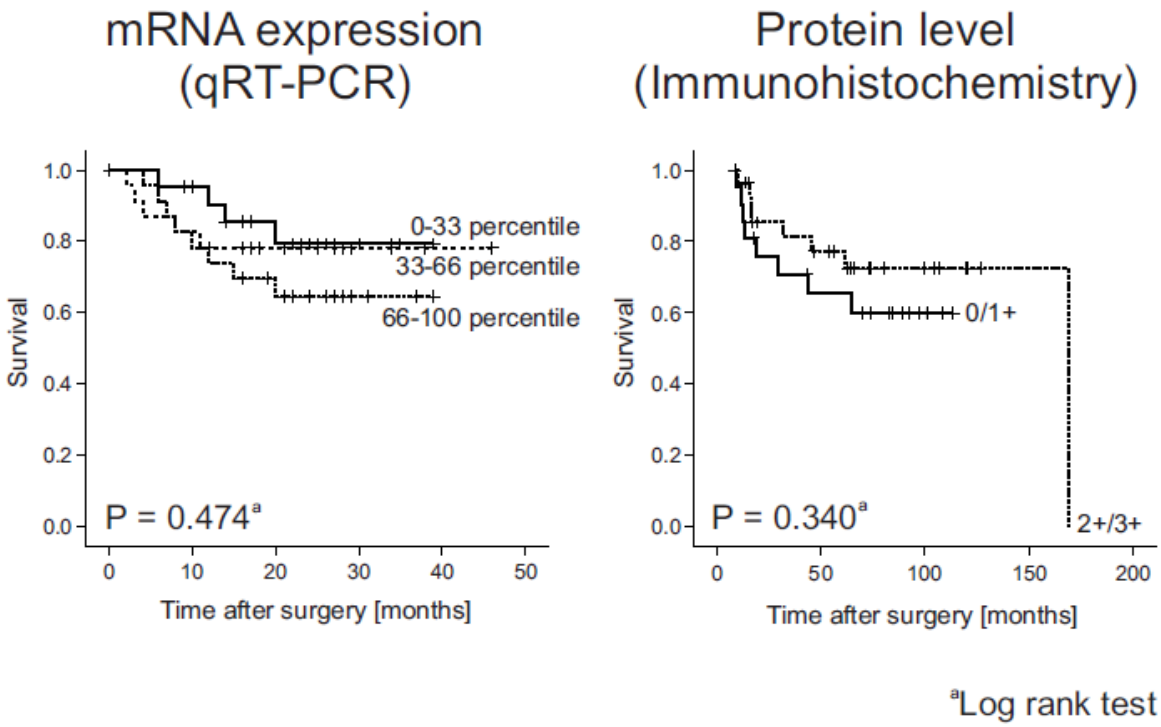

Figure 5 Impact of mRNA and protein levels of BAMBI on patient outcome. *BAMBI* mRNA or protein levels were obtained from independent patient cohorts by qRT-PCR or immunohistochemistry, respectively. As expected, FIGO stages had significant impact on patient overall survival in both patient cohorts, but neither mRNA expression levels (divided into three categories according to the 33.3 and 66.6 percentile) nor protein levels (dichotomized into two groups, 0/1+ compared to 2+/3+, see Fig. 5) had negative impact on overall survival.

Ovarian tumor samples (qRT-PCR)	69	Mean (±SD)
Age at diagnosis [mean in years (range)]	57.9 (36 – 86)	
Follow-up [mean in months (range)]	20.6 (0.0 – 46.0)	P = 0.757[a]
Alive	52 (75.4%)	0.168 (±0.927)
Dead	17 (24.6%)	0.020 (±0.032)
Histology		P = 0.520[b]
Serous	51	0.0361 (±0.098)
Endometrioid	7	0.0544 (±0.102)
Mucinous	4	1.689 (±3.328)
Clear cell	2	0.010 (±0.009)
other (e.g. mixed)	5	0.013 (±0.018)
FIGO		P = 0.819[b]
I	15	0.063 (±0.161)
II	7	0.064 (±0.105)
III	31	0.239 (±1.197)
IV	16	0.016 (±0.021)
Grade		P = 0.642[b]
1	1	0.006
2	34	0.230 (±1.142)
3	34	0.131 (±0.805)
Recurrences (1 missing)		P = 0.378[a]
w/o recurrence	35	0.240 (±1.127)
w/ recurrence	22	0.014 (±0.017)
Progressive disease	11	0.028 (±0.038)

Table 2 mRNA expression of *BAMBI* and correlation with clinicopathologic characteristics of 69 primary ovarian tumor tissues.

6.3.4 BAMBI Protein Expression in Four Normal and 51 Ovarian Tumor Tissues and Correlation with Clinicopathologic Parameters

To assess the impact of BAMBI on patient outcome on the more disease-relevant protein level, we performed immunohistochemical staining of 51 paraffin-embedded ovarian tumor tissues, which did not overlap with the pattient cohort of the mRNA expression study. In addition, four paraffin-embedded normal ovaries (two pre-menopausal and two post-menopausal) were used as references. Distribution of clinicopathologic characteristics was representative for ovarian cancer patients frequenting an university hospital, namely 63% had a serous type cancer histology and 65% were in late stages (FIGO III and IV). The mean follow-up time was 60.6 months with 16 cases of death (31.4%). BAMBI localized to the cytoplasmic and

nuclear cellular compartment and was uniformly distributed within the tumor. Consequently, we classified the staining of tumor tissues solely according to staining intensity into 4 groups (‘0’ virtually no staining, ‘1+’ weak staining, ‘2+’ intermediate staining, and ‘3+’ strong staining) (Fig. 4). Whereas BAMBI was undetectable in all of the controls, we observed a positive staining in 48 out of 51 tumor tissues, indicating that *BAMBI* overexpression in ovarian cancer is a relatively common event. Frequencies of staining intensities are outlined in Table 3. However, we detected no differential staining intensities between tumors of different histologies, different FIGO stages, or different Grades. Equally *BAMBI* mRNA expression, protein staining intensities did not influence overall survival rates in univariate or multivariate analysis when patients were dichotomized in 0/1+ and 2+/3+ staining intensities (Fig. 5). The only significant predictor of overvall survival was again FIGO stage (Fig. 5).

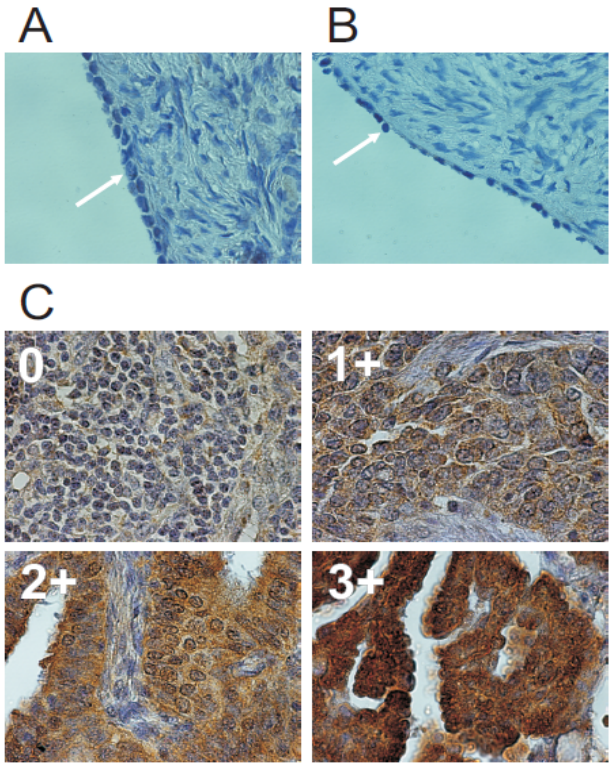

Figure 4
Immunohistochemical staining of BAMBI in normal and malignant ovarian tissues. Pre-menopausal (A) and post-menopausal (B) ovarian surface epithelial cells (arrows) displayed no detectable BAMBI levels. BAMBI staining intensities of malignant ovarian tumor tissues were uniform and therefore classified solely according to their staining intensities into four groups (0, 1+, 2+, and 3+) (C).

6.4 Discussion

During the course of carcinogenesis TGF-ß signalling is frequently altered to overcome its antiproliferative effect. Six serin/threonine kinase receptors (TßRI-III, ActR-IB, BMPR-IA/IB) are known to mediate TGF-ß signalling which is involved in diverse cellular functions. BAMBI has been described as a protein with weak homology to TGF-ß receptors, containing a membrane domain but no active kinase domain. Co-immunoprecipitation experiments revealed interactions between BAMBI and most of the TGF-ß receptors leading to inhibition of functional TGF-ß type I- and type II-complex formation, thus impairing downstream signalling events, as shown by several reporter gene assays (Onichtchouk et al. 1999a).

Upon *BAMBI* overexpression in the ovarian cancer cell line SKOV3 all examined *in vitro* physiological parameters point to enhanced oncogenic characteristics: significantly increased proliferation, migration, (invasion, albeit not significant), and decreased sensitivity to TGF-ß-mediated growth inhibition.

Translocation of phosphorylated Smad2/3 into the nucleus upon activation of TGF-ß receptors provides a simple and direct model for investigation of BAMBI function as an inhibiting pseudoreceptor. Therefore we performed immunostained BAMBI, Smad2/3, and p-Smad2 in TGF-ß-treated cells (Figs 2 and 3A). Surprisingly, TGF-ß-mediated Smad2/3 translocation and Smad2 phosphorylation was not impaired by BAMBI (over)expression (Fig. 2 and 3). Even more unexpectedly, increased amounts of BAMBI were observed in TGF-ß-treated cells by immunocytochemical as well as immunofluorescenc staining experiments (Fig. 2, 3A), together indicating a co-translocation of Smads and BAMBI into the nucleus. In order to verify this novel finding and to get some quantitative information about the putative TGF-ß-induced Smad-BAMBI co-translocation, we performed Western blotting analysis of subcellular fractions. As demonstrated in Fig. 3B, Smad2/3 accumulated in the nuclear fraction

together with a nearly proportional amount of BAMBI upon TGF-ß treatment, proving the model of Smad-BAMBI co-translocation in ovarian cancer cells.

Although we could show that BAMBI is involved in TGF-ß signalling, we propose that BAMBI modulates rather than inhibits TGF-ß signalling. This conclusion is further supported by the very weak homology between TGF-ß superfamily receptors and BAMBI. Amino acid identities vary between 6.1 (to BmprIA) and 9.1 (to BmprIB) percent. Values above 10% are commonly considered to allow functional predictions of homologous proteins. Other pseudoreceptor systems show significant higher homologies (e.g. TRAIL receptors DR4 and DR5 compared to their pseudoreceptors DcR1 and DcR2 showed amino acid identities between 21.9% and 45.9%). Intriguingly, the only BAMBI interaction partner found by protein-protein interaction screenings so far was SOX30, a known transcription factor containing a HMG box DNA-binding domain (Rual et al. 2005).

Since the *in vitro* characterization of the *BAMBI* overexpression models suggest a pro-oncogenic effect, we evaluated the impact of *BAMBI* expression on ovarian cancer patient outcome. *BAMBI* mRNA and protein levels were assessed using quantitative real time RT-PCR and immunohistochemistry staining of ovarian tumor and normal ovarian tissues. Human ovarian epithelial cells (HOSE) from two pre-menopausal and two post-menopausal ovarian sections showed no staining (Fig. 4A and B), indicating that *BAMBI* expression is not detectable in HOSE cells. However, *BAMBI* expression was detectable in 94% of 51 tumor samples (Fig. 4C), showing that *BAMBI* overexpression is a common event in ovarian cancerogenesis. Staining intensities – classified in four groups – did not correlate with any clinicopathologic parameters (Table 3). Despite the frequent event of *BAMBI* mRNA and protein overexpression in ovarian tumors and indications for oncogenic activities *in vitro*,

BAMBI staining intensities had no impact on overall survival of patients (Fig. 5, Table 2).

As conclusion, BAMBI – initially described as a pseudoreceptor, inhibiting TGF-ß superfamiliy signalling – a) cotranslocates together with Smads into the nucleus upon TGF-ß treatment of the cells, b) modulates rather than inhibits TGF-ß signalling, c) is overexpressed in nearly all ovarian cancer tissues, d) rendering a new non-prognostic tumor marker without impact on patient outcome.

The very weak homology of BAMBI to its corresponding receptors, the absent overlap of TGF-ß and BAMBI regulated genes, and the nuclear localisation of BAMBI upon TGF-ß treatment raises the interesting question whether BAMBI functions as a novel modulator of Smad-mediated transcriptional regulation which warrants further investigations.

6.5 Materials and Methods

6.5.1 Cell lines, BAMBI Cloning, and Transfection of SKOV3

The human ovarian carcinoma cell lines MDAH 2774 was cultured in RPMI medium with 10% FCS (fetal calf serum), 50 units ml^{-1} penicillin G, and 50 µg ml^{-1} streptomycin sulfate at 37°C in a humidified atmosphere of 95% air with 5% CO_2. SKOV3, SKOV3 Co, and SKOV3 BAMBI cells were cultured in McCoy's medium supplemented with 10% FCS, 50 units ml^{-1} penicillin G, and 50 µg ml^{-1} streptomycin sulfate. Selection of stable transfectants was archieved by growth in the presence of 200 µg ml^{-1} G418 and subculturing with 100 µg ml^{-1} G418. Growth with TGF-ß was performed in growth medium supplemented with 1 or 2.5 ng ml^{-1} TGF-ß for at least one week with medium change every second day. For *BAMBI* overexpression, the full length ORF of *BAMBI* (acc. no. BC019252) was cloned from the vector pOTB7 (*Sma* I, *Xho* I) into the pLP-IRES neo vector (*Eco R*V). This construct and pLP-

IRESneo as a control were transfected into SKOV3 cells using Lipofectamine 2000 (Invitrogen, Carlsbad, CA, USA). Stable clones were selected, picked and subcultured.

6.5.2 Patient Material

For mRNA expression analysis, ovarian tumor samples from primary tumors and corresponding clinicopathologic parameters were obtained from 69 patients who underwent optimal debulking surgery at the Charité hospital in Berlin, Germany. For immunohistochemical studies on paraffin-embedded tissues, 51 ovarian tumor samples were obtained from ovarian tumor patients at primary diagnosis who underwent optimal debulking surgery, and four normal ovaries were obtained from patients without malignant disease, both surgically removed at the Medical University of Vienna (AKH). Relevant clinical information was collected, and tissue samples and clinical data anonymized. Informed consent for the scientific use of biological material was obtained from all patients in accordance to the requirements of the ethics committee of the institutions involved.

6.5.3 Phenotypical Characterization of Cell Lines

Expression of *BAMBI* was measured by quantitative real time RT-PCR essentially as described previously (Pils et al. 2005) using the TaqMan® Gene Expression Assays Hs00180818_m1 for BAMBI, and Hs99999909_m1 for HPRT1 or Hs99999907_m1 for beta-2-microglobulin as house-keeping controls (Applied Biosystems, Foster City, CA, USA). Expression is given in arbitrary units. For the BAMBI Western blot analysis, 30 µg of total protein prepared with RIPA^{+}-buffer was separated by 12% SDS-PAGE and blotted on PVDF membranes. The antibodies used were: monoclonal mouse anti-BAMBI (Abnova corp., Taipei, Taiwan) in a 1:400 dilution, polyclonal goat anti-mouse HRP-conjugate (Calbiochem, Darmstadt, Germany) in a

1:10,000 dilution, and rabbit anti-actin HRP-conjugate (Santa Cruz Biotechnology, Santa Cruz, CA, USA) in a 1:500 dilution.

Proliferation (doubling time) was measured in triplicates by subsequent cultivation and cell counting by CASY cell counter (Innovatis AG, Bielefeld, Germany). Doubling time (t_d) was calculated as follows: $\mu=(\ln(x_t)-\ln(x_0))/t$, $t_d= \ln(2)/\mu$ (x_t, cell number at time t; x_0, cell number at start of experiment; t, duration of experiment).

Migration and invasion assays were performed in a 24-well plate trans-well system (BD Biosciences, San Jose, CA, USA). For migration and invasion assays, 2.5 10^4 cells were seeded in triplicates on the 8.0 µm pore size control chambers for migration and the BD Matrigel invasion chambers (pore size: 8.0 µm) for invasion. 30% FCS was used as chemoattractant. After 24 h incubation cells from both sides of the membrane were trypsinised, harvested and reseeded in 96-well plates in appropriate densities. After 4 h of cell-settlement, cell numbers were estimated by the Cell Titer-Blue® cell viability assay, based on conversion of resazurin to fluorescent resorufin (Promega, Madison, WI, USA). Results were given in percent calculated as follows: after subtraction of blank values, the fluorescence ($560_{Ex}/595_{Em}$ nm) in cells from the lower side of the membrane (corresponding to the migrated/invaded cells) was divided by the sum of fluorescence values in cells from both sides of the filter (corresponding to all seeded cells) and multiplied with 100.

6.5.4 Immunocytochemical and Immunohistochemical Staining

For immunocytochemical staining cells were grown overnight on sterile four-well Lab-Tek™ Chamber Slides™ (Nagle Nunc International, Rochester, NY, USA). After washing with PBS, cells were fixed in 3% formaldehyde/PBS for 20 minutes at room temperature and permeabilized with 0.5% Triton X-100/PBS for five minutes. Endogenous peroxidase activity was blocked by a ten minute incubation with 3% H_2O_2/PBS. Subsequently, cells were blocked for 30 minutes with 0.2% fish

gelatine/PBS and incubated with the primary antibody diluted in 0.2% fish gelatine/PBS for 60 minutes at room temperature. Dilutions in 0.2% fish gelatine/PBS of primary antibodies were as follows: anti-BAMBI, 1:200; anti-Smad2/3 (BD Biosciences, San Jose, CA, USA), 1:100. After washing with PBS, biotin-conjugated secondary antibody goat-anti mouse, 1:200 in 0.2% fish-gelatine/PBS (BA9200, Vector Laboratories, Burlingame, CA, USA) was applied for 30 minutes followed by incubation with the streptavidin ABComplex-HRP (ABC-Kit from Dako, Glostrup, Denmark) for 45 minutes and subsequent DAB+ (Dako) staining performed according to the manufacturer's instruction. Finally cells were stained with hematoxyline/eosin and mounted in Eukitt (O. Kindler GmbH, Freiburg, Germany). Microscopy was performed on an Olympus BX50 upright light microscope (Olympus Europe, Hamburg, Germany) equipped with the Soft Imaging system CC12.

For immunohistochemical staining (Pils et al. 2007), 5 µm paraffin sections of the paraffin-embedded tissues were deparaffinized with xylenes and rehydrated by incubation in serial dilutions of ethanol. Subsequently, antigen retrieval was performed based on a citrate buffer protocol (incubation in 1:20 diluted citrate buffer (pH 9) DEPP-9 (Eubio, Vienna, Austria) at 96°C for 20 minutes). Sections were treated with 3% H_2O_2/PBS (pH 7.4) to quench endogenous peroxidases and blocked with 10% normal goat serum for 30 min. Afterwards the sections were incubated with monoclonal mouse anti-BAMBI antibody at a 1:200 dilution in 10% serum at RT for 60 minutes. After washing with PBS, biotin-conjugated goat anti-mouse antibody (BA9200, Dako, Carpinteria, CA, USA) was applied at a 1:200 dilution in 10% serum/PBS for 30 minutes, followed by washing and incubation with the streptavidin ABComplex-HRP (ABC-Kit, Dako) for 45 minutes. Finally DAB+ (Dako) staining was performed for 10 minutes according to the manufacturer's instruction. Meyer's

hematoxyline was used for counterstaining the nuclei. Staining intensities were rated by two individual physicians under the supervision of a pathologist.

6.5.5 Immunofluorescence Staining

Cells were grown overnight on sterile polystyrene slides (Nagle Nunc International, Rochester, NY, USA). After washing with PBS, cells were fixed in 3% formaldehyde/PBS for 20 minutes at room temperature and permeabilized with 0.5% Triton X- 100/PBS for 5 minutes. Subsequently, cells were blocked for 30 minutes with 0.2% fish gelatine/PBS and incubated with the primary antibody diluted in 0.2% fish-gelatine/PBS for 60 minutes at room temperature. Dilutions of primary antibodies were as follows: mouse anti-BAMBI, 1:100; mouse anti-Smad2/3, 1:100; mouse anti-p-Smad2 (Millipore Corporation, Billerica, MA, USA), 1:100; rabbit anti-calnexin (personal gift of Dr. Ivessa), 1:200; and rhodamine-phalloidin (Invitrogen, Carlsbad, CA, USA), 1:75. Cye-dye-conjugated secondary antibodies (The Jackson Laboratories, Bar Harbor, ME, USA) were applied for 45 minutes at room temperature at a dilution of 1:100 in 0.2% fish gelatine/PBS. Nuclei were stained by incubation with DAPI (Sigma-Aldrich, St. Louis, MO, USA) or ToPro3 (Invitrogen) together with the secondary antibody dilutions. Conventional microscopy was performed on an Olympus BX50 upright light microscope (Olympus Europe, Hamburg, Germany) equipped with the Soft Imaging system F-View for fluorescence image acquisition.

6.5.6 Subcellular Fractionation and Western Blotting Analysis

Cells grown in T75 flasks were rinsed with 5 ml PBS, harvested in RPMI medium with a rubber policeman and collected at 270 g_{max} for 10 minutes. The cells were resuspended in medium and treated with 20 ng ml^{-1} TGF-□ for 9 minutes at room temperature. Then the cells were immediately harvested at 4300 g_{max} and 4°C for 4 minutes, resuspended in 3 ml buffer A (250 mM sucrose, 10 mM triethanolamine, pH

7.4, 1 mM EGTA) complemented with Complete protease inhibitors (F. Hoffmann-La Roche Ltd, Basel, Switzerland) and phosphatase inhibitor cocktail II (Sigma-Aldrich, St. Louis, MO, USA) and lysed with a tightly fitting Potter teflon pestle for 4 minutes. Nuclei and unbroken cells were pelleted at 1000 g_{max} for 10 minutes and resuspended in 4 ml 2.2 M sucrose, 1 mM $MgCl_2$, 10 mM Tris, pH 7.4 with a loose Potter pestle. Pure nuclei were repelleted at 70,000 g_{max} for 80 min in a Beckman L8-M ultracentrifuge (SW 50.1 rotor) and washed with 4 ml buffer A at 1000 g_{max}. The mitochondria and lysosomes were pelleted from the post-nuclear supernatant at 20,200 g_{max} for 15 minutes. The microsomes were pelleted from the last supernatant at 182,000 g_{max} for 40 minutes and washed with 4 ml buffer A. The post-microsomal supernatant was kept as the cytosolic fraction. The final pellets were resuspended in buffer A and stored at -20°C. All centrifugation and resuspension steps were performed at 4°C. For Western analysis, 5 µg protein of each subcellular fraction (except 15 µg for the cytoplasmic fraction) was loaded. The antibodies used were: anti-BAMBI, anti-Smad2/3, anti-nucleoporin p62 (1:1000, BD Biosciences, San Jose, CA, USA), rabbit anti-actin HRP-conjugate, polyclonal goat anti-mouse HRP-conjugate (specifications as described above).

6.5.7 Statistical Analysis

Continuous variables are presented as mean with standard deviation, categorical variables as absolute and relative frequencies. The significance of differences in doubling time, migration and invasion was calculated using t-test analysis. Correlation of TGF-ß concentration and *BAMBI* expression was calculated with Pearson correlation. In order to compare frequencies between two or more groups, Pearson's Chi-Square test was performed. In case of a sufficient approximation to a normal distribution, means and 95% confidence intervals for *BAMBI* expression were calculated on a logarithmic scale and then transformed back to the original scale. In

order to compare *BAMBI* expression between two or more groups, a t-test or one-way ANOVA, respectively, was performed using the log-transformed expression as independent variable. The potential influence of *BAMBI* expression and of FIGO stage on overall survival is presented in plots of the corresponding Kaplan-Meier estimates and quantified using the Cox proportional hazards regression model. P-values ≤ 0.05 were considered to be statistically significant. All computations have been performed using SPSS software version 15.0 (SPSS Inc. Headquarters, Chicago, Illinois, USA).

Acknowledgements: We gratefully acknowledge Dr. Erwin Ivessa for providing antibodies (rabbit anti-calnexin), Dr. Thomas Grunt for providing the ovarian cancer cell line H134 and Dr. Bernd Mayer for a critical review of the manuscript. This work was supported by the Austrian Science Fund (FWF) grant no. P17891.

6.6 References

Baldwin RL, Tran H and Karlan BY. (2003). *Cancer Res,* **63,** 1413-1419.

Barrios-Rodiles M, Brown KR, Ozdamar B, Bose R, Liu Z, Donovan RS, Shinjo F, Liu Y, Dembowy J, Taylor IW, Luga V, Przulj N, Robinson M, Suzuki H, Hayashizaki Y, Jurisica I and Wrana JL. (2005). *Science,* **307,** 1621-1625.

Bierie B and Moses HL. (2006a). *Nat Rev Cancer,* **6,** 506-520.

Bierie B and Moses HL. (2006b). *Nat Rev Cancer,* **6,** 506-520.

Bierie B and Moses HL. (2006c). *Nat Rev Cancer,* **6,** 506-520.

Degen WG, Weterman MA, van Groningen JJ, Cornelissen IM, Lemmers JP, Agterbos MA, Geurts van KA, Swart GW and Bloemers HP. (1996). *Int J Cancer,* **65,** 460-465.

Derynck R and Zhang YE. (2003). *Nature,* **425,** 577-584.

Gotzmann J, Mikula M, Eger A, Schulte-Hermann R, Foisner R, Beug H and Mikulits W. (2004). *Mutat Res,* **566,** 9-20.

Jemal A, Siegel R, Ward E, Murray T, Xu J and Thun MJ. (2007). *CA Cancer J Clin,* **57,** 43-66.

Massague J, Blain SW and Lo RS. (2000a). *Cell,* **103,** 295-309.

Massague J, Blain SW and Lo RS. (2000b). *Cell,* **103,** 295-309.

Miyazono K, ten DP and Heldin CH. (2000). *Adv Immunol,* **75,** 115-157.

Moustakas A and Heldin CH. (2005). *J Cell Sci,* **118,** 3573-3584.

Nilsson EE and Skinner MK. (2002). *Reprod Biomed Online,* **5,** 254-258.

Onichtchouk D, Chen YG, Dosch R, Gawantka V, Delius H, Massague J and Niehrs C. (1999d). *Nature,* **401,** 480-485.

Onichtchouk D, Chen YG, Dosch R, Gawantka V, Delius H, Massague J and Niehrs C. (1999a). *Nature,* **401,** 480-485.

Onichtchouk D, Chen YG, Dosch R, Gawantka V, Delius H, Massague J and Niehrs C. (1999b). *Nature,* **401,** 480-485.

Onichtchouk D, Chen YG, Dosch R, Gawantka V, Delius H, Massague J and Niehrs C. (1999c). *Nature,* **401,** 480-485.

Pils D, Horak P, Gleiss A, Sax C, Fabjani G, Moebus VJ, Zielinski C, Reinthaller A, Zeillinger R and Krainer M. (2005). *Cancer,* **104,** 2417-2429.

Pils D, Pinter A, Reibenwein J, Alfanz A, Horak P, Schmid BC, Hefler L, Horvat R, Reinthaller A, Zeillinger R and Krainer M. (2007). *Br J Cancer,* **96,** 485-491.

Rodriguez GC, Haisley C, Hurteau J, Moser TL, Whitaker R, Bast RC, Jr. and Stack MS. (2001). *Gynecol Oncol,* **80,** 245-253.

Rual JF, Venkatesan K, Hao T, Hirozane-Kishikawa T, Dricot A, Li N, Berriz GF, Gibbons FD, Dreze M, yivi-Guedehoussou N, Klitgord N, Simon C, Boxem M, Milstein S, Rosenberg J, Goldberg DS, Zhang LV, Wong SL, Franklin G, Li S, Albala JS, Lim J, Fraughton C, Llamosas E, Cevik S, Bex C, Lamesch P, Sikorski RS, Vandenhaute J, Zoghbi HY, Smolyar A, Bosak S, Sequerra R, Doucette-Stamm L, Cusick ME, Hill DE, Roth FP and Vidal M. (2005). *Nature,* **437,** 1173-1178.

Sekiya T, Adachi S, Kohu K, Yamada T, Higuchi O, Furukawa Y, Nakamura Y, Nakamura T, Tashiro K, Kuhara S, Ohwada S and Akiyama T. (2004a). *J Biol Chem,* **279,** 6840-6846.

Sekiya T, Adachi S, Kohu K, Yamada T, Higuchi O, Furukawa Y, Nakamura Y, Nakamura T, Tashiro K, Kuhara S, Ohwada S and Akiyama T. (2004b). *J Biol Chem,* **279,** 6840-6846.

Sekiya T, Oda T, Matsuura K and Akiyama T. (2004c). *Biochem Biophys Res Commun,* **320,** 680-684.

Sekiya T, Oda T, Matsuura K and Akiyama T. (2004d). *Biochem Biophys Res Commun,* **320,** 680-684.

Siegel PM and Massague J. (2003). *Nat Rev Cancer,* **3,** 807-821.

Sunde JS, Donninger H, Wu K, Johnson ME, Pestell RG, Rose GS, Mok SC, Brady J, Bonome T and Birrer MJ. (2006). *Cancer Res,* **66,** 8404-8412.

Yamada SD, Baldwin RL and Karlan BY. (1999). *Gynecol Oncol,* **75,** 72-77.

Curriculum Vitae

EDUCATION:

2006 – present: **PhD studies**
Medical University of Vienna
Expected graduation December 2008

1998 - 2006: **BSc and MSc in Genetics/Microbiology**
Specialization in Immunology and Bioinformatics
University of Vienna

2005: **Course for Science Communications**
University of Vienna

1997 – 1998: **Military Service**

1992 – 1997: **Grammar School, Upper Austria**

WORK EXPERIENCE:

2006 – present: **PhD – Studies**
Medical University of Vienna
Molecular and clinical characterization of the potential tumor suppressor gene HCRP1

2004-2006: **Diploma Thesis**
University of Veterinary Medicine, Vienna
Expression profiling of mitochondrial biogenesis genes in cloned vs wildtype sheeps

Winter 2003/2004: **Research Project**
Department of Developmental Biology, Vienna
Working on MAPK Pathway in *A. thaliana*

Summer 2003: **Research Project**
Department of Microbiology and Genetics, Vienna
In silico sequence analysis and protein structure prediction

Summer 2001: **Industry Practical**
Sanofi Aventis, Frankfurt (Germany)
Expression and purification of PKC-δ

SKILLS:

Sound knowledge of: **Mammalian cell culture techniques** (stable transfections, inducible shRNA sileincing, viability-, apoptosis- and proliferation assays, flow cytometry)

Molecular biology and biochemical techniques (vector cloning, RNA/DNA/Protein preparation, SDS-PAGE and Western blotting, Microarrays, qRT-PCR, IHC, ICC)

In-silico **techniques** (Vector NTI, BLAST, Sequence Navigator, Primer Express, biological databases)

Imaging techniques (conventional and confocal microscopy)

Computer Skills: MS Office, SPSS

Languages: Native in German, Fluent in English, Basics in French

---

PUBLICATIONS:

Publications: The Human Homologue of Vps37A, a Key Component of the ESCRT-mediated Sorting Process in Yeast, is a Potential Biomarker for EGFR-Driven Tumors (submitted)

Methylation of N33 (TUSC3) Independently Predicts Ovarian Cancer Patient Outcomes, Caused by Altered N-Glycosylation Patterns (submitted)

BAMBI Translocates into the Nucleus after TGF-ß Treatment, Promotes Oncogenic characteristics In-vitro but without Negative Impact on Patient Outcome in Ovarian Cancer

Deciphering the role of the TRAIL pathway as potential tumour escape mechanism in ovarian cancer (in process)

Talks and Posters:

AACR PI3K Special Conferene 2008, Boston

HCRP1 contributes to degradation of activated EGFR and can be regarded as potential biomarker for targeted cancer therapies

Annual AACR Meeting 2008, San Diego, California

HCRP1 contributes to degradation of activated EGFR *(Abstract #3427)*

Deciphering the role of the TRAIL pathway as potential tumour escape mechanism in ovarian cancer *(Abstract #824)*

PhD Symposium 2008, Vienna, Austria

HCRP1 contributes to degradation of activated EGFR, a mechanism highly relevant for ovarian cancer

Annual Meeting of the Austrian Society of Human Genetic 2006, Vienna, Austria

HCRP1 – A novel tumor suppressor gene in ovarian cancer

GRANTS AND AWARDS:

PRIZE – Award for prototype development (2009)

GlaxoSmithKline Outstanding Clinical Scholar Award 2008

Mayor Grant of the City Vienna (€ 40 000.-)

REFERENCES:

Prof. Michael Krainer; MD
michael.krainer@meduniwien.ac.at
+43-1-40400-7572

Prof. Thomas Grunt, PhD
thomas.grunt@meduniwien.ac.at
+ 43-1-40400-5487

Prof. Maria Sibilia, PhD
maria.sibilia@meduniwien.ac.at
+43-1-40160-63011

Prof. Pavel Kovarik, PhD
pavel.kovarik@univie.ac.at
+43-1-4277-546 08